SLR

global environmental solutions

UPPSALA UNIVERSITET

FINAL REPORT ON PROSPECTIVE SITES FOR THE GEOLOGICAL STORAGE OF CO_2 IN THE SOUTHERN BALTIC SEA

ELFORSK

Swedish Energy Agency

GLOBAL CCS INSTITUTE

ccsp Carbon Capture and Storage Program

February 2014

SLR Ref: 501-00302-00001

CONTENTS

TABLES

FIGURES

PLATES

APPENDICES

1.0 EXECUTIVE SUMMARY

SLR was commissioned by Elforsk to identify and characterise the potential CO_2 storage sites in the southern Baltic Sea, in a project sponsored by the Swedish Energy Agency, the Global Carbon Capture and Storage Institute and Swedish industrial partners.[1] The project cooperates with the Finnish program CCSP under the management of the VTT Technical Research Centre

The study determined that there is a theoretical regional capacity to store some 16Gt of CO_2 in the Middle Cambrian sandstone beneath 900 metres of caprock and 1.9Gt in the Dalders Monocline. There is theoretical storage capacity of some 743Mt CO_2 in hydrocarbon and saline structures, which are located mainly offshore Latvia. On the basis of the data available, there is no effective capacity proven within these totals, although the Dalders Structure, with 128Mt, could be considered better defined, albeit still within the theoretical category range. Thus the study has established a relatively large theoretical storage capacity for captured CO_2.

The southern Swedish sector, where dynamic modelling was undertaken by Uppsala University, has relatively poor permeability and porosity characteristics. Maintaining the reservoir pressure at 50% above the hydrostatic pressure, limits the injection rate to 0.5Mt per well per annum over a 50 year period if five wells were to be used. The preliminary and indicative dynamic modelling for this area suggests that with 5 injection wells, a total injection capacity of 2.5 Mt per annum could be achieved. Reducing the injection period to say 25 years and increasing the number of wells could increase the total injection rate somewhat above this level. There may also be reservoir intervals with higher porosity and permeability where higher injection rates could be safely achieved. Thus it is possible that this area, including the Dalders structure, could be suitable as a storage site for CO_2 captured from a limited number of industrial facilities.

Other areas to the north east of the Monocline, such as the eastern Swedish sector and offshore Latvia where limited data is available, may have better reservoir qualities and where a higher rate of injection could be achieved, and thus be more suitable for regional industrial CO_2 storage. Furthermore, the regional storage capacity assessment demonstrated that there are sweet spots in the Cambrian reservoir such as onshore Latvia, where there is commercial gas storage, and both onshore and offshore Kaliningrad, where there is ongoing hydrocarbon production.

Three possible modes of seal failure have been identified. These include top seal failure, migration up the bounding fault planes and leakage across fault planes. All three possible modes of potential failure were investigated. The risk associated with all of these is considered low, based on currently available data. However the sealing integrity will require further investigation once new data becomes available and an injection site is selected. This will characterise small, site specific fault structures.

A test injection methodology has been designed with the objective of assessing the viability of CO_2 injection in the Baltic Sea region. This includes the characterisation of reservoir, caprock and hydraulic properties, pump testing as well as CO_2 migration and trapping using a phased approach methodology.

[1] SSAB, Jernkontoret, Svenska Petroleum Exploration, Cementa, Nordkalk, SMA Mineral, Minfo, Vattenfall, Fortum and Preem

An outline MMV programme has been developed based on the results of the dynamic modelling and the development phases of a CO_2 injection site. However, the details of this will be subject to site specific conditions and will need to be updated once new data is available.

Since the potential of the Swedish part of the Dalders Monocline to act as a regional storage site for significant quantities of CO_2 appears to be limited based on the present information, exploration efforts should be focused on areas where the best reservoir quality and regional storage potential are likely to be found. As offshore and onshore well data indicate that the north eastern portion of the Dalders Monocline appears to have better reservoir qualities than the current study area, new well data covering this area, in particular offshore Latvia would help to identify more suitable sites for CO_2 storage. Regional reservoir quality maps based on the limited data available indicate that onshore and offshore Kaliningrad would also appear to have better reservoir qualities.

Recommendations for further work include a study of the Cambrian sandstone interval to better understand the heterogeneity and distribution of good quality reservoir; a seismic attribute study to investigate the porosity trends in the Cambrian reservoir; a structural geology study to understand the influence of faulting on diagenesis and fracture porosity within the Cambrian; and a fracture gradient study of the Cambrian interval.

2.0 DEFINITION OF THE STUDY AREA

The study area is defined as previously mapped Palaeozoic sedimentary basins in the Baltic Sea Area, as described in the document *Geology and hydrocarbon prospects of the Paleozoic in the Baltic region*, 1993 by Brangulis, Kanev, Margulis and Pomerantseva. This assessment by SLR is searching for a geological formation that is ultimately capable of storing 50 million tonnes of dense phase CO_2 per year for a minimum of 25 years. This is based on calculations that show carbon dioxide emissions from stationary sources of up to a gross volume of some 100 million tonnes per year in the Baltic Sea region (Nilsson, 2011).

The report assesses the potential for geological storage of carbon dioxide (CO_2) in sedimentary basins in the Baltic Sea area. Storage potential may exist in depleted oil and gas fields or saline aquifer formations at depths greater than 800m, the minimum depth for CO_2 stability. The Precambrian crystalline basement of the Baltic Sea Basin lacks porosity and permeability for CO_2 storage. The principal stage of basin development was during deposition of a thick Middle Cambrian-Lower Devonian (Caledonian) sequence. This sequence contains sandstone and limestone aquifers that could store CO_2 that are sealed by shale and claystone aquifers (see Figure 1 below). Mesozoic rocks that unconformably overlie the Paleozoic are not deeply buried enough for CO_2 storage and are confined to the south and southwest of the Baltic Sea area.

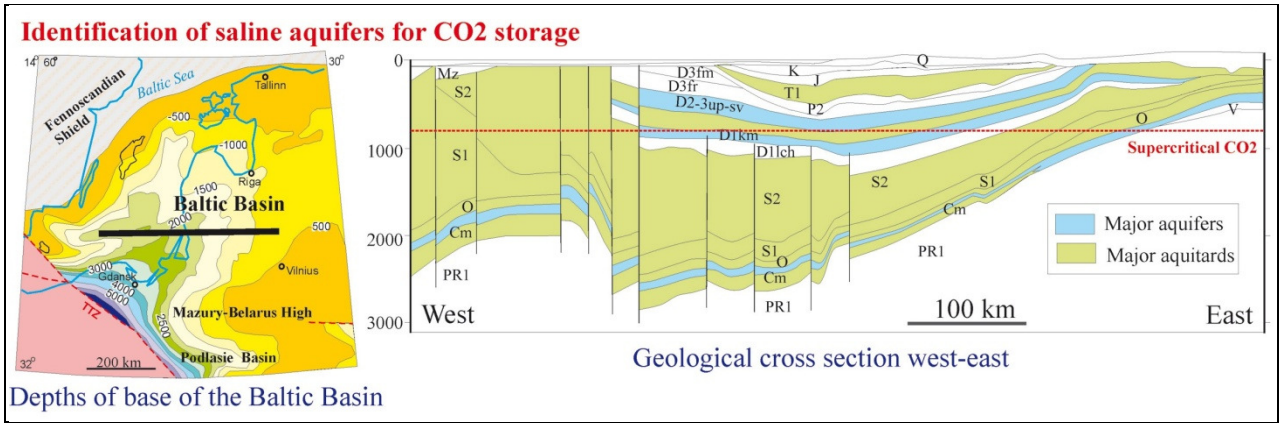

Figure 1 Map showing depth in metres of the Caledonian Baltic Sea Basin with a geological cross section indicating the aquifers that could store CO2 in supercritical state below 800m[2]

The Baltic Sea Basin is a marginal platform depression, deepening from 1 km in the northwest to more than 4km in the southwest, containing un-deformed Palaeozoic rocks underlain by Proterozoic crystalline basement (Figure 1). The area of the basin is about 200,000km^2 with the long axis being approximately 700 km and the maximum width in the southwest being 400-500 km (A.P. Brangulis, 1993). The structural elements with Caledonian sedimentary deposits are the Slupsk-Latvian-Estonian Border Zone (or Gotland Monocline), the Lithuanian Border Zone, the Liepaja Depression, and the Gdansk-Kura Depression (Plate 1). The sub-basins are separated by the Leba High and Liepaya-Saldus Ridge where structural traps are abundant. Palaeozoic terrigenous and volcanic rocks overlie the crystalline basement. There is a 100-150m thick Lower to Middle Cambrian sandstone that is the main hydrocarbon bearing reservoir of the Baltic region (Figure 3). The overlying Ordovician rocks comprise interbedded sand and shale members including the

[2] Cm, Cambrian; O, Ordovician; S1, Lower Silurian (Llandovery and Wenlock series); S2, Upper Silurian (Ludlow and Pridoli series); D1, D2, and D3, Lower, Middle, and Upper Devonian; P2, Middle Permian;T1, Lower Triassic; J, Jurassic; K, Cretaceous; Q, Quaternary (after Sliaupa S., 2009).

Alum Shale. This is followed by interbedded shale and limestone including shallow shelf carbonate rocks. Further limestone and shale was deposited in the Silurian. In the south west graptolitic shales are found. The shales grade to the northeast into marls, limestone, clays and shoal carbonates facies with barrier reefs. The upper part of the Caledonian sedimentary sequence is composed of lagoonal, continental deposits. Within this sequence the Cambrian and Devonian sandstones and the Ordovician and Silurian carbonates have the reservoir potential to store CO_2.

The main targets for CO_2 storage sites are faulted anticlines, step and nose features associated with the monoclines that occur on the northwest margin of the Baltic Basin. These structures contain the Lower to Middle Cambrian sandstone (Deimena Formation in Latvia, Faludden Sandstone in Sweden) that is the main hydrocarbon bearing reservoir of the Baltic region. There is also the possibility of stratigraphic traps, particularly in the Ordovician shelf carbonate rocks that are porous but not very permeable. There are indications on seismic sections offshore Latvia (A.P. Brangulis, 1993) of possible Ordovician shelf carbonates offshore (see L&OG Report) but poor reservoir quality and small size makes them inappropriate for CO_2 storage (Sweden Baltic Sea OPAB Farmout Prospectivity Appraisal, 1990).

The offshore Dalders Prospect Structure (Figure 2), which straddles Swedish, Lithuanian and Latvian territory, has been identified as a potential site for storage (Svenska Petroleum Exploration OPAB, 2010). Associated with the Dalders structure is the Dalders Monocline that extends NW to Gotland in Sweden. While storage in confined aquifers and closed structures is the preferred CO_2 sequestration mechanism (e.g. in the CCS-directive from the EC), it would significantly increase the potential of aquifers offshore Sweden if it can be shown theoretically and by demonstration and monitoring projects that CO_2 can be trapped in monoclinal structures (Erlstrom, 2008).

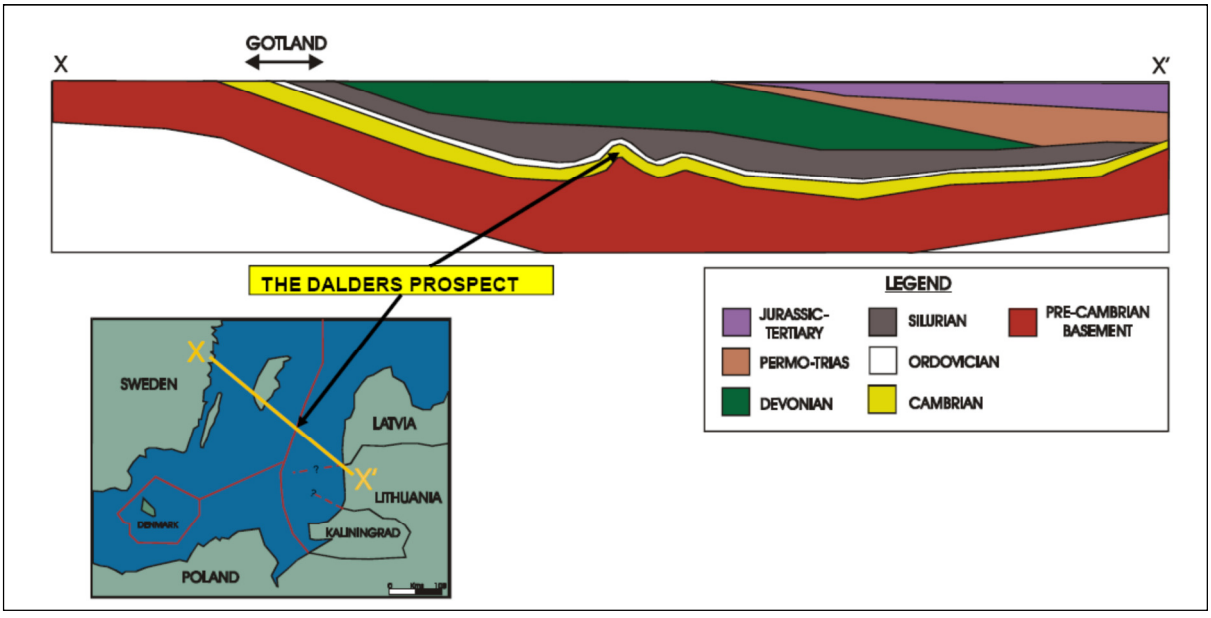

Figure 2 Location of the Dalders Prospect and the Dalders Monocline (from OPAB)

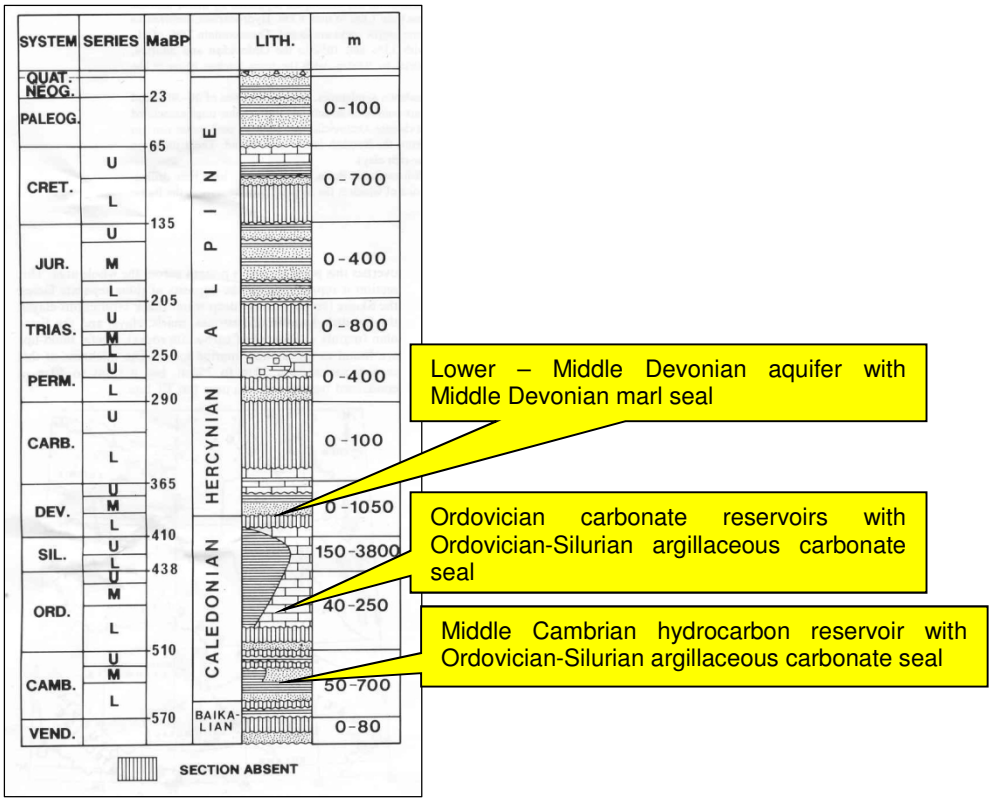

Figure 3 Geological section of the sedimentary basins in the Baltic Sea area[3]

[3] From Brangulis, A.P., Kanev, L.S., Margulis, L.S. and Pomerantseva, R. A., 1993 *Geology and hydrocarbon prospects of the Paleozoic in the Baltic region.* Geology of Northwest Europe: Proceedings of the 4th Conference edited by J.R. Parker, Geol. Soc. Lon.

3.0 GEOLOGICAL OVERVIEW

3.1 Introduction

Within the East Baltic region the main area for hydrocarbon exploration is the Baltic Depression. The Baltic Basin has an approximate latitude of 56° 30° N and longitude of 19° 00° E. The Baltic Basin is a large synclinal structure located in the south-western part of the East European Craton (EEC). The area of the basin is about 200,000km^2. The synclinal structure is approximately 700km long and 500km wide. The axis of the syneclise plunges to the southwest. Towards the north, east and southeast the syneclise is bounded by the Baltic Shield, the Latvian Saddle and Byelorussian Anteclise, respectively, (Brangulis, A.P. et al 1993). The basin is bounded to the south west by the Trans-European Suture Zone that strikes north-west to south-south-east. The area of interest covers parts of onshore Latvia, Lithuania, Kaliningrad and northern Poland, as well as the Baltic Sea. The central Baltic Sea is located in a transitional zone between an area of present day uplift to the north and an area of slight subsidence to the south. Four principal sub-basins (Plate) are considered as part of this study:

- **Slupsk Border Zone (SBZ)** located in the South-western Baltic Sea between Poland and Sweden, has an approximate surface area 2500km^2.
- **Gdansk-Kura Depression (GKD)** located in the south-eastern Baltic Sea, covers parts of Poland Russian and Lithuania and has an approximate surface are of 8000km^2.
- **Liepaja Saldus Ridge (LSR)** located in the southern part of the Baltic Sea and extends southwest to northeast across the Baltic Sea into Latvia. The Liepaja Saldus Ridge has a surface area of 2500 km^2.
- **Latvian, Estonian, Lithuanian Border Zone (LEL)** is located in the mid Baltic Sea and extends southeast to northwest covering parts of Estonia, Latvia and Gotland Island. The border zone has an approximate surface area of 2500 km^2.

3.2 General Geology

The Baltic Sea Basin contains a full sedimentary sequence from the Archean to the Cenozoic. The general geology of the Baltic Sea Area can be broken down into four major complexes (Brangulis et al, 1993):

- The Baikalian Complex
- The Caladonian Complex
- The Variscan Complex
- The Alpine Complex

3.2.1 The Baikalian Complex

The Baikalian Complex made up of a sequence of sandstones, siltstones and claystones up to 200m in thickness and includes up to 120m of early Cambrian claystones. This complex varies across the Basin and fills two northeast trending depressions.

3.2.2 The Caledonian Complex

The Caledonian Complex covers the four main sub-basins that contain the identified CO_2 storage targets. It is made up of the Middle and Upper Cambrian succession of up to 170m of sandstone, siltstone and shale. The upper part of the complex is characterised by between 40m and 250m of Ordovician shaly carbonates, approximately 1,000m Silurian shales, as well as lower Devonian claystone, sandstone and marlstone.

3.2.3 The Variscan Complex

The Variscan Complex contains the rest of the Devonian sequence of about 1100m of interbedded marly-carbonates and sandstones. The upper part of the complex is characterised by Lower Carboniferous siliciclastic carbonates. There were no CO_2 storage sites identified in the Variscan Complex.

3.2.4 The Alpine Complex

The Alpine Complex contains rocks in age from the Middle to Upper Carboniferous up to the Quaternary. The Permo-Triassic part of the complex includes 100m of Upper Permian carbonates and evaporates and approximately 250m of Lower Triassic mudstones, 120m of Jurassic sandstones, claystones and limestones as well as 140m Cretaceous glauconitic sand and chalky marl. The Cenozoic sequence is characterised by 80m of siliciclastic lithologies and confined to the south western part of Lithuania. There were no CO_2 storage targets identified in the Alpine Complex.

3.3 Structural History

The Baltic Sea Basin has a long and complex structural history. The Precambrian East European Continent (EEC) comprises several continental and arc-related terranes developed during a sequence of orogenic cycles spanning Archean, Early Proterozoic and Riphean times. The Baltica terrane forms the core of the EEC. During the Late Riphean and Vendian, Baltica formed part of a supercontinent from which it was separated at the end of the Vendian. During Cambrian to Late Silurian times, Baltica was an independent plate. During the Caledonian orogeny, it formed part of the Laurussian plate which was integrated into Permo-Triassic Pangea during the Variscan-Appalachian orogenic cycles. The EEC has remained geologically stable since late pre-Cambrian times.

Table 1 List of events which directly affected Baltica (Cocks et al 2005)

Events on Baltica	Millions of Years Ago (Ma)
Start of Rodinia break-up	**c. 800**
Timanian Orogeny end	**c. 555**
Completion of Iapetus Ocean opening	**c. 560**
Tornquist Ocean closure	**c. 445**
Iapetus Ocean closure	**c. 420**
Pangea assembly	**om 330**

The Baltic Depression is a large marginal synclinal structure in the south-western part of the EEC and formed during a period of extensions associated with the breakup of the Rodina supercontinent (Poprawa et al, 1999). The basin developed as a flexural foreland basin during the Silurian collision of Baltica and Eastern Avalonia.

The structural elements of the Baltic Depression are mainly associated with the movements of the basement blocks. The throws of the largest faults reach 200-500m and the lengths of the fault zones can be up to a few hundred kilometres. The majority of faults have accompanying fold structures; most of these interestingly do not cut the Variscan and Alpine complexes.

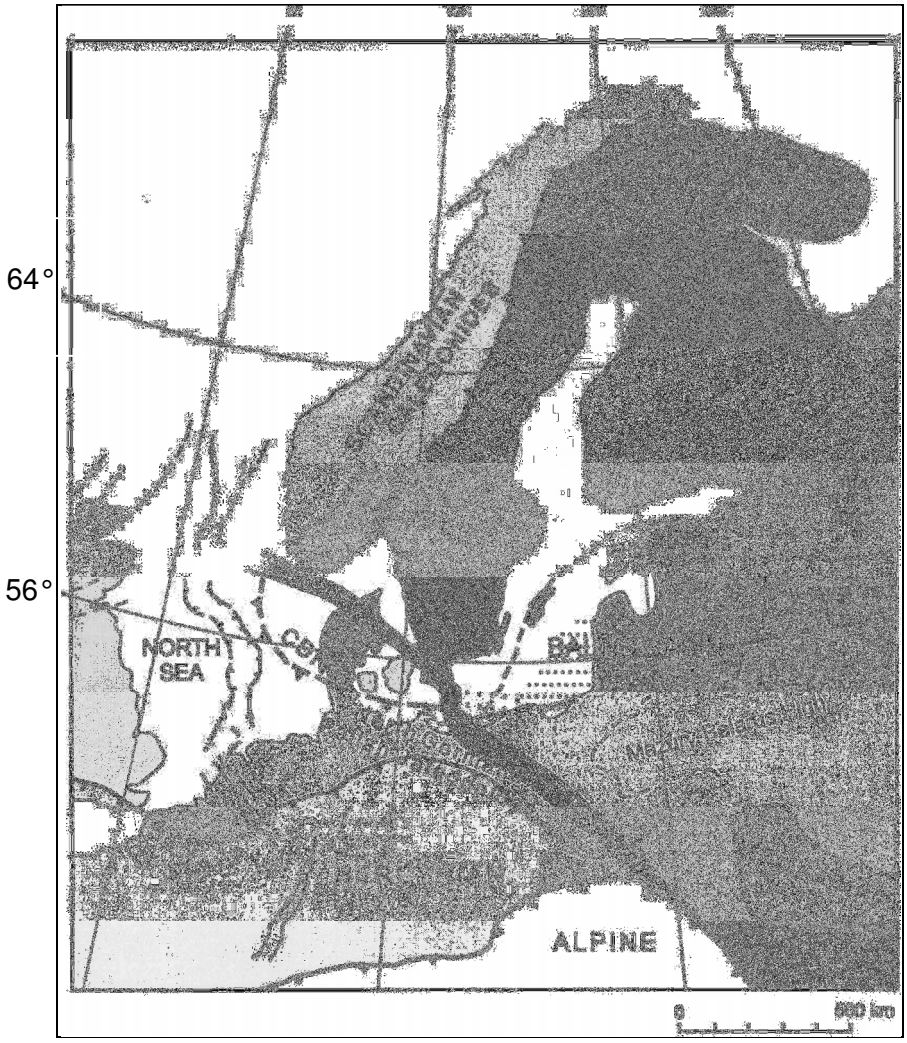

Figure 4: Major Tectonic structures and orogenic belts surrounding the Baltic Basin[4]

The main stage in the evolution of the Baltic Sea Basin was the Caledonian period. Rapid subsidence in the Silurian followed by deformation in the early Devonian produced the major structural features of the basin. The Hercynian and Alpine tectonic cycles modified the regional basin geometry only slightly.

3.4 Sub-Basin Structure

3.4.1 Slupsk Border Zone (SBZ)

The Slupsk Border Zone is a gently sloping monocline at the West northwest margin of the Baltic Basin.

3.4.2 Gdansk – Kura Depression (GKD)

The Gdansk-Kura Depression is affected by Caledonian minor faulting and folding that creates the best structural closures for hydrocarbon and CO_2 storage.

3.4.3 Liepaja Saldus Ridge (LSR)

The Liepaja-Saldus Ridge is a complex zone of faulted highs striking West-southwest/East-northeast. It traverses from the central part of the Baltic Sea onshore to central Latvia over a

[4]Poprawa et al, 1999

distance of more than 300 km. The Liepaja-Saldus Ridge is bounded by major faults, with a displacement of Caledonian sediments up to 600 m. The southern border of the ridge is particularly distinct. The ridge contains several untested potential CO_2 storage structures offshore Sweden and Latvian including the Dalders structure.

3.4.4 Latvian, Estonian, Lithuanian Border Zone (LEL)

The Latvian-Estonian and the Lithuanian Border Zones are stable areas of gently dipping crystalline basement overlain by a thin sedimentary succession. The surface of the basement rocks is buried to depths ranging from 500 to 1200-1400 m, and the monoclines have small anticlinal structures. An example is the significant structure that contains the Inčukalns underground gas storage facility.

3.5 Depositional Setting and Stratigraphy

The continental crust of the Baltic region was formed between 3.5 and 1.5 Ga. during four periods of orogenic activity. After its formation the crust underwent major reworking during the Sveconorwegian – Grenvillian and Caledonian orogenies (1.2 - 0.9 Ga). The Variscan and Alpine orogenies (about 300 and 100Ma respectively) influenced the south-western parts of the EEC. The anorogenic periods succeeding the orogenies saw erosion, sedimentation and a moderate amount of igneous activity. The Baltic Basin includes the Vendian at the base and most Phanerozoic systems. Four separate successions, the Bailkalian, Caledonian, Hercynian and Alpine, can be distinguished and are separated by angular unconformities.

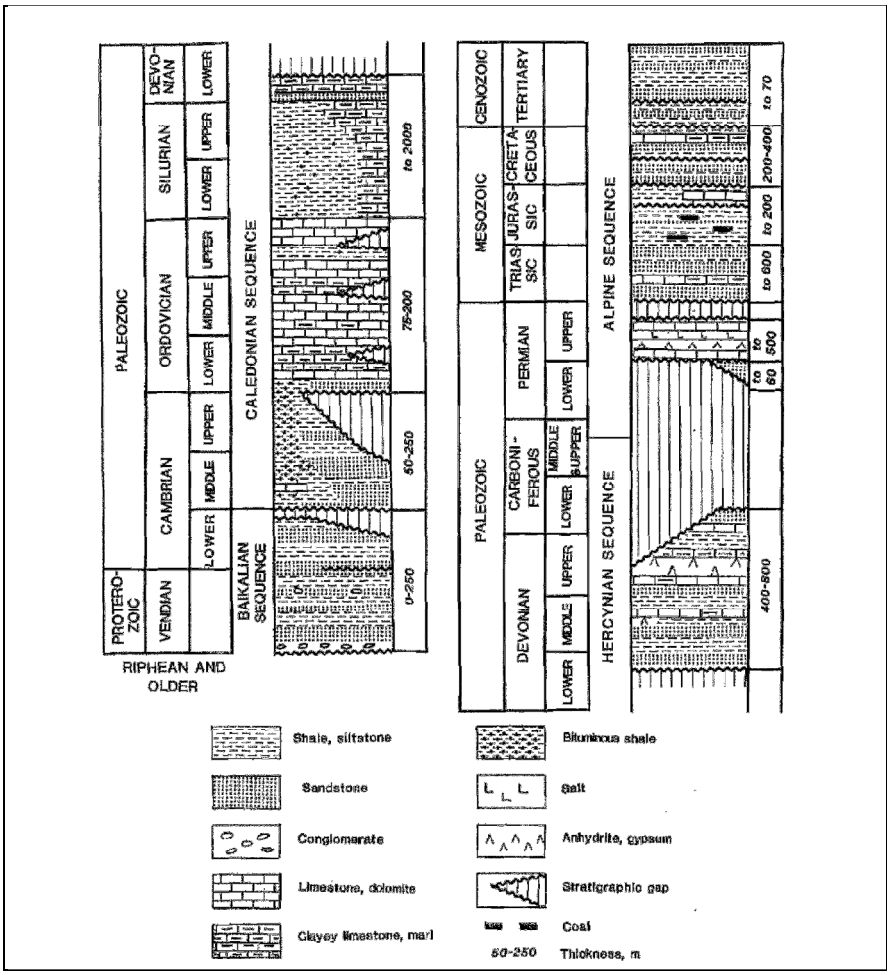

Figure 5 Stratigraphic Column of the Baltic Sea Basin showing the main depositional sequences[5].

The basement structures of the Baltic basin formed part of Baltica. Baltica consisted of three terranes, Fennoscandia, Sarmatia and Volgo-Uralia. They consolidated to form the supercontinent of Rodinia (c1300-1000Ma) during the Sveconorwegian Orogeny. At about 770-750 Ma, Rodinia broke up with the opening of the proto-Pacific, separating East Gondwana from the western margin of Laurentia. Subduction of the Mozambique and Brazilide oceans led to the collision of East Gondwana, and several continental blocks forming West Gondwana and produced the Pan African-Bailkalian-Brasiliano orogens about 620Ma. This orogen formed a second, Late Proterozoic 'Vendian' supercontinent comprising Gondwana, Laurentia and Baltica (Woodcock and Stracken, 2000).

[5] Ulmishek G, 1990

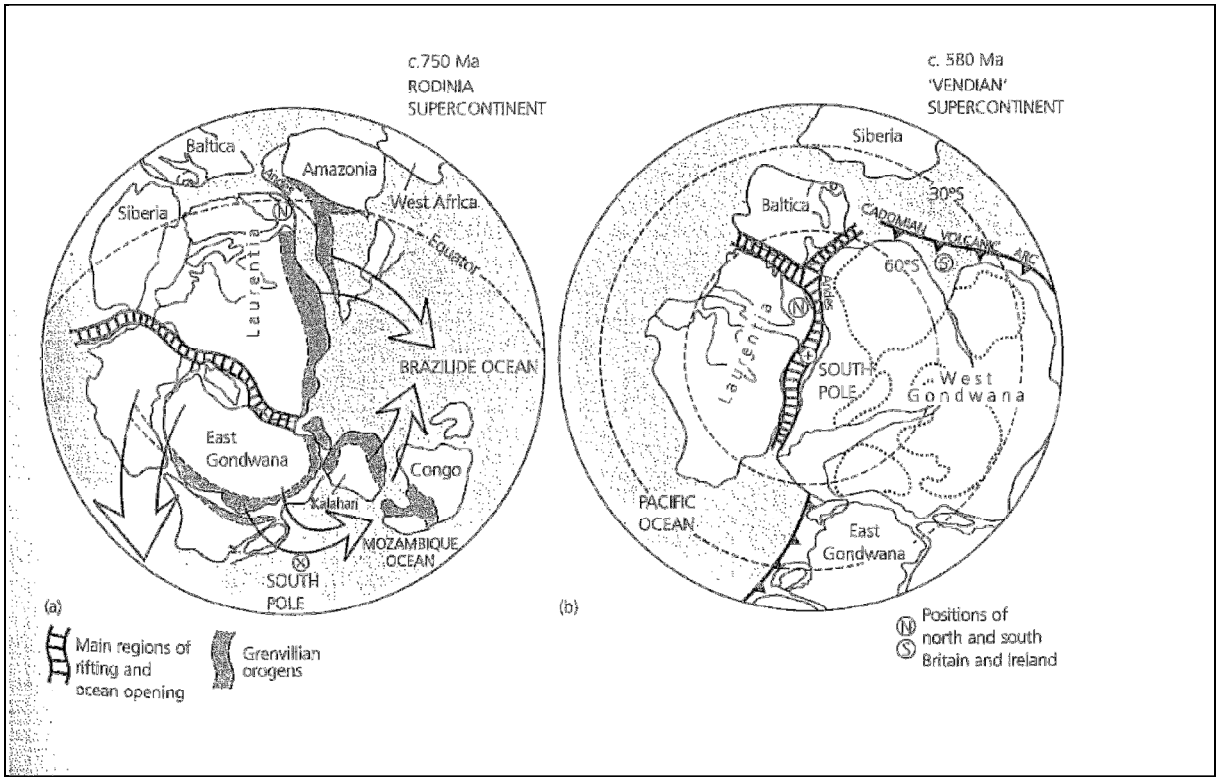

Figure 6 Global Paleocontinent reconstruction from the Neoproterozoic.

3.5.1 Proterozoic

The Proterozoic resulted in the deposition of a considerable thickness of the Jotnian red quartzites, aleurolites and conglomerates that make up the oldest non-metamorphosed cover of the Baltic Shield. Mid Riphean sandstones (c.1.3Ga), were uniformly deposited but can only be observed in a few tectonic depressions as a result of post depositional erosion forming the sub-Cambrian peneplain. This erosion continued into the Late Vendian as the Baltic Region remained uplifted. Late Vendian arkose sedimentation occurred in the narrow basins located along the future Baltica continental margin.

3.5.2 Cambrian

The Cambrian contains the best candidate reservoirs for CO_2 storage. The transgressive Cambrian sea created an embayment in the Baltic region and resulted in both near shore and open marine depositional sequences. Open marine conditions prevailed in the western and offshore area during the Early Cambrian whilst shallow marine conditions prevailed to the east. The oldest rocks in the Baltic Basin are found in Estonia. They are represented by the Rovno and Lontova regional stage (the Baltoji group) of the Manykayan stage. (Usaityte,D, 2000.) The Rovono stage comprises of greenish grey clays with interbedded silt and sand with glauconite grains.

The Lontova regional stage in the NW of the Baltic Basin is approximately 90m thick. The sequence is comprised of greenish, grey, violet, brown fine-laminated clay with beds of glauconitic sandstone and silt. Clay occurs in the lower parts of the upper units to the east whilst silt and sandstone replace the clay in the western regions.

Regional stages can be distinguished in the Lower, Middle and Upper Cambrian.

3.5.3 Lower Cambrian

The Lower Cambrian is characterised by mainly deep marine sequences with sediment sourced from land to the northwest and southeast of the Baltic Basin. Most of Latvia and Lithuania were covered in a shallow sea environment at this time.

The lower unit is the Talsi Formation, consisting of mainly sandstone with some pyroclastic rocks towards the northwest of the basin. This indicates a marine environment to the south, with some volcanic activity on the north western border of Baltica, possibly on the Baltic Continent, (Figure 7). The volcanism is consistent with rifting that was taking place during the Cambrian period. The thickest sandstones in the Cambrian are in this lower unit with a thickness of approximately 157m (Grigelis, 2011).

The middle unit is the Vergale Formation characterised by mainly sandstone in the south and interbedded sandstone, limestone, siltstone and argillite in the northwest. This is still a marine sequence with some quiet water conditions, as well as reef build up.

The upper formation is the Raus Formation. This sequence is fairly compact and consists of interbedded sandstone siltstone, argillite and limestone across the Baltic Basin. This indicates the continuing marine paleoenvironment during the Cambrian. There was a reduction in the sedimentation at this time.

The end of the Lower Cambrian is represented by a widespread unconformity.

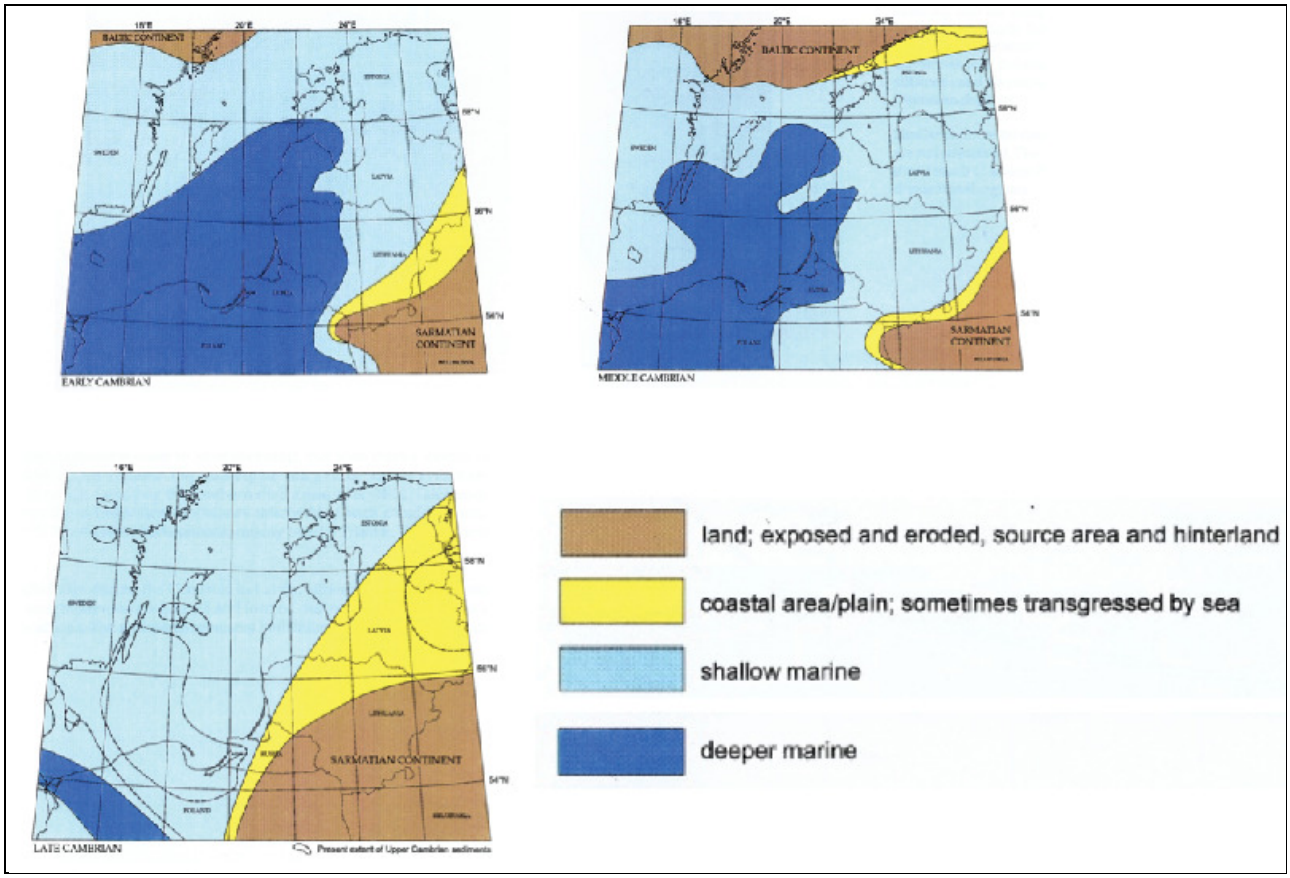

Figure 7 Reconstruction of the Cambrian paleoenvironment, separated into Early, Middle and Late Cambrian[6]

[6] Tarvis, T. 2007

3.5.4 Middle Cambrian

There was a marine transgression in the middle Cambrian with an increase in sedimentation. Subsidence occurred to the east of the Baltic Basin. Parts of Russia, Lithuania and Latvia were subsiding at this time and continued to subside into the Upper Cambrian period.

The Middle Cambrian is split into the Upper and Lower units.

The lower unit consists of the Kybartai Formation comprising argillite and siltstone lithologies, with thin interbedded sandstone and limestone in the north of the basin. This argillite shale dominance indicates quiet water, deep marine depositional conditions, with the basin shallowing towards the north with the introduction of sandstone and limestone.

The upper sequence is made up of the Deimena Group consisting of 82m thick sequence sandstones in the north of the Basin with the introduction of interbedded siltstones and argillite in the south. Marine conditions prevail throughout the upper-Middle Cambrian.

3.5.5 Upper Cambrian

During the Upper Cambrian there was a vast reduction in the number of deep marine deposits as the basin dramatically shallowed. Shallow marine sequences were widespread across the Baltic Basin. Terrigenous sediments were deposited in the Lithuanian region during this period and extensive coastal deposits were also formed.

The Upper Cambrian is not very well constrained. It is found mainly in the south of the Baltic Basin and consists of argillites and a thin bed of limestone.

The bituminous organic rich Alum Shales make up most of the argillites in the Upper Cambrian sequence.

3.5.6 Ordovician

The Ordovician contains argillaceous limestone deposits associated with algal reefs on the northern and north eastern flanks of the Baltic Basin. The reef structures are relatively shallow, small in size and therefore unsuitable for CO_2 storage.

3.5.7 Silurian

Thick Silurian argillaceous carbonates act as an effective seal to Cambrian reservoirs. The Silurian also contains barrier reef build ups with secondary dolomites but the size of individual structures is likely to be too small for matched CO_2 storage.

3.5.8 Devonian & Carboniferous

Devonian and Carboniferous terrigenous and carbonate deposits up to 800m thick are found in the east of the Baltic Basin.

3.5.9 Permian

Lower Permian continental sandstones, conglomerates and siltstones are up to 70m thick but are too shallow to be considered for CO_2 storage. The upper Permian is made up of carbonate and evaporitic deposits.

3.5.10 Mesozoic & Cenozoic

Mesozoic and Cenozoic terrigenous rocks unconformably overly the Caledonian sequence (Figure 8).

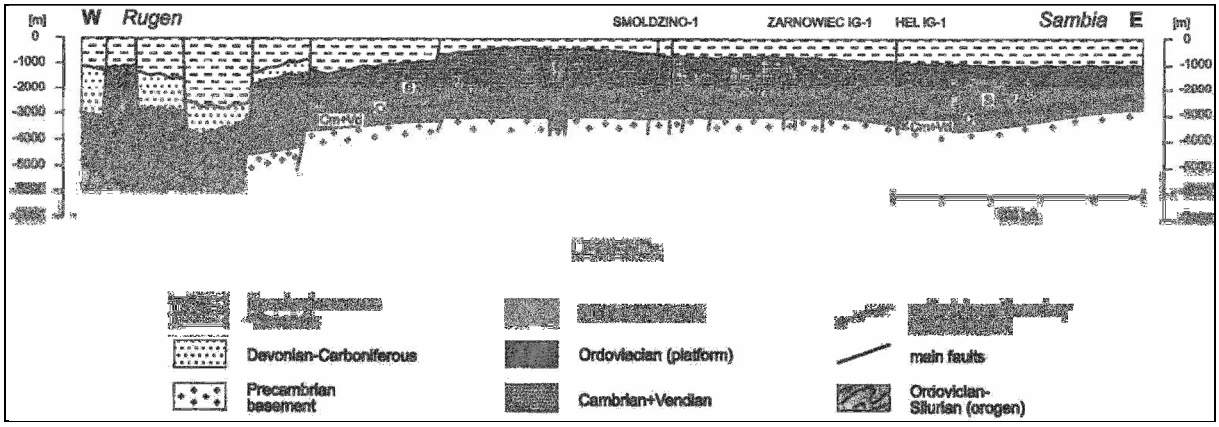

Figure 8 Sambia-Rugen Cross Section Through the Central Western Part of the Baltic Basin and the Caledonides.

3.6 Reservoir and Seal Pairs

The first oil field in the Baltic basin was discovered in 1962. It was located in the Middle-Late Cambrian sandstones. Several gas shows were encountered in the Devonian and older rocks. (Ulmishek, G. 1990) The Middle-Upper Cambrian sandstones form the major CO_2 storage reservoir of interest in the Baltic Sea Basin. The Cambrian reservoirs are sealed by thick Ordovician-Silurian carbonates and a 20m thick Upper Cambrian – Lower Ordovician shale horizon.

3.6.1 Reservoir Rocks

The best reservoir rocks in the Baltic Sea Basin are the Middle-Upper Cambrian sandstones that alternate with shales and siltstones. Diagenetic alteration controls the properties of the sandstones. Quartz grains went into dissolution and reprecipitation occurred between the grains in open pore spaces. This controls the porosity and to a lesser extent the permeability of the sandstones. The sandstones are well sorted with porosities of up to 25% and permeabilities of several hundred millidarcies in places. Below 2km the porosity deteriorates to values of 5% to 7%. The Middle Cambrian Deimena sandstones contain Skolithos ichnofossils that locally increase the vertical porosity and permeability (Brangulis et al 1993).

The Ordovician has little potential as a CO_2 storage reservoir due to the variability of carbonate porosity and permeability as well as size of individual reef structures (Ulmishek, G. 1990).

3.6.2 Cap Rocks

The upper Cambrian and Lower Ordovician shales and the thick Ordovician marls and argillaceous carbonates form the cap rock for most of the reservoirs in the Baltic Basin. A thick sequence of Silurian mudstones, shales and siltstones overlie the Ordovician lithologies. The overall cap rock thickness across the Baltic Basin exceeds 800m in many areas (Modliński, 2010).

3.6.3 Mod

In the southeast part of the Baltic Sea Basin most of the known hydrocarbon fields are located in a narrow area east of the basin axis in the Mid-Upper Cambrian sequence. The Ordovician carbonates and marls form the cap. The traps are controlled by local structures intersected by reverse faults. These structures are relatively small in area with vertical closures between 30-70m in height (Ulmishek, G. 1990).

3.7 Geological Targets for CO_2 Storage

The conclusion of the geological overview is that the only workable reservoir seal pair for CO_2 storage is the Cambrian sandstones sealed by the Ordovician Silurian argillaceous carbonates and shales.

In the Baltic Basin four sub-basins of interest have been identified, Slupsk Border Zone (SBZ), Gdansk-Kura Depression (GKD), Liepaja-Saldus Ridge (LSR) and the Latvian, Estonian Lithuanian Border Zone (LEL). These areas contain almost all of the oil and gas fields in the Baltic Basin (Plate 1).

The basin screening in Section 4.0 concentrates on the assessment of these sub-basins for CO_2 storage.

4.0 BASIN SCREENING

Bachu (2003) developed a quantitative evaluation of a sedimentary basin's suitability for CO_2 storage. In the table below fifteen assessment criteria are shown with three to five classes defined from the least favourable to the most favourable.

Table 2 Criteria for assessing sedimentary basins for CO_2 geological sequestration (Bachu 2003)

	Criterion	Classes				
		1	2	3	4	5
1	Tectonic setting	Convergent oceanic	Convergent intramontane	Divergent continental shelf	Divergent foredeep	Divergent cratonic
2	Size	Small	Medium	Large	Giant	
3	Depth	Shallow (<1,500 m)	Intermediate (1,500–3,500 m)	Deep (>3,500 m)		
4	Geology	Extensively faulted and fractured	Moderately faulted and fractured	Limited faulting and fracturing, extensive shales		
5	Hydrogeology	Shallow, short flow systems, or compaction flow	Intermediate flow systems	Regional, long-range flow systems; topography or erosional flow		
6	Geothermal	Warm basin	Moderate	Cold basin		
7	Hydrocarbon potential	None	Small	Medium	Large	Giant
8	Maturity	Unexplored	Exploration	Developing	Mature	Over mature
9	Coal and CBM	None	Deep (>800 m)	Shallow (200–800 m)		
10	Salts	None	Domes	Beds		
11	On/Off Shore	Deep offshore	Shallow offshore	Onshore		
12	Climate	Arctic	Sub-Arctic	Desert	Tropical	Temperate
13	Accessibility	Inaccessible	Difficult	Acceptable	Easy	
14	Infrastructure	None	Minor	Moderate	Extensive	
15	CO_2 Sources	None	Few	Moderate	Major	

Sedimentary basins were selected for their suitability for storage of CO_2 in depleted oil and gas fields or saline aquifers using a basin-by-basin approach applying the minimum criteria, secondary qualifiers and weightings as defined in Table 3 and Table 4 (modified from Bachu, 2003). Bachu's suitability criteria were broadly classified into three:

1. Basin characteristics, such as tectonism, geology, geothermal and hydrodynamic regimes (these are "hard'' criteria because they do not change).
2. Basin resources (hydrocarbons, coal, salt), maturity and infrastructure (these ''semi-hard'' or ''semi-soft'' criteria because they may change with new discoveries, technological advances and/or economic development).
3. Societal, such as level of development, economy, political structure and stability, public education and attitude (these are ''soft'' criteria because they can rapidly change or vary from one region to another).

Table 3 Minimum criteria for consideration of sedimentary basins for CO_2 storage

	Suitability Criterion	Suitability threshold	Weight
1	Depth	>800 m	0.07
2	Size at surface	>2500 km^2	0.06
3	Seismicity	<High (i.e., not in subduction zones)	0.06
4	Reservoir/Seal	At least one major extensive and competent seal	0.08
5	Faulting and/or fracturing	Low to moderate	0.07
6	Pressure regime	Not overpressured	0.05
7	Regulatory status	Accessible	0.03
		TOTAL	**0.42**

Table 4 Proposed secondary qualifiers for assessing the potential of sedimentary basins for CO_2 storage

	Potential Criterion	Poor Potential	Good Potential	Weight
1	CO_2 sources	At >500 km distance	At <500 km distance	0.08
2	Physical accessibility	Difficult	Good	0.03
3	Infrastructure	None or poor	Developed	0.05
4	Hydrogeology Flow systems	Shallow, short	Deep and/or long	0.08
5	Geothermal regime[1]	Warm	Cold	0.10
6	Hydrocarbon potential and industry maturity	None, poor	Large, mature	0.08
7	Coal	Too shallow or too deep	Between 400 and 1000 m depth	0.04
8	Coal value[2]	Economic	Uneconomic	0.04
9	Climate	Arctic and sub-arctic	Temperate	0.08
			TOTAL	**0.58**

The combined weights of Table 3 and Table 4 are equal to 1.0. Individual basins can be ranked according to these criteria to give a value between 0 and 1.

The Baltic Sea Basin is potentially a good candidate for CO_2 storage because it is a stable divergent cratonic basin with limited faulting and extensive sealing shale (Plate 1and Ulmishek, G. 1009). It has regional long range flow systems. The cold climate and geothermal gradient increase CO_2 storage capacity and decrease CO_2 buoyancy. There is a proven hydrocarbon system with oil and gas production. However the monoclines around the margins are relatively shallow. In the relatively shallow monocline structures where the target saline aquifer storage reservoirs are less than 800m deep, CO_2 sequestration and storage is inefficient (low CO_2 density) and unsafe because of very high CO_2 buoyancy (Chadwick, A. 2008). The Baltic Sea sub-basins are all of suitable size but the structures within them are not. The monoclines that form the boundary to the basin may be candidates for CO_2 storage in saline aquifers but further reservoir engineering studies are required to establish the integrity of CO_2 trapping in monoclines where no structural closure exists. This applies in to the Dalders Monocline in Sweden.

With respect to physical accessibility and regulatory status the Baltic sub basins were ranked from the point of view of transporting CO_2 from point sources surrounding the Baltic Sea. Both pipeline and shipping transport are considered. In Table 4, Table 6, Table 8 and Table 10 the distance is calculated for point sources in Finland which are the furthest away from the potential storage sites in the Baltic Sea sub basins. Clearly distances from other countries will be much less. The Baltic Sea sub-basins could provide accessible CO_2 storage sites below 800m onshore and offshore in shallow water. There are major CO_2 sources surrounding the Baltic Sea Basin and there is a moderate level of pipeline and hydrocarbon production infrastructure. The regulatory status refers to legal and commercial access by Finland and Sweden to CO_2 sinks in the host country.

The results of the screening exercise for sedimentary basins of the Baltic Sea are shown below with additional weightings applied by SLR using a variation of Bachu's methodology (Bachu, 2003).

4.1 Slupsk Border Zone

The Slupsk Border Zone (Plate 1) is a monocline at the WNW margin of the Baltic Basin. It contains part of the Dalders Monocline.

Table 5 Criteria for consideration of Slupsk (including Dalders) Monocline for CO_2 storage

	Criterion	*Threshold*	*Slupsk Monocline*	*Weight*
1	Depth	>800 m	Deep (1000+ m)	0.07
2	Size at surface	>2500 km^2	Moderate size structures	0.06
3	Seismicity	Low (i.e., not in subduction zones)	Low (intracratonic)	0.06
4	Reservoir/Seals	At least one major extensive and competent seal	Excellent	0.08
5	Faulting/fracturing	Low to moderate	Low	0.07
6	Pressure regime	Not overpressured	Normal	0.03
7	Regulatory status	Accessible	Moderately accessible	0.03

Table 6 Secondary qualifiers for assessing the potential of Slupsk for CO_2 storage

	Potential Criterion	*Poor Potential*	*Good Potential*	*Weight*
1	CO_2 sources	--	~300 km distance	0.04
2	Physical accessibility	--	Good	0.03
3	Infrastructure	--	No developed pipelines	0.01
4	Flow systems	--	Deep but untested	0.03
5	Geothermal regime	--	Cold	0.10
6	Hydrocarbon potential and industry maturity	--	Good data	0.08
7	Coal	N/A	N/A	0.00
8	Coal value	N/A	N/A	0.00
9	Climate	--	maritime, sub arctic	0.08

Total weightings of Table 4 and Table 5 for Slupsk Monocline = 0.76

COMMENTS:

- A potential siliciclastic saline aquifer is present in the Cambrian.
- A significant structure closure (161 km^2)has been mapped at the storage reservoir level at the Dalders Prospect.
- Oilfields in Poland, Lithuania and Russia are producing from the Middle Cambrian sandstone reservoir and therefore the Cambrian has proven capacity to store CO_2.
- A significant part of the Dalders monocline is accessible in Swedish territory.
- When the Latvia/Lithuania border is agreed, all of the Dalders structure could be accessible for oil field development with CO_2 Enhanced Oil Recovery (EOR).

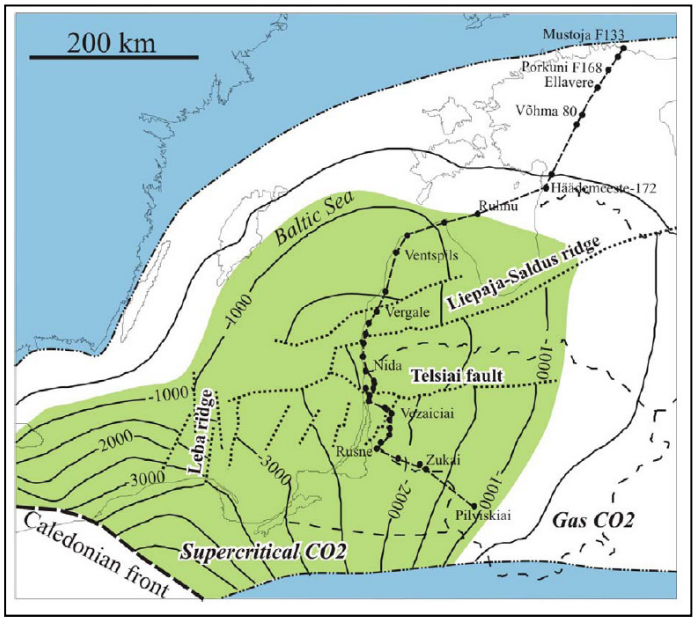

Figure 9 Depth of top of the Cambrian aquifer.[7]

The score of 0.76 for the Slupsk Border Zone makes it a potential candidate for CO_2 storage. The Dalders Prospect anticline structure (Figure 2) is located in water depth of 120m in the central Baltic across Swedish, Latvian and Lithuanian territory. It has a volume estimate of about 300 million barrels of recoverable oil in Cambrian sandstone (Petroswede Svenska Petroleum Exploration, 2010). Structurally it lies on the SE edge of the Slupsk-Latvian-Estonian Monocline on the Liepaya-Saldus High. The Dalders structure and associated monocline is a potential candidate for CO_2 storage based on its favourable depth, size, low seismicity, limited faulting, accessibility and good reservoir seal pair.

4.2 Latvian Estonian and Lithuanian Border Zone (LEL)

The Latvian Estonian and Lithuanian Border Zone (Plate 1) is a monoclonal structure that surrounds the margins of the Baltic Basin. The Latvian Estonian Monocline is largely offshore and the Lithuanian Monocline is largely onshore. There are a number of oilfields onshore Latvia and Lithuania producing from Cambrian sandstone reservoirs in small anticline traps (e.g. Kuldiga Field). The Devonian aquifer is not buried sufficiently deep to act as a reservoir for CO_2 storage (Figure 9). There is onshore pipeline infrastructure in Latvia and an underground gas storage facility at Inčukalns which proves the CO_2 storage capacity of the Cambrian sandstone reservoirs and the physical accessibility. The area is also less than 400kms from CO_2 point sources in Finland.

[7] The line of the geological cross-section shown in Figure 10 is indicated. The green area indicates the pressure temperature field for supercritical CO_2 (after Sliaupa S., 2009).

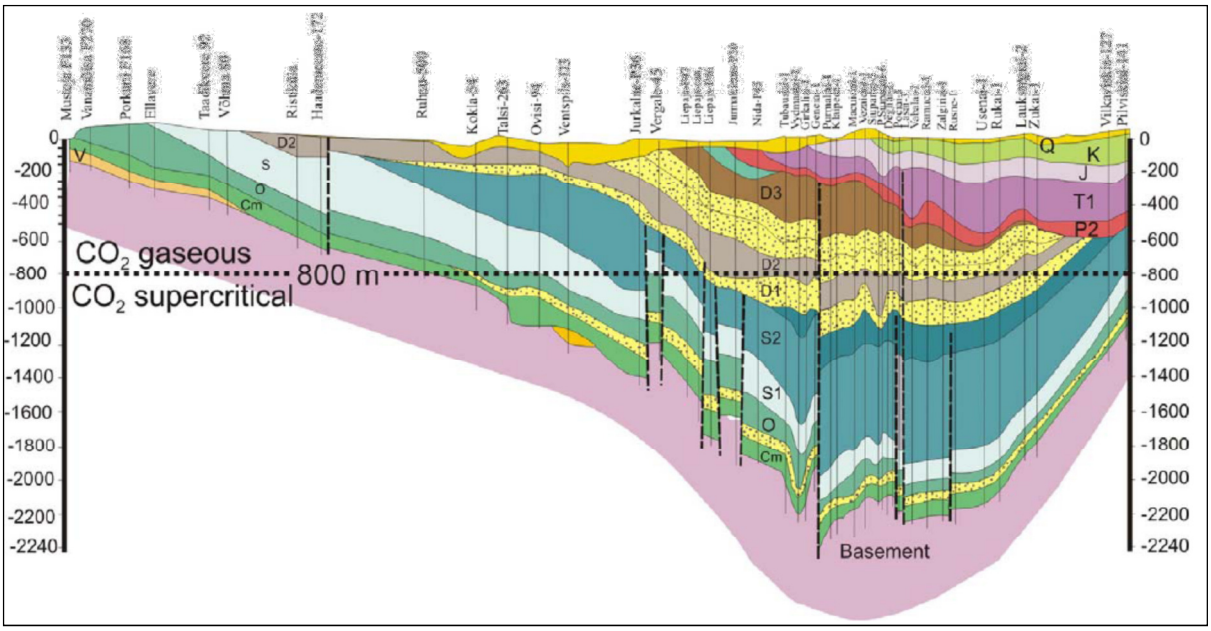

Figure 10 Geological cross section across Estonia, Latvia, and Lithuania[8]

Table 7 Criteria for consideration of Latvian Estonian and Lithuanian Monocline for CO_2 storage

	Criterion	*Threshold*	*Latvian Estonian Lithuanian Monocline*	*Weight*
1	Depth	>1000 m	Deep (1000+ m)	0.07
2	Size at surface	>2500 km^2	Small structures	0.02
3	Seismicity	Low (i.e., not in subduction zones)	Low (cratonic)	0.06
4	Reservoir/Seals	At least one major extensive and competent seal	Excellent	0.08
5	Faulting/fracturing	Low to moderate	Low	0.07
6	Pressure regime	Not overpressured	Normal	0.03
7	Regulatory status	Accessible	Moderately accessible	0.07

[8] **Modified after Sliaupa et al. 2008**

Table 8 Secondary qualifiers for assessing the potential of Latvian Estonian and Lithuanian Monocline for CO_2 storage

	Potential Criterion	Poor Potential	Good Potential	Weight
1	CO_2 sources	--	~400 km distance	0.08
2	Physical accessibility	--	Good	0.01
3	Infrastructure	--	Some pipelines onshore	0.03
4	Flow systems	--	Deep and/or long	0.03
5	Geothermal regime	--	Cold	0.10
6	Hydrocarbon potential and industry maturity	--	Moderate, mature	0.05
7	Coal	N/A	N/A	0.00
8	Coal value	N/A	N/A	0.00
9	Climate	--	Maritime, sub arctic	0.08

Total weightings of Table 6 and Table 7 for Latvian Estonian and Lithuanian Monocline = 0.71

COMMENTS:

- Ten sources in Lithuania emit more than 0.1Mt of CO2 per year from an oil refinery (Mazeikiai), an ammonia plant, two cement plants (Akmene) and power plants.
- Two prospective siliciclastic saline aquifers are present in the Cambrian and Lower Devonian. There are no significant structures in the Lower Devonian (Sliaupa S., 2009)
- Oil production onshore Gotland is from Ordovician reefs at shallow depths unsuitable for CO_2 storage.
- Ordovician and Upper Silurian carbonate reefs with storage potential are interpreted on seismic data acquired in the northern part of offshore Latvia.
- Eleven oilfields are producing from the Middle Cambrian sandstone reservoir in Lithuania, but the structures are small and enhanced oil recovery and storage potential is estimated to be negligible, about 5.6Mt (Sliaupa S., 2009).
- One of the 17 major West Latvian structures identified with Cambrian reservoirs, Inčukalns, has been used for underground gas storage since 1968, proving the stability of the sealing cap rock (Shogenova, A. 2009), (Latvijas Vides, Geolgijas, un Meteorlogijas Agentura, 2007).
- The storage capacity of the Lithuanian Monocline is limited by the size of structures with Cambrian sandstone reservoirs and the restricted area that is sufficiently deep for CO_2 storage.

The LEL, with a score of 0.71, is a possible candidate for CO_2 storage based on its favourable depth, low seismicity, good Cambrian and Devonian reservoir/seal pairs, onshore infrastructure and accessibility. Only two structures of capacity greater than 1 Mt CO2 were identified in Lithuania. Ordovician algal reefs occur at shallow depths in small structures in Gotland and onshore Latvia. Thirty large structures (greater than 600Mt CO_2 storage capacity) are identified in Latvia, onshore and offshore (Sliaupa S., 2009).

4.3 Liepaja-Saldus Ridge

The Liepaja-Saldus Ridge (Plate 1) is a regional faulted zone with a complex structure, oriented SW-NE. It extends more than 300 km from the central part of the Baltic Sea to central Latvia onshore. It is bounded by major faults that displace Caledonian sediments up to 600m. The Liepaja-Saldus High has several structures with associated oil prospects offshore Latvia. The Dalders Prospect (Figure 2) extends onto the Liepaja-Saldus Ridge.

Table 9 Minimum criteria for consideration of Liepaja-Saldus High for CO_2 storage

	Criterion	Threshold	Liepaja-Saldus High	Weight
1	Depth	>800 m	Deep (1000+ m)	0.07
2	Size at surface	>2500 km^2	Medium size structures	0.06
3	Seismicity	Low (i.e., not in subduction zones)	Low (passive margin)	0.06
4	Reservoir/Seals	At least one major extensive and competent seal	Excellent	0.08
5	Faulting and/or fracturing	Low to moderate	Low	0.07
6	Pressure regime	Not overpressured	Normal	0.03
7	Regulatory status	Accessible	Accessible	0.02

Table 10 Secondary qualifiers for assessing the potential of Liepaja-Saldus High for CO_2 storage

	Potential Criterion	Poor Potential	Good Potential	Weight
1	CO_2 sources	--	~400 km distant	0.08
2	Physical accessibility	--	Fair (marine)	0.02
3	Infrastructure	Limited	--	0.01
4	Flow systems	--	Deep and/or long	0.03
5	Geothermal regime	--	Cold	0.10
6	Hydrocarbon potential and industry maturity		Mature	0.05
7	Coal	N/A	N/A	0.00
8	Coal value	N/A	N/A	0.00
9	Climate	--	Maritime, sub-arctic	0.08

Total weightings Table 8 and Table 9 for Liepaja-Saldus High = 0.75

COMMENTS:

- Adjacent to Latvian coast.
- Two wells offshore Latvia, E6-1 and P6-1, proved a saline aquifer in Middle Cambrian sandstones and some oil production from Late Ordovician carbonates. No current production.
- A number of structures with prognosed Cambrian sandstone reservoirs have been identified offshore Latvia including the Dalders Structure.
- Good potential licence access given Svenska's licence holding in Latvia.

The Liepaja-Saldus Ridge, with a score of 0.75, is a potential candidate for CO_2 storage based on its favourable depth, low seismicity, excellent reservoir/seal pairs, and accessibility.

4.4 Gdansk-Kura Depression

The Gdansk-Kura Depression is a large regional structure, extending SW-NE from Poland to the southern part of Western Latvia (Plate 1). There are oil discoveries in Poland, Lithuania and Kaliningrad District and several oil prospective structures offshore Latvia.

Table 11 Minimum criteria for consideration of Gdansk-Kura Depression for CO_2 storage

	Suitability Criterion	Gdansk-Kura Depression	Weight
1	Depth	Deep (1000+ m)	0.07
2	Size at surface	Moderate size structures (in Poland ~8,000 km^2)	0.03
3	Seismicity	Low	0.06
4	Reservoir/Seals	Proven excellent	0.05
5	Faulting and/or fracturing	Low to moderate	0.04
6	Pressure regime	Normal	0.05
7	Regulatory status	Reasonably accessible	0.02

Table 12 Secondary qualifiers for assessing the potential of Gdansk-Kura Depression for CO_2 storage

	Potential Criterion	Poor Potential	Good Potential	Weight
1	CO_2 sources	--	~400 km distant	0.01
2	Physical accessibility		Good	0.03
3	Infrastructure		Present--	0.05
4	Flow systems	--	Deep and/or long	0.08
5	Geothermal regime	--	Cold - moderate	0.10
6	Hydrocarbon potential and industry maturity		Mature	0.08
7	Coal	N/A	N/A	0.00
8	Coal value	N/A	N/A	0.00
9	Climate	--	Maritime, sub-arctic	0.08

Total weightings of Table 10 and Table 11 for Gdansk-Kura Depression = 0.75

COMMENTS:

- Contains producing fields offshore Poland and Russia and onshore Russia and Lithuania.
- Existing platforms and pipelines.
- Potential access to storage offshore Poland.
- Possible access to storage offshore Kaliningrad.

The Gdansk-Kura Depression, with a score of 0.75, is a potential candidate for CO_2 storage based on its favourable depth, moderate size, low seismicity, proven reservoir/seal pairs and possible licence access through Poland.

4.5 Liepaja Depression

The Liepaja Depression is located north of the Liepaja-Saldus High and extends onshore Latvia (Plate 1). The Liepaja Depression is not a candidate for CO_2 storage based on its unfavourable depth. The prospective reservoirs are less than 800m deep.

5.0 BASIN RANKING

In the previous section, a modified version of Bachu's criteria was used to score the sub-basins of the Baltic Sea Basin. Based on the weightings shown in Table 5 to Table 12 above the basins are ranked as follows Slupsk Border Zone (0.76), Gdansk-Kura Depression (0.75), Liepaja Saldus Ridge (0.75), and Latvian Estonian Lithuanian Border Zone (0.71).

Table 13 Ranking of Baltic Sea sub-basins in terms of suitability for CO_2 geological sequestration

Rank	Basin	Characteristics	Score
1	Slupsk Border Zone	Proven reservoir/seal pair, moderate size structures, offshore, large saline aquifer, limited faulting, good accessibility, <500kms to strategic CO_2 sources	0.76
2	Gdansk-Kura Depression	Existing oil and gas production infrastructure, moderate sized structures, offshore, fair accessibility, >500kms to some strategic CO_2 sources	0.75
3	Liepaja Saldus Ridge	Proven reservoir/seal pair, moderate size structures, offshore, fair accessibility, <500kms to strategic CO_2 sources	0.75
4	Latvian Estonian Lithuanian Border Zone	Proven reservoir/seal pairs, small structures, potential saline aquifer, only small area sufficiently deep for CO_2 storage, accessible, 250kms to strategic CO_2 sources	0.71

In this initial ranking the Slupsk Border Zone has the highest priority because it contains the Dalders Monocline which is a probable CO_2 storage structure that is accessible to Swedish CO_2 point sources. The Gdansk-Kura Depression is geologically suitable for CO_2 storage and has existing oil production infrastructure at PetroBaltic's B3 field and Lukoil's Kratsovskoye field. However access may be restricted depending on the storage capacity of the depleted oil and gas reservoirs when they become available. There are existing plans to use the offshore facilities in Poland to store CO_2 from the Lotos refinery in Gdansk. The Liepaja Saldus Ridge is closer to CO_2 sources in Finland and has potential CO_2 storage in saline aquifers offshore Latvia. The LEL Border Zone has the lowest rank because only a small area is sufficiently deep for CO_2 storage.

6.0 STORAGE CAPACITY CALCULATION METHODOLOGY & RESULTS

6.1 Introduction

Following the ranking of the Baltic Sea sub-basins, storage capacity calculations have been completed using the GeoCapacity (2009) methodology. Hydrocarbon exploration and production data obtained in the initial phases of the project was integrated into a GIS database and used to estimate the potential theoretical storage capacity for the Baltic Sea sub basins. The calculations were undertaken as regional estimates for both hydrocarbon fields and saline aquifers. The specific methodologies used for individual fields, the data origins and the results are discussed below.

6.2 Hydrocarbon Field Storage Capacity Estimates

6.2.1 Generic Hydrocarbon Fields:

Based on the available data for specific hydrocarbon fields, two separate calculation methodologies were used. Where limited data is available the Generic Hydrocarbon Fields method is used. A simplified formula using the ultimate recoverable reserves (UR) and formation volume factors (FVF) for the oil and gas fields shown in Table 14 was used (Schuppers, *et al.*, 2003).

Table 14 Oil and Gas Fields where Generic Hydrocarbon Fields method is used

LITHUANIA	SUB-BASIN	POLAND	SUB-BASIN	KALININGRAD	SUB-BASIN
S. Blidinziai	GKD	B34	LSR	Slavinsk	GKD
Lapgiriai	LEL			Gajevsk	GKD
Lauksargiai	GKD			Laduskino	GKD
Plunge	GKD			Veselovsk	GKD
Girkaliai	GKD			Slavsk	GKD
Ablinga	GKD			**Gusevskij**	GKD
Vezaiciai	GKD			**Solnečnaja**	GKD
Siupariai	GKD			**Zverevskaja**	GKD
P. Siupariai	GKD			**Rjazanskaja**	GKD
Degliai	GKD			**Borokskaja**	GKD
Silale	GKD			**Dubravnaja**	GKD
Pociai	GKD			**D158**	GKD
Vilkyciai	GKD			**D30**	GKD
Sakuciai	GKD			**D160**	GKD
Kybartai	LEL			**C32**	GKD
Kudirka	LEL			**d21**	GKD
				d22	GKD
				Kravtsovskoye (D-6)	GKD

$$M_{CO_2} = \rho_{CO_2} \times UR_p \times B$$

where:

ρ_{CO_2} = CO_2 density at reservoir conditions

UR_p = Proven Ultimate Recoverable Oil or Gas

B = Oil or Gas Formation Volume Factor

The proven recoverable oil or gas data from the LO&G, 2007 report was used to estimate the CO_2 storage potential of the Lithuanian, Polish and some of the Kaliningrad fields. Zytner et al (2008), Otomas (2011) and Sliaupiene and Sliaupa (2011) provided the proven recoverable oil and gas reserve data for the other Kalinigrad fields. For the Lithuanian fields FVFs based on those reported for the Genciai, Nausodis and Kretinga fields by Svenska, 1996 were used. No FVF data was available for the Kaliningrad fields and a value of 1.08 similar to the onshore Lithuanian fields was assumed. In the case of the Polish fields, FVF data and CO_2 density was obtained from the data included in the LOTOS, 2010 presentation.

CO_2 density values based on published information and temperatures and pressures recorded for the Lithuanian fields as published by Streimikiene, 2010 was used in the calculations.

For the Kaliningrad fields a default CO_2 density value of 0.650t/m^3 was used due to the lack of specific formation data.

6.2.2 Detailed Hydrocarbon Fields:

Calculations of CO_2 storage capacity in hydrocarbon fields where detailed reservoir and formation data are available have been undertaken based on Bachu, *et al.*, 2007. The following formulae were applied:

Gas Fields: $\boldsymbol{M_{CO_2} = \rho_{CO_2} \times R_f \times (1 - F_{ig}) \times OGIP \times B_g}$

Oil Fields: $\boldsymbol{M_{CO_2} = \rho_{CO_2} \times (R_f \times OOIP \times B_o - V_{iw} + V_{pw})}$

where:

$\boldsymbol{\rho_{CO_2}}$= CO_2 density at reservoir conditions (best estimate based on available data & using the CO_2 State Equations for Pressure and Temperature Conditions; http://webbook.nist.gov/chemistry/fluid/)

$\boldsymbol{R_f}$ = Recovery Factor

$\boldsymbol{F_{ig}}$ = Fraction of Injected Gas

$\boldsymbol{OGIP}$ = Original Gas in Place (at surface conditions)

$\boldsymbol{B_g}$ = Gas Formation Volume Factor <<1

$\boldsymbol{OOIP}$= Original Oil in Place (at surface conditions)

$\boldsymbol{B_o}$ = Oil Formation Volume Factor >1

$\boldsymbol{V_{iw}}$ = Volume of Injected water

$\boldsymbol{V_{pw}}$ = Volume of Produced water

Detailed information from a very limited number of hydrocarbon fields in the Baltic Sea region was available to perform a trap or structure specific theoretical storage capacity calculation. **Table 15** below summarises the fields where detailed Recovery Factor (RF) and FVF data was available to perform these detailed calculations. No information was available with regard to volumes of produced and injected water and these values were omitted from the calculations.

Table 15 Hydrocarbon Fields with Detailed Reservoir Information

POLAND	Trap / Structure Name	Sub-Basin	LITHUANIA	Trap / Structure Name	Sub-Basin
B3	Total	LSR	**Genciai**	Total	GKD
B4	B4-1	LSR	**Nausodis**	Total	GKD
B6	B6-1	LSR	**Kretinga**	Total	GKD
B8	B8-1	LSR			

The Polish field data was primarily based on data published in the LOTOS, 2010 presentation where more up to date information on the Middle Cambrian Zona Paradoxides Paradoxissimus formation reservoir conditions was available for the B3, B4, B6 and B8 fields.

A detailed assessment of the Genciai Lower and Upper Sand reservoirs was performed using this method based on the information compiled in the Svenska 1996 pre-development study report. For this field an average recovery factor of 47% was used.

Storage Capacity calculations for the A Upper and A Lower Sand were undertaken for both Nausodis and Kretinga as well as for the B Sand in the Kretinga field. Average RF values of 14% and 22% respectively were used for these calculations.

The OOIP values used were those published by Svenska in 1996. For all of the Lithuanian fields a FVF of 1.08 was used based on the published values from the Genciai field.

6.3 Saline Aquifer Storage Capacity Estimates:

6.3.1 Regional, Bulk Volume Estimate:

A storage capacity calculation for the Cambrian below 900m and for the Dalders Monocline was performed using the modified formula by Bachu *et al.* (2007) as published in the GeoCapacity (2009) report:

$$M_{CO_2} = A \times h \times NG \times \emptyset \times \rho_{CO_2} \times S_{eff}$$

where:

ρ_{CO_2}= CO_2 density at reservoir conditions (best estimate based on available data & using the CO_2 State Equations for Pressure and Temperature Conditions; http://webbook.nist.gov/chemistry/fluid/)

A = Area of the regional trap of aquifer

h = Height of the regional trap of aquifer

NG = Net to Gross Ratio (NG)

$\emptyset$ = Average reservoir porosity of regional or trap aquifer (best estimate)

S_{eff} = Storage Efficiency Factor (for bulk volume of regional aquifer or trap specific)

The outline of the Cambrian below 900m (LO&G, Enclosure 2, 2002) was digitised into GIS and an area of 193,192km^2 was calculated. The Dalders Monocline as outlined in the structural elements of the Baltic Syneclise (Tarvis, 2007) and mapped below 900m (LO&G, Enclosure 2, 2002) was calculated as 19,634km^2. An average height of the reservoir of 70m and average porosity of 13% were used based on data in Skirius, 1996 (Amoco report) and data for the Faludden sandstone from the B-9 and P6 wells.

A storage efficiency factor of 2% was used for all the bulk regional aquifer assessment whilst the CO_2 density was calculated based on reservoir temperature and pressure data from the B-9 well composite log.

6.3.2 Trap Volume Estimate:

A trap specific theoretical storage capacity calculation was carried out for 8 offshore Latvia closures and for the Dalders Structure as presented in the Amoco 1996 report. The calculation was undertaken assuming the structures are open or semi-closed and assuming the Middle Cambrian Faludden sandstone is an unconfined aquifer. The structures modelled are listed in Table 16 below.

Table 16 Closure specific Calculations for the Dalders Structure

Structure Name	Sub-Basin
Dalders Structure	LSH
E5	LSR
E6	LSH
E7	LSH
E5	LSH
P1	LSH
E17	LSH
P4	LSH
E12-E13-E2-D10	LSH
E23	LSH

This conceptual model assumes that the storage space is generated by displacing existing fluids and distributing the pressure increase in the surrounding and connected aquifer. This approach therefore assumes that available space is essentially the pore volume and the storage efficiency factor is dependent on the connectivity of the surrounding aquifer (GeoCapacity, 2009).

Storage capacity calculations for the eight structures mapped in the Latvian offshore were completed using digital Top Cambrian depth structure isopach maps and fault outlines at a scale of 1:25,000 and 1:50,000 purchased from the Latvian Environment, Geology and Meteorology Centre (LEGMC). Outlines of the structures were digitised using the deepest closing contour and the fault structures.

Average reservoir height, average porosity values and CO_2 density values based on the observed reservoir formation data (including temperature and pressure) from the E6-1 and E7-1 wells were used in the storage capacity calculations for the E6 and E7 structure. Net to Gross (NG) ratio values published in the Amoco Enclosure 24 map were used.

The LEGMC Top Cambrian depth structure digital data was combined with fault structures and used to define the outlines of the E5, E17, P4 and E23 structures. Combined data from E12-E13-E2-D10 was used to determine overall area of the structure. An average reservoir thickness of 55m and average porosity of 15% was used based on the values from the E6-1 and E7-1 wells and an estimated CO_2 density of 0.603 t/m^3 was used in the calculation with the NG ratio values derived from the Amoco, Enclosure 24 map.

The P4 structure located within the area of the Dalders Monocline was also modelled based on the information available from the P6-1 well. An average reservoir thickness of 83m and a porosity value of 12% were used. However, it important to note that the digital Top Cambrian structure map coverage did not provide an accurate way of determining the boundary of this structure.

The Middle Cambrian depth map showing contours of the Middle Cambrian Sandstone in the Dalders Structure (Amoco, 1995) was combined with the digital Top Cambrian E7 structure map and the fault structure outlines to define the boundary of the Dalders Structure. The NG ratios of 76% and an average formation porosity of 13% based on information from Donoho, 1996 and Amoco Enclosure 24 was used. An average reservoir formation thickness of 55m, as published in the Structural Analysis section by Donoho *et* al (1996), was used for the Dalders structure.

The 'cartoon approach' of the GeoCapacity (2009) methodology was used to estimate the storage efficiency factor for these structures. The reservoir can be considered high quality based on the porosity and permeability values recorded for the Faludden sandstone in the E6-1, E7-1 and P6 wells. This is supported by permeability values in the B3 field (Lotus 2011). However, there are a small number of mapped structural features that limit the apparent connectivity in the reservoir between the individual trap structures. There are variations in permeability of between 10mD to 100mD observed in the cores from the E6-1, E7-1 and P6-1 well within the bulk aquifer volume. Based on these observations a storage efficiency value of 20% was chosen.

6.4 Theoretical Storage Capacity Calculation Results:

The summary tables below show the storage capacity calculation results for the Baltic Sea region based on the methodology described above. The best prospects are the Dalders Monocline and the Cambrian across the Baltic Sea region below 900m depth Table 17. The Cambrian has an estimated theoretical storage potential 16,222Mt of which 1,924Mt is in the Dalders Monocline and 128Mt in the Dalders Structure, located in the central part of the Baltic Sea Area (Table 17). The total individual field storage capacity is estimated to be 943Mt of which the individual hydrocarbon fields are estimated to have theoretical storage potential of 210Mt.

Table 17 Theoretical Storage Capacity Summary

	Estimated CO_2 Storage Capacity (10^6 tonnes)
Regional Cambrian Below 900m	16,222
of which Dalders Monocline	1,924
Individual Baltic Sea Field Total	743
Dalders Structure	128

. The estimates for onshore theoretical storage capacity are summarised below:

Table 18 Proportion of onshore CO_2 storage capacity

	Estimated CO_2 Storage Capacity (10^6 tonnes)	Estimated CO_2 Storage Capacity onshore (10^6 tonnes)	Percentage of the overall CO_2 storage capacity
		-	-
Regional Cambrian Below 900m	16,222	9151	56
of which Dalders Monocline	1,924	157	8
of which Dalders Structure	128	0	0
Individual Baltic Sea Field Total	743	88	12
of which in Poland	6	0	0
of which in Latvia	633	0	0
of which in Lithuania	31	31	100
of which in Kaliningrad	73	57	78

Results from the individual hydrocarbon fields, saline aquifer structure and bulk assessments are discussed in more detail below.

6.4.1 Generic Hydrocarbon Fields:

The results from the theoretical capacity calculations using the Generic Hydrocarbon Fields method show relatively small storage potential associated with individual hydrocarbon fields across the Baltic Sea region.

Table 19 Hydrocarbon Field Theoretical Storage Capacity
(* indicates the onshore fields)

LITHUANIA	Estimated CO_2 Storage Capacity (10^6 tonnes)
S. Blidinziai*	0.32
Lapgiriai*	0.32
Lauksargiai*	0.16
Plunge*	0.28
Girkaliai*	3.75
Ablinga*	0.66
Vezaiciai*	2.78
Siupariai*	2.50
P. Siupariai*	5.51
Degliai*	1.89
Silale*	1.23
Pociai*	0.50
Vilkyciai*	5.05
Sakuciai*	1.90
Kybartai*	0.48
Kudirka*	1.53
TOTAL	**28.87**

POLAND	Estimated CO_2 Storage Capacity (10^6 tonnes)
B34	3.28
TOTAL	**3.28**

KALININGRAD	Estimated CO_2 Storage Capacity (10^6 tonnes)
Slavinsk*	4.97
Gajevsk*	1.14
Laduskino*	26.22
Veselovsk*	1.87
Slavsk*	3.17
Gusevskij*	0.32
Solnečnaja*	0.31
Zverevskaja*	0.05
Rjazanskaja	0.13
Borokskaja*	0.07
Dubravnaja*	0.08
D158	0.94
D30	1.47
D160	0.70
C32	2.71
d21	1.03
d22	1.97
Kravtsovskoye (D-6)	7.17
TOTAL	**54.33**

Country	Estimated CO_2 Storage Capacity (10^6 tonnes)
Lithuania	28.87
Poland	3.28
Kaliningrad	54.33
TOTAL	**86.47**

UR data were collected from LO&G (2002), Zytner et al (2008), Otmac (2011) and Sliaupiene and Sliaupia (2001) for the Kaliningrad fields. FVF values based on the Lithuanian field values and a CO_2 density value of 0.6500 t/m^3 were used for the fields from the LO&G report and 0.7300 t/m^3 for the other fields. The total theoretical storage capacity value is 54.33 Mt of CO_2 for the Kaliningrad fields.

Individual Lithuanian hydrocarbon fields are estimated to have a total theoretical storage capacity of just under 29 Mt using the data that was available from the UR estimates (LO&G, 2002), the FVF and CO_2 density values (Streimikiene, 2010).

A theoretical storage capacity for the B34 field was calculated to be 3.3Mt.

Overall, 27 of the 35 fields considered for the Generic Hydrocarbon Fields class are onshore and correspond to 77.71% of the 86.47 Mt theoretical storage capacity.

Storage capacity calculations were not completed for hydrocarbon fields where no data was available. These include:

- Poland: B16, B21
- Lithuania: Saukenai

- Kaliningrad: Kulikovsk, Jagodnoje, Kaliningrad, Gusev, Neman

6.4.2 Detailed Hydrocarbon Fields:

The results from the theoretical capacity calculations using the Detailed Hydrocarbon Fields Method also show relatively small storage potential associated with individual hydrocarbon fields across the Baltic Sea region.

Table 20 Hydrocarbon Field Detailed Theoretical Storage Capacity (* indicates the onshore fields)

	Trap/ Structure Name	Hydrocarbon Field CO_2 Storage Capacity (10^6 tonnes)
POLAND		
B3	Total	1.20
B4	B4-1	0.29
B6	B6-1	0.24
B8	B8-1	0.89
	TOTAL	**2.62**
LITHUANIA		
Genciai*	Total	1.48
Nausodis*	Total	0.18
Kretinga*	Total	0.19
	TOTAL	**1.86**

The B3 and B8 oil fields have the greatest theoretical storage potential with 4.75Mt and 3.63Mt respectively based on the limited available information for the Polish offshore sector of the Baltic Sea. Detailed field data from the Genciai, Nausodis & Kretinga fields show a combined theoretical storage capacity of 1.86Mt.

All the fields in Lithuania are onshore, this implies 3 structures from the 7 described in table 20 are onshore and 41.52% of the storage capacity is onshore for the detailed hydrocarbon fields class.

6.4.3 Saline Aquifer Regional Bulk Storage Potential:

The regional saline aquifer bulk storage assessments show the highest theoretical storage potential with a combined total of 18,145 Mt. The largest proportion of this is the generic regional estimated CO_2 storage potential for the Cambrian below 900m which is 16,221Mt of the 18,145 Mt total. The additional 1,923Mt theoretical storage capacity has been calculated for the area of the Dalders Monocline. While both of these numbers are encouraging, more data on reservoir thickness, porosity and FVFs across the regional Cambrian reservoir target and better definition from seismic of the 19,634km^2 extent of the Dalders Monocline is required as the current estimates are based only on the values observed in the P6-1 and B-9 wells.

Table 21 Regional Saline Aquifer Theoretical Storage Capacity

Saline Aquifer Bulk - Storage Potential	Estimated CO_2 Storage Capacity (10^6 tonnes)
Cambrian below 900m	**16,221.56**
Dalders Monocline	**1,923.55**

The confidence in these calculated storage capacity calculations was improved significantly by the inclusion of the LEGMC Cambrian structure map and fault line data resulting in accurate boundaries for the individual structure being selected.

6.4.4 Saline Aquifer Field Storage Potential:

A field storage potential calculation for four Middle Cambrian sandstones structures in the Dalders structure shows a total theoretical storage capacity of 127.91Mt.

The combined total of the seven bulk trap assessments in the Latvian offshore, the Kaliningrad fields and the Dalders structure represent a theoretical storage capacity of 780.35 Mt with the highest values recorded in the E23, the combined E12-E13-E2-D10 structure and Dalders structure with 266.05 Mt, 144.09 Mt and 127.91 Mt respectively (Table 22).

Table 22 Saline Aquifer Field Theoretical Storage Capacity

Structure Name	Saline Aquifer Field CO_2 Storage Capacity (10^6 tonnes)	Structure Name	Saline Aquifer Field CO_2 Storage Capacity (10^6 tonnes)
Dalders Structure	127.91	Cheremuhovo	0.2769
		Hrustalninskaya	0.3474
LATVIA		Lesnaya	1.1017
E5	36.31	Volodarovskaya	0.2493
E6	35.26	Ključevaja	1.1749
E7	18.01	Gusevskaya	1.5629
E12-E2-13-D10	144.09	Aleshkinskoe	0.251
E17	104.70	Deyminskoe	1.1097
P4	29.03	Western Krasnoborskoe (+ south)	2.5817
E23	266.05	Krasnoborskoe	2.5045
		Malinovskoe (North & South)	3.0772
KALININGRAD		Northern Krasnoborskoe	0.0545
Bobruisk	0.7208	Semenovskoe	0.1409
Bolshakovskaya-2	0.1901	Ushakovskoe (+ west)	3.6508
		TOTAL	**780.35**

The assessment for the seven individual Latvian offshore closures is based on formation data obtained from summarised information from the E6-1, E7-1 and P6 boreholes including formation pressure data recorded during the testing operations. The outline of the structures has been mapped based on 1:25,000 and 1:50,000 digital LEGMC data Top Cambrian depth structure maps and fault data. The assessment demonstrates that structures with CO_2 storage capacity > 100Mt are present in the Latvian offshore region with the E23, E17 and combined E12 structures of particular interest. Estimates of the NG ratios and average porosity values are based on data from the E6-1 and E7-1 wells. Further data from future exploration drilling and testing of the offshore Latvian structures should be used to confirm the porosity, NG ratios as well as formation temperature and pressure data and further increase the confidence in the theoretical storage capacity calculations.

In Kaliningrad, 16 saline aquifer structures are described based on detailed data supplied by VNIGRI. The volumes and the NG ratios of the remaining eight structures are based on Otmas (2011), CO_2 density and the average reservoir thickness is based on well data provided by VNIGRI.

7.0 STATIC MODEL:

Based on the well and Cambrian depth structure map data available for the Baltic Sea area, four areas of interest have been identified for further study as CO_2 storage sites. This section describes the methodology used to develop the static model for the selected structures shown in Table 23.

Table 23 Static Model Structure Sizes

	Area in km^2	Area in m^2
Dalders Structure	161	160,784,104
Dalders Monocline	72,169	72,169,300,000
E-6 Structure	26	26,368,579
E-7 Structure	26	26,298,247

For the four areas of interest, the depth of the Top of the Middle Cambrian sandstone reservoir has been selected as the reference layer for the static models as it extends throughout the whole Baltic Sea region. The Middle Cambrian is composed of several sandstone (SST) intervals of which the top one is the main reservoir, known as the Faludden SST (Sweden), Paradoxides Paradoxissimus (Poland) and Deimena SST (Latvia and Lithuania). The three additional surfaces are the bottom of the Middle Cambrian, the top of the Alum Shale (Upper Cambrian) and the top of the Ordovician. The Alum Shale and Ordovician act as cap rocks overlying the Faludden SST reservoir. Details of the available data are summarised in Table 24 below.

Table 24 Depth of the Top Ordovician, Top Alum Shale, Top Middle Cambrian, Bottom Cambrian, Thickness Ordovician, Thickness Alums Shale and Thickness Faludden SST from well data (m.b.R.T.).

	Top Ordovician	Top Alum Shale	Top Middle Cambrian	Thickness Ordovician	Thickness Alum Shale	Thickness Faludden SST
Dalders Monocline						
B-3	679	736	742	57	6	30
B-3A	-	767	771	-	4	32
B-5	633	713	750	80	37	27
B-7	751.1	823.5	829.6	72.4	6.1	41
B-9	928.2	994.6	998.4	66.4	3.8	48.1
B-10	433	439	522	-	6	22.6
B-11	688.8	-	773.2	84.4	0	49.8
B-12	463.9	-	569.3	105.4	0	-
BO-13	597.4	-	689	91.6	0	33
BO-21	564.5	-	688.7	124.2	0	29.8
P6	1181	-	1254	73	0	83
B6-1	1334	1410	1431	76	21	69.5
E-6 Structure						
E6-1	729	871.5	875	142.5	3.5	53
E-7 Structure						
E7-1	1256	1378.9	1389	122.9	10.1	57

Other Locations						
D1-1	2256		2338	82	0	-
Yoldia-1	703	753	783	50	31	59

The methodology used to compile the individual static models and the assumptions made are described below.

7.1 Dalders Monocline

7.1.1 Principal data set used:

Digitised A0 Top & Base Cambrian Depth Map (1:1,000,000) *Source*: LO_G report

7.1.2 Assumption relating to the Top Cambrian:

The depth of the top Cambrian is based on 17 wells throughout the Dalders Monocline. The wells are located south and east of Gotland in Swedish territorial water (12 wells), close to the southernmost boundary of the Dalders Monocline in Polish territorial waters (4 wells) and in offshore Latvia (1 well). The top Cambrian map is based on the base of the Cambrian map from the LO_G report and the thickness of the Cambrian from Ūsaitytė (2000).

7.1.3 Interpolation of the Top Cambrian Layer:

Digitised isolines from the original map were used for the interpolation using the Determination of Earth Surface Structures (DEST) algorithm (Favalli *et al.*, 2004) on a square grid of 1,000m*1,000m. Figure 12 below shows the surface of the Top Cambrian in the Dalders Monocline.

7.1.4 Determination of the Base Faludden Sandstone Layer:

The thickness of the Faludden SST was determined using the available wells in and around the Dalders monocline in offshore Sweden, offshore and onshore Poland as well as offshore and onshore Latvia (see Table 24). The thickness values in these wells show that the thickest reservoir unit is located offshore Latvia (83m in the P6 well), decreasing toward the northwest with values reaching 25m offshore Gotland. The other values observed in the Monocline suggest the thickness varies between 30m and 70m. An additional constraint to the thickness is the Faludden SST map from Erlström *et. al* (2011) that indicates the limit of the Faludden SST. The base of the Faludden SST has been determined based on the thickness values in the wells, the limits of the Faludden SST (0m values along the northwest boundary) and the top of the Middle Cambrian.

7.1.5 Determination of the Top Alum Shale:

The thickness of the Alum shale was determined using well data from the Baltic Sea region. The Alum shale does not cover the whole Dalders Monocline and only overlies the reservoir in the southernmost half of the monocline. The limit of the Alum Shale within the Dalders Monocline follows a southeast northwest line that starts from south Gotland (Figure 11). The thickness of the Alum shale decreases from 20m in the Polish offshore to only a few meters in the Latvian and Swedish offshore.

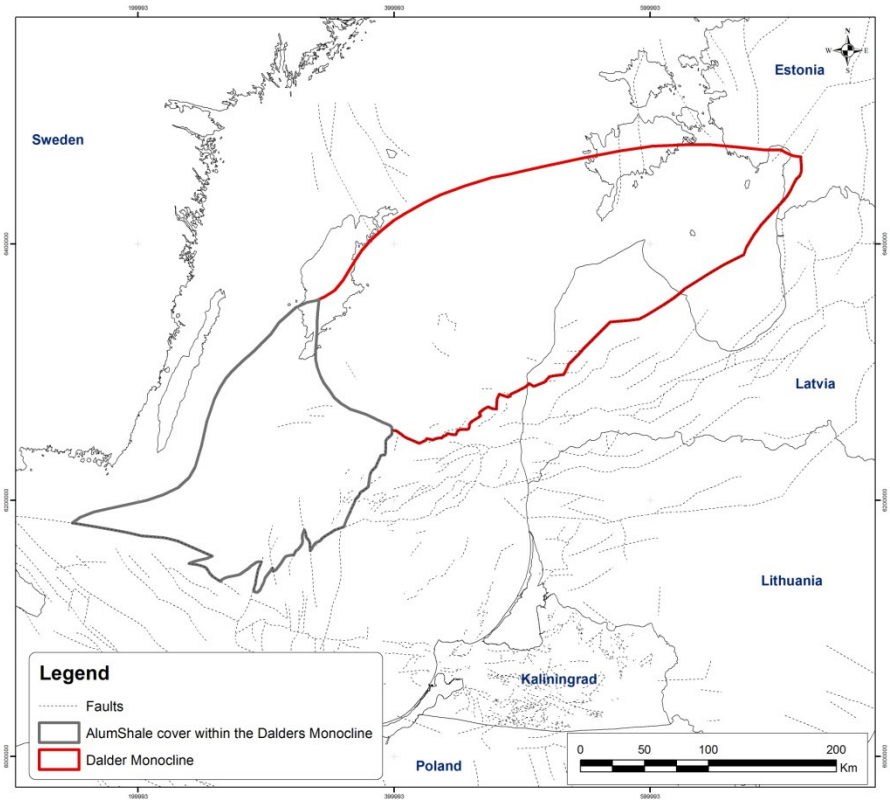

Figure 11 Boundaries of the Dalders Monocline (red polygon) and area covered by the Alum Shale within the Dalders Monocline (grey Polygon – OPAB, 2011).

7.1.6 Determination of the Top Ordovician:

The thickness of the Ordovician follows a general northeast-southwest trend with low values recorded in the Sweden sector and increasing in offshore Poland and onshore Latvia. The thickness remains relatively low along a northwest-southeast trend between the southern part of offshore Sweden and offshore Kaliningrad. Ūsaitytė (2000), maps the thickness of the Ordovician with low values of less than 80m in the central part of the Dalders monocline, reaching 200m in the southern part of onshore Latvia. These values are supported by Ordovician formation thickness values recorded in offshore wells.

7.1.7 Boundary of the Dalders Monocline:

The northern boundary of the Dalders monocline is controlled by the limit of the Faludden Sandstone in Sweden (Erlström et al, 2011) and the Middle Cambrian in Poland (Modliński and Podhalańska, 2010) and Estonia (Raukas and Teedumäe, 1997). The southern boundary is controlled by the major faults to the north of the Liepaja Saldus Ridge.

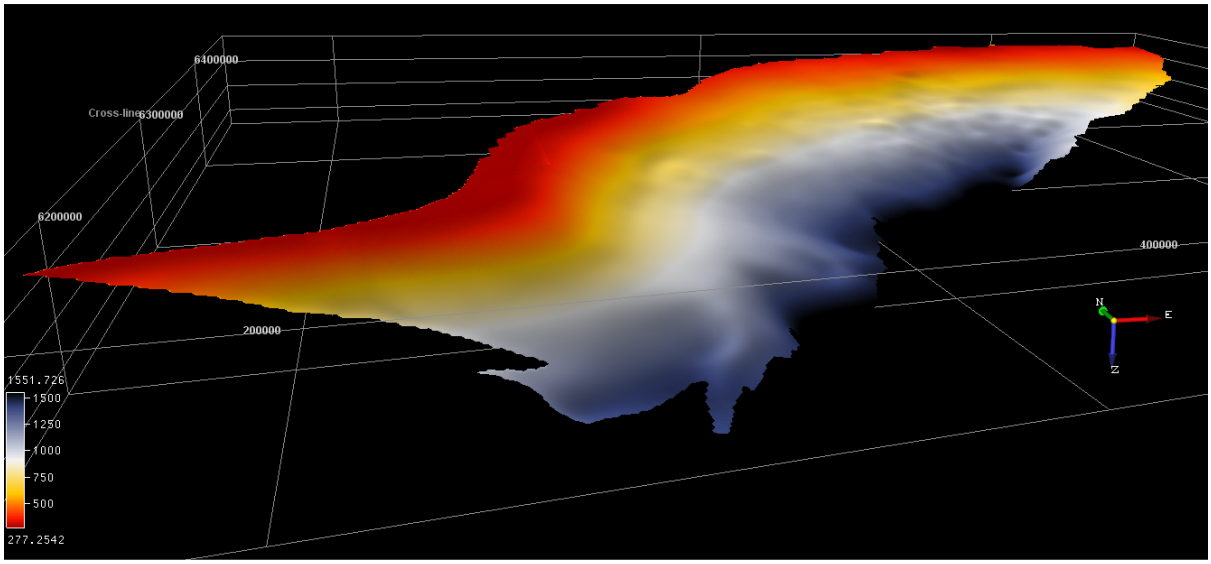

Figure 12 Top Cambrian Layers of the Dalders Monocline.

7.1.8 Porosity and Permeability in the Dalders Monocline:

The porosity of the Middle Cambrian in the Monocline was interpolated using effective porosity values measured in core samples from offshore wells. A general trend as low as 3% offshore Poland, increasing up to 20% in Latvia is observed. A low anomalous value of 12% is noticeable in the well P6 located in the central part of the Dalders Monocline, which could be due to the local depositional environment.

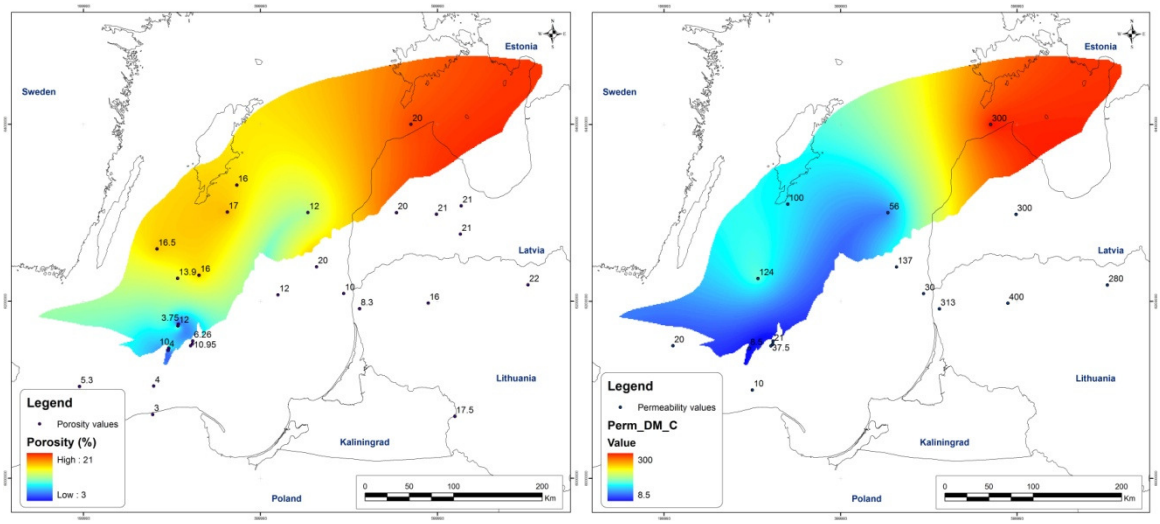

Figure 13 Porosity (to the left) and Permeability (to the right) of the Dalders Monocline.

The permeability of the Middle Cambrian in the Dalders Monocline has been defined using permeability values from measurements in wells and core samples. The trend is similar to that observed for the porosity with low values in the southwest and higher values in the northeast. The lowest value is 10mD in the B16 well (offshore Poland) and a maximum of 400mD in the Syderiai structure (onshore Lithuania).

7.2 Dalders Structure

The static model for the Dalders structure was developed based on the lithofacies distributions of the Middle Cambrian sandstone unit observed in the B3 field in the Polish offshore sector. This was considered to be the best analogue to use for reservoir heterogeneity in the Dalders Structure and was used to map individual lithological sub-layers within the Middle Cambrian reservoir section. Well data from the B3 structure (B3-1, B3-2 and B3-3) were used to create five sub-layers.

7.2.1 Principal data set used:

Digitised Dalders Middle Cambrian Depth Map (Enclosure 21) Source (AMOCO, 1995)

7.2.2 Interpolation of the Top Cambrian Layer:

Digitised isolines from the original map were used for the interpolation using the DEST algorithm on a square grid of 200m*200m. The top Surface in Figure 14 below shows the Top of the Middle Cambrian in the Dalders Structure.

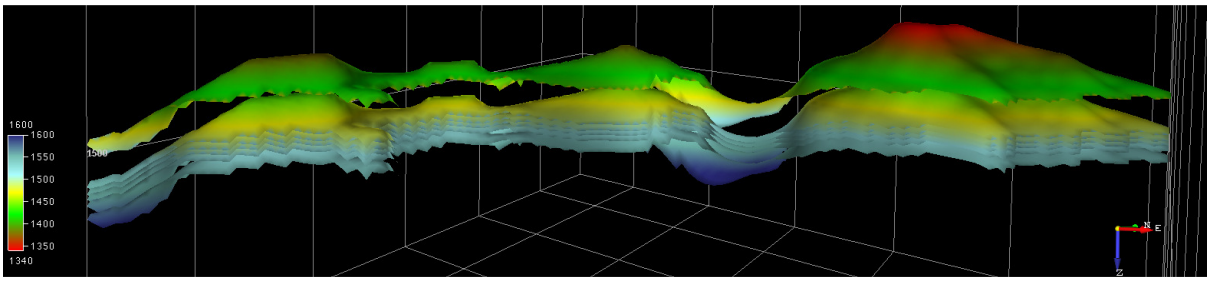

Figure 14 Middle Cambrian Layers of the Dalders structure.

7.2.3 Determination of the Base of the Middle Cambrian Layer:

The total thickness of the Middle Cambrian is 100m, this is based on the values from the B-9 (147m) and E7-1 (97m) wells, which are the closest wells to the Dalders Structure. The sub-layers have been defined using the logs from the wells in the B3 structure (located in the northern part of the offshore Poland).

The total Middle Cambrian thickness in the B3 well is 50m. For this reason the thickness of the individual sub-layer was doubled to obtain consistent results with the anticipated Middle Cambrian values in the Dalders Structure.

The individual sub-layer thicknesses and the related lithologies are presented in Table 25 and show a main sandstone reservoir at the top (i.e. the Faludden SST reservoir) with a thickness of 56m, which is in agreement with the Faludden SST thickness values in the B-9 (48.1) and E7-1 (57) wells. Given the extension of the Dalders Structure, the thickness has been considered as constant over the whole area. Figure 14 show the layers of the Dalders Structure.

Table 25 Sub-layers and their lithology for the Dalders Structure.

Layer	Thickness (m)	Lithology
Middle Cambrian 1	56	Sandstone with shale influence
Middle Cambrian 2	10	Sandstone
Middle Cambrian 3	7	Sandstone with silt/shale
Middle Cambrian 4	9	Sandstone
Middle Cambrian 5	18	Sandstone with high shale content

7.2.4 Boundary of the Dalders Structure:

The boundary of the Dalders Structure was determined using the mapped fault structures to the north and the 1,460m Middle Cambrian contour.

7.2.5 Permeability and Porosity of the Dalders Structure:

The porosity and permeability values representing the heterogeneity of the reservoir are compiled from detailed measurements of the porosity and the permeability from core (i.e. effective porosity and permeability) in the B3 field wells (see Figure 15). Both porosity and permeability have been assigned for the B3-1*, B3-2* and B3-3* synthetic wells created in the Dalders Structure. This information is based on the well recorded from the B3 field.

B3-1* was used to define the southern apex of the Dalders Structure, B3-2* the central part of the structure with B3-3* defining the northern apex.

Table 26 demonstrates the porosity and the permeability values for each well that have been used for the interpolation of the sub-layer properties for the whole structure.

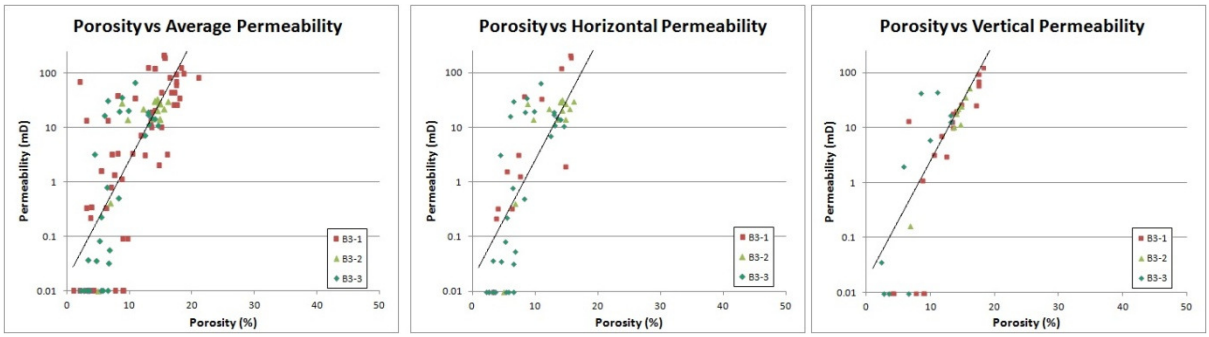

Figure 15 Porosity vs Permeability from the three wells in the B3 structure.

Table 26 Porosity and permeability of the defined sub-layers in the Dalders Structure.

Porosity (%)	B3-1	B3-2	B3-3
Middle Cambrian 1	10	8	5
Middle Cambrian 2	18	12	4
Middle Cambrian 3	10	15	8
Middle Cambrian 4	16	15	14
Middle Cambrian 5	8	5	6

Permeability (mD)	B3-1	B3-2	B3-3
Middle Cambrian 1	30	12	12
Middle Cambrian 2	70	20	0.01
Middle Cambrian 3	30	25	6
Middle Cambrian 4	50	20	13
Middle Cambrian 5	40	1	1

7.3 E6 Structure

7.3.1 Principal data set used:

Digital E6 Top Cambrian Depth structure contours and fault structure shapefiles (LEGMC, Latvia).

7.3.2 Interpolation of the Top Cambrian Layer:

Top Cambrian Depth structure contours were used for the interpolation using the Determination of Earth Surface Structures (DEST) algorithm on a square grid of 50m*50m. Figure 16 below shows the surface of the Top Cambrian in the E6 structure.

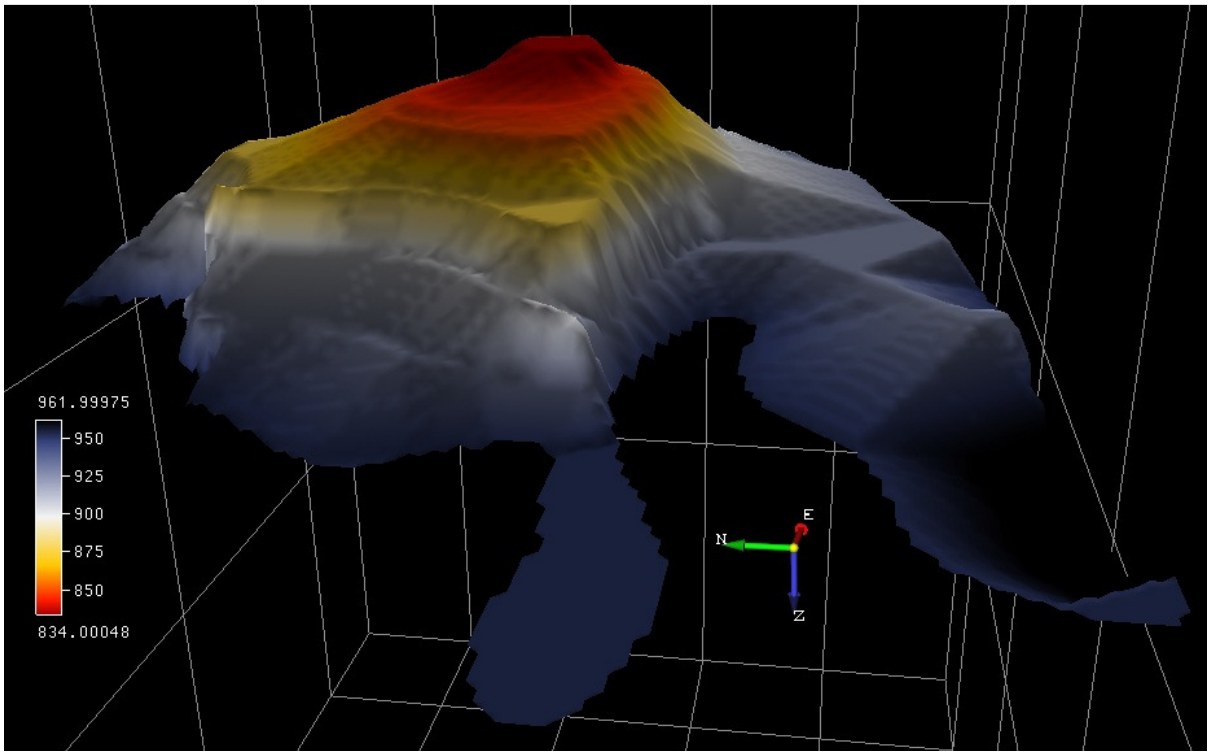

Figure 16 Top Cambrian Layers of the E6 Structure.

7.3.3 Determination of the Base Faludden Sandstone Layer:

The thickness of the Faludden SST based on the thickness recorded in the E6-1 well and a constant value of 57m for the E6 structure.

7.3.4 Boundary of the E6 Structure:

The boundary of the E6 structure was determined using the mapped fault structures and the 1425m contour.

7.4 E7 Structure

7.4.1 Principal data set used:

Digital E7 Top Cambrian Depth structure contours and fault structure shapefiles (LEGMC, Latvia).

7.4.2 Interpolation of the Top Cambrian Layer:

Top Cambrian Depth structure contours were used for the interpolation using the DEST algorithm on a square grid of 50m*50m. Figure 17 below shows the surface of the Top Cambrian in the E7 structure.

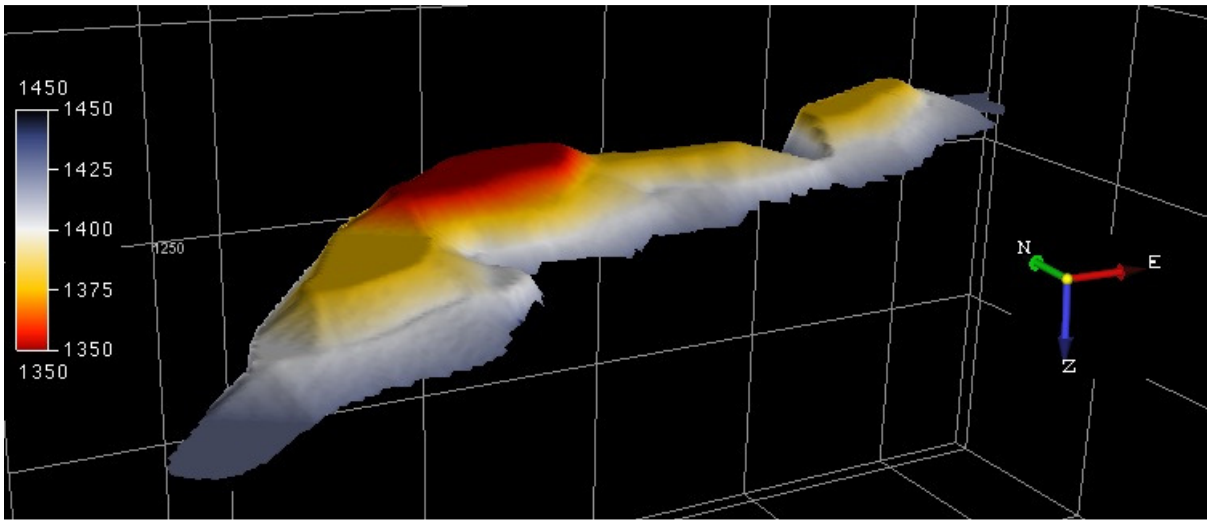

Figure 17 Top Cambrian Layers of the E7 structure.

7.4.3 Determination of the Base Faludden Sandstone Layer:

The thickness of the Faludden SST based on the thickness recorded in the E7-1 well and a constant value of 53m for the all E7 structure.

7.4.4 Boundary of the E6 Structure:

The boundary of the E6 structure was determined using the mapped fault structures and the 950m contour.

7.4.5 Conclusions of the Static Modelling

The Dalders Monocline and the Dalders Structure were selected for dynamic modelling. Both structures are large enough for industrial scale CO_2 storage. The Dalders Structure is also potentially a target for hydrocarbon exploration. The dynamic modelling is discussed in Section 9 below.

8.0 SEALING INTEGRITY

8.1 Methodology

The seal integrity study investigates basic overburden properties above the Middle Cambrian reservoir including stratigraphy, lithology and thickness as well as the nature of any faulting and fracturing observed in the two candidate structures for CO_2 storage. Favourable overburden properties may include the presence of shallow aquifers that could, through monitoring, give early warning of upward CO_2 migration (Chadwick, 2008).

There is a significant thickness of overburden composed of low permeability argillaceous lithologies that exceed 800m overlying the two target storage sites. These cap rocks are sufficient to contain CO_2 within the underlying Middle Cambrian aquifer. Where the cap rocks lack faulting and have low structural dips (which means that most of the cap rock succession is in direct contact with the seabed), the overburden will form a satisfactory regional seal. Results from a research cruise undertaken by the University of Gdansk over the B3 field were investigated as a possible analogue for the Dalders Structure (Sokołowski, A., Tęgowski, J. 2012). However, differences between the geological structure and stratigraphy of both sites, highlights the possible limitations of such a correlation.

The seal integrity study also assesses the leakage risk from pathways other than faults such as high permeability sediment stringers in the immediate overburden by examining shallow gas occurrence as indicators of previous or ongoing gas leakage.

In addition to physical trapping and structural traps CO_2 can be trapped by dissolution in the aquifer or trapped as residual gas. A longer migration distance towards a potential leak point would imply a greater degree of CO_2 trapping by dissolution and residual gas trapping. Before CO_2 can make its way out of the aquifer to surface, the residual gas trapping and dissolution alone may secure all of the CO_2 to be stored (Qiang Xu, 2009).

With respect to cap rock integrity, one would not expect major pathways for CO_2 migration along fault plans unless the complete cap rock is penetrated by a single fault. This can be identified from the existing seismic data. Due to high confining stresses at depths greater than 1,000m it can be expected that faults are closed and that shear zones would be filled with sealing debris of the sheared wall rock. Fault analysis using 3D seismic mapping should be used to fully evaluate the sealing potential of faults including clay smear and fault gauge ratio determinations.

8.2 Sealing Capacity Study Area

The study area is defined as previously mapped Palaeozoic sedimentary basins in the Baltic Sea Area, as described in the document *Geology and hydrocarbon prospects of the Paleozoic in the Baltic region*, 1993 by Brangulis, Kanev, Margulis and Pomerantseva (**Error! Reference source not found.** 1).

The report assesses the sealing capacity of the overburden above potential reservoirs for geological storage of carbon dioxide (CO_2) in sedimentary basins in the Baltic Sea area. The thick Middle Cambrian contains sandstone and limestone aquifers that could store CO_2 that are sealed by shale and claystone aquitards (Figure 18).

The area of the Baltic Sea Basin is about 200,000km^2. There is a 100-150m thick Lower to Middle Cambrian sandstone that is a potential reservoir for CO_2 storage (Figure 3). The overlying Ordovician rocks comprise interbedded sand and shale members including the Alum Shale. This is followed by interbedded shale and limestone including shallow shelf carbonate rocks. Further limestone and shale was deposited in the Silurian. In the south west graptolitic shales are found.

The shales grade to the northeast into marls, limestone, clays and shoal carbonates facies with barrier reefs. The upper part of the Caledonian sedimentary sequence is composed of lagoonal, continental deposits. Within this sequence the Cambrian and Devonian sandstones and the Ordovician and Silurian carbonates have the reservoir potential to store CO_2.

The offshore Dalders Structure (Figure 2 2), which straddles Swedish, Lithuanian and Latvian territory has been identified as a potential site for storage (Svenska Petroleum Exploration OPAB, 2010). Associated with the Dalders Structure is the Dalders Monocline that extends NW to Gotland in Sweden. While storage in confined aquifers and closed structures is the preferred CO_2 sequestration mechanism (e.g. in the CCS-directive from the EC), it would significantly increase the potential of aquifers offshore Sweden if it can be shown theoretically and by demonstration and monitoring projects that CO_2 can be trapped in monoclinal structures (Erlstrom, 2008).

8.3 Sealing Integrity Results

8.3.1 Introduction

The CO_2 storage location, the Dalders Monocline and the Dalders structure, contain Middle Cambrian reservoir formations covered by a thick sealing overburden of Upper Cambrian to Lower Ordovician shales, Ordovician marls, claystones and mudstone and most importantly a thick complex of Silurian shales. The effectiveness of the sealing properties of these formations and their relationships to faults structures were examined with respect to the potential of leakage and migration of CO_2.

The cap rock suitability assessment used wireline logs, from both Swedish and Polish wells and previous seal integrity assessments completed as part of hydrocarbon prospectivity studies (Donoho and Hart, 1996).

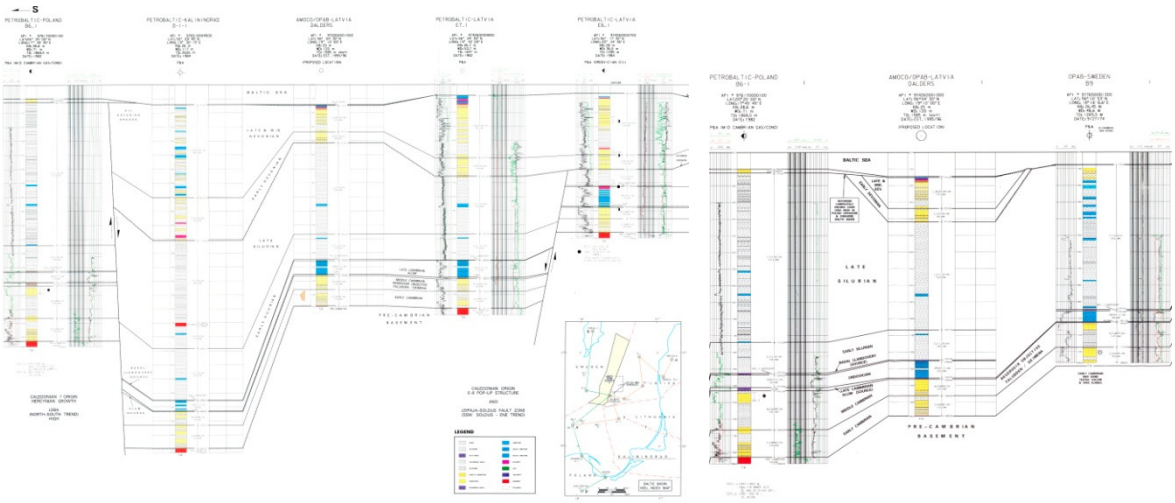

Figure 18 Baltic Basin Well Correlation (Donoho, 1996).

The petrophysical properties of the individual stratigraphic units derived from available wireline log data as well as petrophysical properties measured from cored samples are summarised in Table 27 below.

Table 27 Porosity and permeability of sealing formations from the Central Baltic Sea regions

Latvian Offshore Data	**E7-1**				**P6-1**			
	Depth (m.b.S.L)		Porosity	Permeability	Depth (m.b.S.L)		Porosity	Permeability
	Top	Base	(%)	(mD)	Top	Base	(%)	(mD)
SILURIAN	657	1253			480	1173	10.6	0.09
ORDOVICIAN	1256	1379	6.2	0.08	1180	1248	3.9	0.45
Swedish Offshore Data	**B-3A**				**B-9**			
	Depth (m.b.S.L)		Porosity	Permeability	Depth (m.b.S.L)		Porosity	Permeability
	Top	Base	(%)	(mD)	Top	Base	(%)	(mD)
SILURIAN	77	686			48.6	928		
ORDOVICIAN	686	767	< 1		928	995		
	BO-12				**B-7**			
	Depth (m.b.S.L)		Porosity	Permeability	Depth (m.b.S.L)		Porosity	Permeability
	Top	Base	(%)	(mD)	Top	Base	(%)	(mD)
SILURIAN	118	464			50.1	751		
ORDOVICIAN	464	569	< 3		751	824	< 3	

8.3.2 Cap Rocks

Two stratigraphic units act as seal to the Middle Cambrian reservoir in both the Dalders Structure and the Dalders Monocline. These include Ordovician shaly carbonates and Silurian successions that act as basin-scale aquitards. The overall thickness of the Ordovician and Silurian deposits increases towards the south and south-west reaching a maximum thickness of 2,000m along the Polish coast and reaching a maximum combined thickness of between 500m and 1,000m over the Dalders Monocline and Dalders structure (Figure 19).

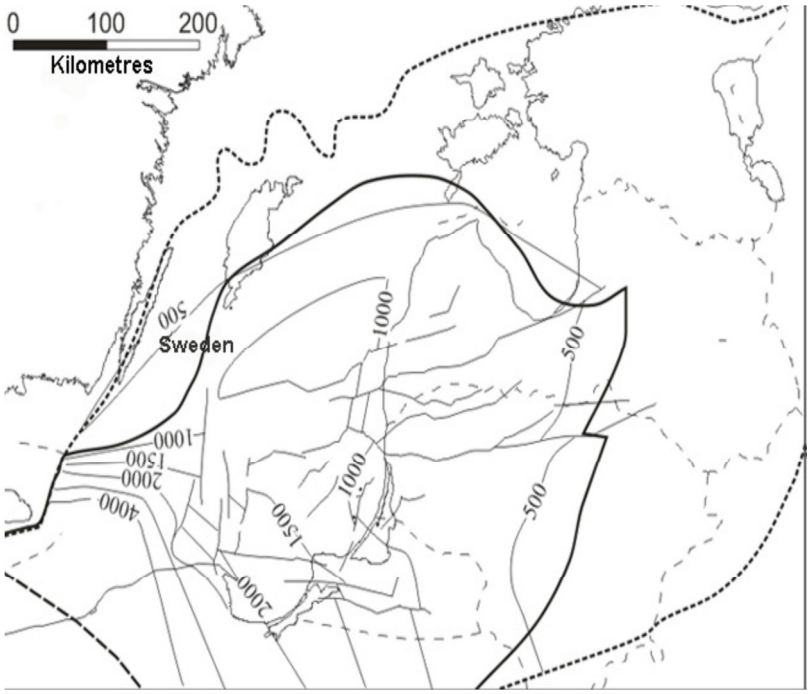

Figure 19: Isopach map of the Ordovician-Silurian succession. Limit of supercritical CO_2 phase is marked by bold line (bold line). Hatchet line shows the limit of distribution of Ordovician–Silurian deposits (Šliaupiene and Sliaupa, 2012).

8.3.3 Upper Cambrian and Ordovician lithologies

Ordovician strata have been recognised in several boreholes, on and offshore in the Baltic depression. Several of these have been fully cored, allowing lithostratigraphical unit boundaries and locations to be precisely distinguished and petrophysical parameters determined. The Ordovician is dominated by claystones and mudstones, with limestone's and marls appearing in the middle Ordovician and the uppermost part composed of marls, shaly marls, mudstones and calcareous shale's.

The main lithologies observed in the southern Baltic Sea region range from limestones and marly limestones in the north western part of the southern Baltic Sea with interbedded calcareous claystones and mudstones in the central and south-western region (Figure 20 & Plate 4).

At the proposed CO_2 storage sites in the southern part of the Dalders Monocline south of Gotland and in the Dalders Structure, the Middle Cambrian reservoir is overlain by between 80m and 115m of Ordovician lithologies with good sealing cap rock properties.

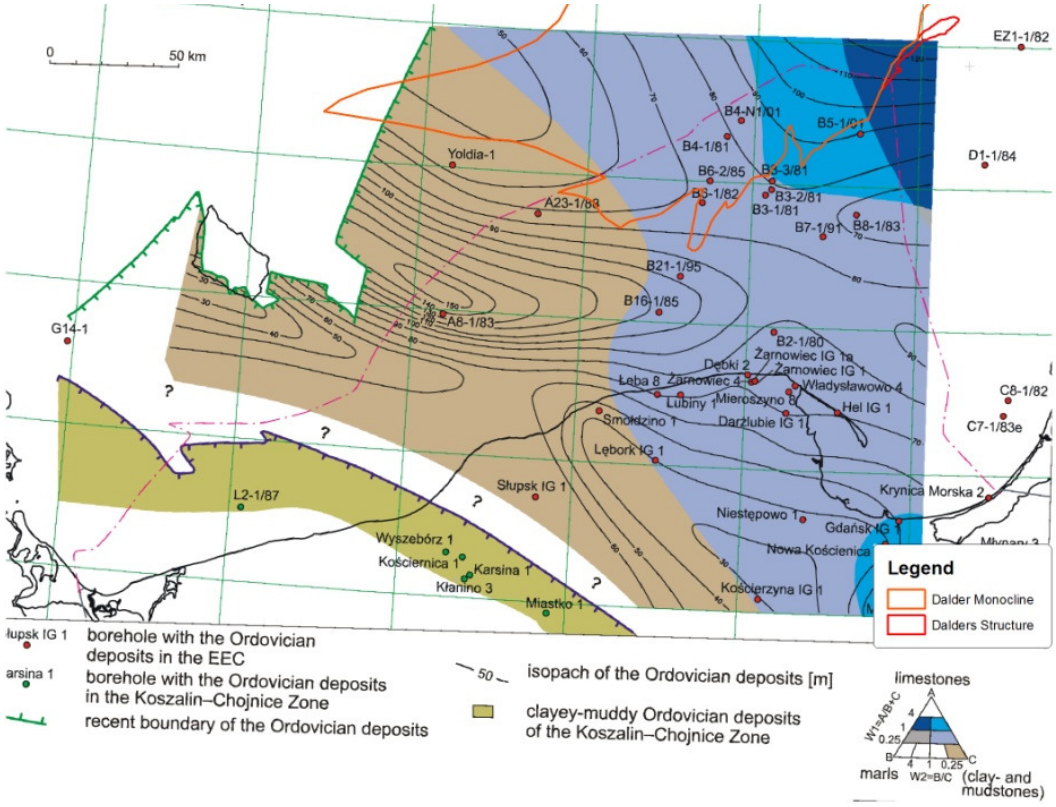

Figure 20 Lithofacies Map of the Ordovician deposits (Modliński and Podhalańska, 2010).

The Upper Cambrian-Tremadocian claystones of the Piaśnica Formation (Modliński and Podhalańska, 2010), corresponding to the Alum Shale in the offshore Swedish sector of the Baltic Sea, represent the primary sealing formation directly overlying the CO_2 storage reservoir. Extensive work on the sealing potential of the Alum Shale and the overlying Ordovician deposits has been undertaken as part of a hydrocarbon prospectivity assessment (Donoho and Hart, 1996). Field data from the producing B3 field offshore Poland represent a good analogue of the potential sealing conditions expected in the Dalders structure.

Isopach depth structure maps for the Alum Shale derived from slow velocities identified from seismic line data, suggest the formation has an overall thickness of 6m across the extent of the Dalders structure. The slow formation velocities are attributed to the ductile nature of the shales that provide an effective seal over the top of the CO_2 storage structure (Donoho and Hart, 1996). Similar properties are observed in the analogous shales that seal the producing B-3 field in Poland (albeit the shale thickness is greater).

In the B3 and B4 fields offshore Poland the thickness of the Alum Shale is approximately 10m and decreases in thickness towards the north west in the Dalders Monocline where it pinches out south of Gotland Island. Isopach depth structure maps for the Alum Shale show a thickness of between 5m and 6m over the CO_2 storage reservoir in the Dalders Structure.

The Upper Cambrian and Lower Ordovician shales and the thick Ordovician marls and argillaceous carbonates form the cap rock for most of the reservoirs in the Baltic Basin. The Upper Cambrian is dominated by thin interbeds and lenses of, often bioclastic, limestone, with the uppermost Cambrian (shelf muds of the Piasnica Formation) corresponding to Alum Shale's of Scandinavia. Similar lithologies are described from the offshore Latvian E7-1 and E6-1 wells, where these constitute up to 61m of the Upper Ordovician succession. Porosity and permeability values of a maximum of 7.1 % and 0.12 mD respectively were recorded in the Ordovician of both wells, which indicates impermeable sealing rock properties.

Similar lithologies are observed in the Polish offshore sector with the Lower Ordovician characterised by the Sluchowo Formation comprising black calcareous shales, green shales and interbedded basal conglomerate beds. The lowermost sequence is overlain by the marly limestones of the Kopalino formation and the Sasino and Pratuby formation comprising shales and interbedded shales and sandstones that characterise the uppermost part of the Ordovician succession and mark the regressive character of the depositional environment (Modliński and Podhalańska, 2010). The total thickness of the Ordovician sequence in the Polish sector of the Baltic Sea varies between 30m (recorded in the Kościerzyna IG1 borehole and up to 150m in the A8-1/83 borehole (Figure 20). This is a significant thickness of impermeable sealing rocks above the target CO_2 storage reservoir.

Upper Cambrian claystone samples from wells Bartoszyce IG1, Barciany 1 Lesieniec and Pieszkowo 1 provide petrophysical properties highlighting the sealing properties of the Ordovician sequence. Permeability values of 0.01-0.001 mD were obtained (within the limit of accuracy of Oil and Gas Institute equipment - for the model one can take a realistic value of 0.005 mD, so it seems even the lowermost and poorest sealing formation is tight enough). The effective porosity of these samples is of 1-3 %. This corresponds to the good seals within the Mesozoic complexes. Additionally, just above the Upper Cambrian and Ordovician there is a thicker (at least 300-400 m) cap rock complex of Silurian that excludes the vertical migration of the injected CO_2 (Wojcicki and Paczesna, 2012).

8.3.4 Silurian Shales

The Silurian is characterised by the bending of the western margin of the Baltica plate, the docking of east Avolonia and the progressive advance of the North-German Polish orogen resulting in an extensive period of subsidence and resulting in the deposition of extensive graptolitic shales dominating the sedimentary succession in the western and central parts of the Baltic basin grading to marlstones in the transitional zone and to the carbonate platform in the shallow eastern margin of the Baltic basin (Šliaupiene and Sliaupa, 2012).

The Silurian has been drilled on and offshore, by a large number of boreholes in the Baltic Depression. A 2,245.2m Silurian succession was observed and almost completely cored, in Lębork IG 1 well, allowing precise location of all stage boundaries and their ranges to be determined. The dominant lithologies are thick claystones, mudstones with thin interbeds of fine-grained quartz sandstone (Modliński and Podhalańska, 2010).

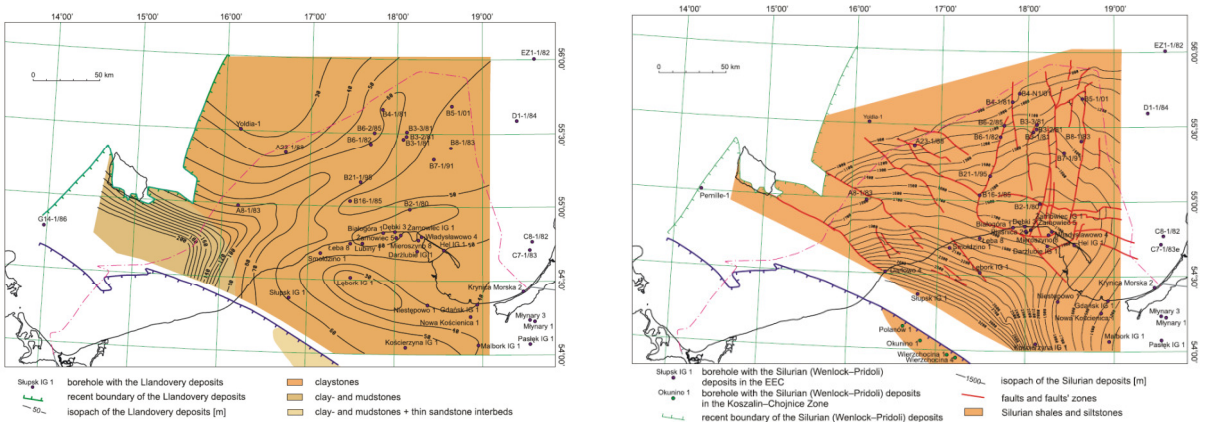

Figure 21 a) Lithofacies Map of Llandovery Deposits ; b) Lithofacies Map of Wenlock-Pridoli Deposits (Modliński and Podhalańska, 2010)

The lowermost sequence of the Silurian deposits is characterised by the Llandovery aged, bituminous shales of the Paslek Formation (Figure 21a) that reach a maximum thickness of up to 100m in the Polish offshore sector. The Pelplin Formation, dominated by grey, black shales with occasional calcareous and marly limestone interbeds occurs at the base of the Wenlock sequence and reaches a thickness of 400m in the Polish offshore sector. The Pridoli Formation, Kociewie Formation and the Puck Shales formations comprising mainly shales and calcareous siltstones constitute the Upper Silurian Wenlock sequence having a thickness of up to 1,000m in the northern Polish offshore sector (B8-1/38) and increasing in thickness towards the south (Figure 21b).

In the northern part of the Baltic Sea region and the northern section of the Dalders Monocline the thickness of the Llandovery strata varies from a few dozen meters up to 160m in southern Estonian offshore and exceeding 300m adjacent to the Caledonian Deformation Front along the boundaries of the Dalders Monocline (Śliaupiene and Podhalańska, 2012).

8.3.5 Discussion

The Ordovician–Silurian shaly package is a reliable cap rock owing to its large thickness and predominance of impermeable lithologies. There is no evident risk from capillary leakage, because the producing hydrocarbon fields in the Cambrian sandstone reservoir overlain by Ordovician carbonates, claystones and mudstones demonstrate that Ordovician cap rock has prevented migration of hydrocarbons from the reservoir.

The possible migration of CO_2 through permeable zones as a result of the interactions between the cap rock and CO_2 is considered negligible due to the extensive thickness of the Ordovician–Silurian aquitard sequence. The risk of migration of CO_2 through carbonate in the sequence is considered as low because of the low porosities (up to 3–4%) and low permeability (<1 mD) values recorded in the Ordovician limestones (Table 27). The extensive thickness of the Silurian succession above the Ordovician would further inhibit any potential CO_2 migration and leakage. The main risk for leakage of CO_2 is via fault structures breaching the cap rock sequence.

The Faludden sandstone reservoir is overlain by a variable thickness of Alum Shale observed from well data as approximately 25m in the south western boundary and thinning towards the northern part of the Monocline north of the B11 well. The Alum Shale is a ductile shale with very effective sealing properties. The absence of the Alum Shale in the northern part of the Monocline connects the Middle Cambrian reservoir with the upper Cambrian sandstones leaving the Ordovician claystones and the overlying Silurian shales as the ultimate top seal.

8.4 Fault Structure Leakage Potential and CO_2 Migration

Both the Dalders Structure and the Dalders Monocline have two stratigraphic units acting as seal to the Middle Cambrian reservoir. The lowermost of these units is a thin sequence of Upper Cambrian to Lower Tremadocian Alum Shales that rests directly above the reservoir in both the Dalders structure and the Monocline. The Alum shale sequence is overlain by a series of Ordovician mudstones, siltstones and clays.

The extent of both stratigraphic units and their relationship with mapped large scale and smaller scale structures varies between the Monocline and the Dalders Structure.

Several tectonic events are identified as affecting the sedimentary pile of the Baltic Sea region with the earliest events occurring during the deposition of Vendian and Cambrian sediments in an extensional regime (Sliaupa & Hoth, 2010). There is little evidence of large scale regional faulting occurring during the Cambrian, Ordovician and early Silurian. Minor faulting occurred as a result of the growth of the Ordovician reefs (Kanev *et al.*, 2000). Basin scale tectonic activity developed in the late Silurian and early Devonian times in a north west south east compressional setting and resulted in the development of large scale, E-W and NE-SW striking reverse fault structures. These are concentrated and best observed along the Lepaya - Saldus High and characterise the main bounding structures of the Dalders Monocline and Dalders Structure. The main characteristics observed are steeply dipping fault planes (70^o-80^o) in a common WNW direction (Šliaupiene and Sliaupa, 2012).

To the south of the Lepaya - Saldus High and in the Leba High, fault structures are coincident with the principal Caledonian fault trends and result in large scale N-S trending fault structures associated with the Polish offshore sector gas fields. In the northern part of the Baltic region smaller scale fault structures with a predominant NW-SE strike are also observed (Plate 4).

Reactivation of most of the regional fault structures described in the Baltic Sea region occurred during the late Carboniferous and Permian stages with the most intense deformation in the SW part of the Baltic Sea adjacent to the Teisseyre–Tornquist Zone (TTZ). This reactivation phase resulted in the development of large scale E-W trending fault structures observed in Gdansk Bay and offshore Kaliningrad.

The Caledonian aged fault structures (NE-SW and E-W trending) show simple geometries developed in a compression basin setting in the case of the NE-SW structures and more complex, transpressional flower structures in the case of the E-W faults. Therefore the compressional NE-SW structures are tight and do not represent a risk from the point of view of CO_2 leakage whilst the transpressional E-W structures bear a higher risk (Šliaupiene and Šliaupa, 2012).

Two large scale, deep seated, NE-SW trending regional fault structures characterise the northern boundary of the Dalders Structure and the eastern boundary of the northern section of the Dalders Monocline. Displacement along these structures is estimated to have terminated around late Devonian times coincident with end of the Caledonian Orogeny with little or no evidence of later reactivation that could result in the breaching of the Dalders structure trap (Donoho and Hart, 1996). The absence of fault reactivation is further supported by the observed accumulations of hydrocarbons along fault bound anticline traps such as the B6 field offshore Poland, suggesting the potential leakage of CO_2 up fault structures is likely to be low.

The southern part of the monocline however is characterised by N-S trending structures that extend from offshore Poland to the offshore Swedish section of the Baltic Basin (Plate 4).

The University of Gdansk conducted a research cruise in 2012 to assess both the location of natural gas emissions from shallow and deep geological layers and to investigate the structure of benthic communities and basic geochemical parameters of the sediment in the

B3 area. Several gas diffusion chimneys and bottom sea craters were identified (Figure 22a, Figure 22b and Figure 22c) extending as shallow as 30m below the seabed. These features may indicate possible leakage of gas from the Middle Cambrian reservoir of the B3 field. The orientation of the features suggests a probable correlation with east west trending structures (Sokołowski and Tęgowski, 2012). The features may also be due to the presence of shallow biogenic gas unrelated to gas leakage from the deeper Middle Cambrian reservoir.

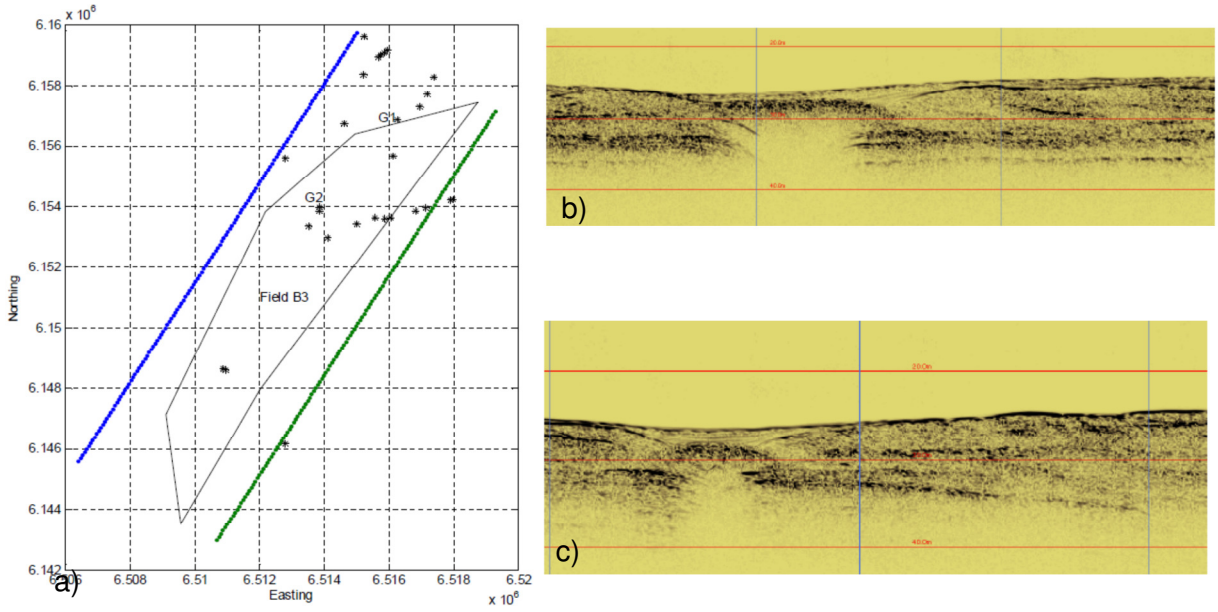

Figure 22 a) Southern Baltic oil field B3 (border depicted by black solid line). Star points show positions of gas diffusion chimneys and bottom sea craters.

b) The sea crater and top part of gas diffusion chimney. The position of this structure is visible in Fig.22a as G1.

c) The sea crater and top part of gas diffusion chimney. The position of this structure is visible in Fig.22a as G2. (Sokołowski and Tęgowski, 2012)

A closer analysis of the fault structures mapped in the B3 field and the location of the recorded diffusion chimneys by the Gdansk University research cruise, suggests that these are not on the main fault structure along the western boundary of the B3 field, but that these are associated with secondary fault structure which in some cases display a more E-W component. These structures potentially represent a greater risk for leakage and migration to the surface. Further evidence of potential leakage from E-W trending structures is suggested where these are described as flower structures or complex intersecting fault structures in other parts of the Baltic Basin. These have led to the migration of hydrocarbons from the Cambrian reservoir to the upper Ordovician limestone lithologies as for example in the E6-1 field (Šliaupiene and Šliaupa, 2012). This suggests that careful consideration needs to be given to any small scale faults associated with individual potential structures considered for CO_2 storage or test injection.

Lateral leakage of CO_2 potentially represents a greater risk across fault structures especially where the Middle Cambrian reservoir juxtaposes Ordovician limestones along the northern flanks of the Dalders structure or the Upper Cambrian sandstone lithologies in the northern part of the Dalders Monocline. However, where this juxtaposition has been observed in association with the predominating NE-SW structures across the Baltic Basin, the offsets recoded on the fault planes is greater than thickness of the Cambrian reservoir, leaving the reservoir juxtaposed against thick sequences of Ordovician claystones or Silurian shales (Šliaupiene and Šliaupa, 2012).

Clay smear and capillary pressure analyses from the B-9 (offshore Sweden) and E7-1 wells adjacent to the Dalders structure suggest that the risk of trans-fault leakage is low (Donoho and Hart, 1996). However these data are sparse and may not be representative across the complete Dalders Monocline region particularly in the southern section.

The nearly hydrostatic pressure regime identified in the reservoir and in the producing B3 field, suggests that whilst the reservoir is not overpressured, CO_2 injection rates and pressures will be critical at maintaining the seal integrity around fault structures and to prevent CO_2 leakage and migration.

8.5 Well Completion and Integrity

A number of hydrocarbon exploration wells were drilled in the Dalders Monocline during the 1970s and 1980s. Boreholes in the Swedish offshore sector have been plugged and abandoned whilst some well in the southern part of the Monocline in the Polish offshore sector are still in production. Table 28 below summarises available well completion information.

In the case of the plugged and abandoned boreholes the issue of corrosion has to be considered with respect to the potential for CO_2 leakage from the storage reservoir. Therefore, careful monitoring of these wells would be necessary to ensure secure CO_2 storage. In some cases it may be necessary to recomplete the well where it is clear that corrosion or a poor cement job has resulted in a potential leak point from the CO_2 storage reservoir.

Table 28: Completion Details of Exploration Wells in the Dalders Monocline (Swedish offshore)

	Well No.	B-3	B-3A	B-7	B-9	B-10	B-11	BO-12	BO-20
Rotary Table Elevation (m)		21.5	20.7	28.2	26.42	25.91	24.99	24.7	25
	Date	1974	1973	1974	1974	1976	1976	1976	1976
Casing String (K55 Buttress)	30"	96	70	96.8	93	92.4	113.1	141.4	127
	13 3/8"	290	292	330.5	501	90.8	111.4	193.3	125.3
	9 5/8"					345.9	392.9	407.5	387.5
	TD	1002	966.7	1037.5	1266	535.8	1036.9	818.2	689
Cement Plugs	Top (m)	0	0	0	451	0	300	356	149
	Bottom (m)	56	54	86	551	133	335	420	302
	Top (m)	209	224	315	451	313	340	458	341
	Bottom (m)	320	304	345	551	393*	457	533	438
	Top (m)	662	681	-	-	420	579	567	600
	Bottom (m)	750	762	-	-	480	920	630	690
	Top (m)	-	-	-	-	-	-	700	-
	Bottom (m)	-	-	-	-	-	-	749	-

8.6 Conclusions of Seal Integrity Study

A geologically and geometrically suitable site for CO_2 sequestration has been identified in the Dalders Structure and Dalders Monocline. Based on the analysis of the stratigraphic and petrophysical properties of the sealing formation at both sites, the following conclusions have been reached:

- Three possible modes of seal failure have been identified for the Dalders Structure, these include top seal failure, migration up the bounding fault planes and leakage across fault plane, with the former two considered to be the lowest risk.

- The potential for top seal failure across the Baltic Basin has been considered in detail as part of this study. Whilst a relatively thin cover of Alum Shale directly overlies the

reservoir in both the Dalders Structure and the Dalders Monocline, a significant thickness of between 500m and 1,000m of combined Ordovician and Silurian deposits comprising mainly shales and claystones act as the ultimate seals. The potential for top seal failure is therefore considered low.

- Seal failure resulting in leakage across fault planes downthrown Ordovician carbonate lithologies is more likely, however the risk of this is still low when the thickness of the reservoir and large throws along the fault planes are considered.

- The potential for migration of CO_2 along fault planes has been considered in the context of the different structural events recorded in the Baltic Basin, the trends of the faults structures and their relationships with the reservoir and seals identified in the Dalders Structure and Monocline. The main boundaries of both structures are considered to be sealed leaving little or no risk of upward leakage or migration of CO_2 along fault planes.

Evidence from analogous fields in the offshore Polish sector demonstrates that smaller scale cross cutting fault structures with particular E-W and NW-SE orientations) are likely to be open. These are associated with the development of gas chimneys and the upward migration of hydrocarbons from the Cambrian reservoir to overlying Ordovician limestones. However there is no current evidence for smaller scale cross cutting faults on the Dalders Structure.

8.7 Recommendations

The principal recommendations for risk assessment of the Dalders Structure are as follows:

- A detailed structural study of the Dalders prospect should be conducted to clarify the probable migration pathways. A risk associated with anticlinal traps is the possibility of the build up of a large, vertical column of CO_2, exerting buoyancy forces on the caprock. (Best practice for the Storage of CO_2 in Saline Aquifers, 2008.) Although a large thickness of caprock with limited faulting has been identified, its structural integrity would need assessing. Long term hydraulic and gas transport testing on the caprock samples initially from existing wells such as the Lebork IG1 onshore Poland should be undertaken in advance of new core samples being obtained from any potential test sites.
- Further seismic interpretation and where necessary, the acquisition of new data will be required in the vicinity of any proposed test injection site to be selected in the Dalders Monocline to map in detail any faults, structures and seismic atttributes that remain poorly indentified in the Swedish offshore sector. This should confirm the integrity of the sealing formations overlying the reservoir and identify any risk for CO_2 leakage and migration where these structures intersect the Ordovician and Silurian sequences.
- A detailed sensitivity analysis with respect to different injection scenarios, resulting reservoir pressures and their potential impact on the preservation of the seal integrity around fault structures where the cap rock is thinnest needs to be undertaken. The current dynamic reservoir modelling is addressing this to some degree. However the results of these sensitivity analyses will have to integrate with the results of the long term hydraulic and gas transport testing of caprock samples.
- Given the results of the biological and geochemical studies at the B3 site, conducted by the University of Gdansk research cruise, a multibeam seabed survey and sub-bottom profiling would need to be undertaken above any potential CO_2 storage or injection test location.
- Detailed analyses of cored Silurian and Ordovician-upper Cambrian sealing formation from newly drilled exploration wells in the proximity of the Dalders Structure and Monocline need to reviewed and the results considered in the context of any future proposed test injection site selection and characterisation.

9.0 DYNAMIC MODELLING

9.1 Introduction

Based on the results of the static model described in Section 7, the Dalders Monocline and the Dalders Structure were selected for dynamic modelling (Plate 2). Both structures are large enough for industrial scale CO_2 sequestration. The Dalders Monocline is a large regional saline aquifer located in the offshore Swedish sector of the Baltic Sea. The Dalders Structure is a fault bounded anticlinal structure located in the central part of the Baltic Sea region that has been the subject of hydrocarbon exploration since the early 1990 but remains undrilled.

The data compiled for the static modelling for both structures comprised existing exploration well data, including core and petrophysical analysis as well as analogous reservoir production data. The dynamic modelling was applied to the static models for both candidate structures.

The University of Uppsala Earth Sciences Department undertook the dynamic modelling of both structures, with a view to assessing the potential of the Middle Cambrian sandstone reservoir and adjacent formations to store CO_2 and to provide a semi-quantitative analysis of the behaviours of the reservoir and CO_2 plume during the course of injection and post-injection periods.

The specific objectives of the modelling included:

- Define the reservoir pressure behaviour with respect to seal integrity for different injection scenarios based on the existing petrophysical reservoir properties and hydrogeological aquifer parameters;
- Calculate the CO_2 plume migration tip speed and distance and the potential for dissolution trapping;
- Identify suitable multi-well injection scenarios in the Dalders Monocline to meet the estimated industrial CO_2 storage requirements identified around the Baltic Sea.

9.2 Modelling Methodology

Three separate modelling approaches were used with a view to characterising different injection scenarios for the Dalders Monocline and Dalders Structure. The objectives and inputs of the three different methodologies are briefly described below. A methodology description for the individual techniques, as well as the results obtained for each are discussed in detail in **Appendix A**.

9.2.1 Analytical Modelling:

A sensitivity analysis was undertaken based on the methodology by Mathias, 2010 a & b to determine the optimum CO_2 injection rates that would not result in cap rock breach or fault re-activation. The analysis was based on the static model reservoir characteristics for the Dalders Monocline. In the absence of detailed formation leak off test data, a threshold 50% excess above the formation pressure was assumed. This is equivalent to 150% overpressure during the injection phase.

Table 29 below presents the modelled reservoir properties used and the resulting base case injection scenario for the Dalders Monocline. The sensitivity analysis demonstrates that the injection rates required to maintain the reservoir pressure below 180 bar are strongly controlled by the permeability, reservoir thickness and the number of injection wells. These values were used as reference values for the modelling techniques discussed below.

Table 29 Sensitive Analysis parameters and base case reservoir properties.

Property	Minimum Value	Intermediate	Maximum	Base Case
Reservoir Pressure	120 bar			180
Porosity	0.12			
Permeability	20 mD	40 mD	80 mD	40mD
No. of Wells	3	5	7	5
Reservoir Thickness	40 m	50 m	60 m	50 m
Injection Time	50 years			
Injection Rate				0.5 Mt/yr

9.2.2 TOUGH2 Modelling:

The TOUGH2/ECO2N and TOUGH2MP simulators were used to simulate CO_2 migration in the reservoir (Pruess et.al, 1999; Pruess, 2005) in 3D and pseudo 3D. Several modelling scenarios were used based on the available datasets for reservoir porosity and permeability properties interpolated across the Monocline area, assuming a homogenous reservoir.

An initial model of CO_2 migration was conducted for the entire Monocline region (see boundaries A-B-C in – Plate 3). This model focussed on injection from one well (Inj_0) whilst two subsequent models focussed on the injection in the southern part of the Dalders Monocline only (A-B'-C) where the Ordovician Alum Shale cap rock provides a seal directly above the top of the reservoir.

The third and last model, of greatest interest to the industrial viability of CO_2 injection in the Dalders Monocline, focussed on potential impacts of pressure build up and CO_2 migration in a multi well injection scenario (Inj_1, Inj_2, Inj_3).

A similar single well model was also conducted for the Dalders Structure (Figure 23). The available information from drilled boreholes close to the structure allowed a heterogeneous reservoir model to be developed, based on analogous lithofacies and reservoir properties observed in the B3 field in the Polish offshore sector, the E7-1 well data offshore Latvia and the B-9 well data from offshore Sweden (Plate 1).

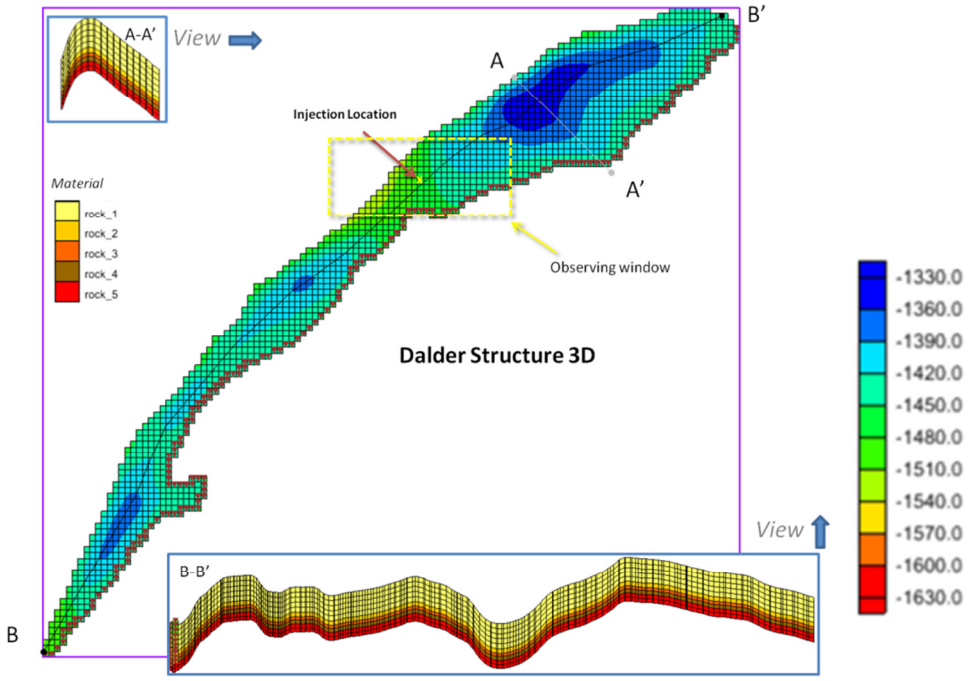

Figure 23 Dalders Structure - Conceptual model extent, location of the injection well. Heterogeneous reservoir characteristics shown in the colours that indicate the depth as expressed in meters in mean sea level.

Several different boundary conditions for the Dalders Monocline and the Dalders structure were considered. Based on the available structural data at the time of modelling, the most likely boundary conditions were chosen. These are listed in Table 30 below.

Table 30 Boundary Conditions for TOUGH 2 Models.

Dalders Monocline	Boundary Condition	Description
A to B	Open	Hydrostatic Pressure Boundary
A to B'	Open	Hydrostatic Pressure Boundary
A, C to B	Closed	Sealed Regional Scale Fault Structure
Dalders Structure		
B to A to B'	Closed	Sealed Regional Scale Fault Structure
B to A' to B'	Open	Hydrostatic Pressure Boundary

As part of the TOUGH 2 modelling several modelling parameters were used for the different scenarios presented above. Some of the reference values with respect to comparable injection rates for the different models are listed below.

- Irreducible water saturation, Sl,r [-] 0.300
- Residual gas saturation, Sg,r [-] 0.050
- Van-Gnuchten parameter, m [-] 0.457
- Reference for Leverett scaling on capillary pressure, Pref [Pa] 1.98×10^{4}
- Reference permeability - *regional Dalders Monocline* , kref [mD] 100
- Pore compressibility [Pa-1] $4.5\text{x}10^{-10}$

- Brine Salinity (% NaCl) 11.54
- Formation temperature (^oC) 50

Several injection rates were considered for the Dalders Monocline and the Dalders Structure models. These are summarised in Table 31 below

Model Domain	Description	No. of Injection Wells	Injection Rates Modelled ($MtCO_2$/year)			Injection Location	Injection Time (yrs)	Post Injection Monitoring (yrs)
Dalders Monocline	Regional Model for the entire Dalders Monocline Area	1	3.0			Inj_0	50	1000
Southern Dalders Monocline Area	Southern Dalders Monocline Area	1	1.0			Inj_0	50	1000
	Southern Dalders Monocline Area	1	0.5			Inj_1	50	1000
	Southern Dalders Monocline Area - Multiple Well, Simultaneous Injection	3	0.5	0.5	0.2	Inj_1,2&3	50	1000
Dalders Structure	Single Well Injection into the lowermost part of the reservoir	1	0.3				20	1000
	Single Well Injection into the lowermost part of the reservoir	1	0.5				20	1000

Table 31 TOUGH2MP Model scenarios and Injection Rates

The TOUGH2/ECO2N was used to simulate the migration of CO_2 in the Cambrian reservoir within the Dalders Monocline. The model was run using the static model parameters and based on the following assumptions:

- Plume width 1km
- Plume depth 1,200m
- Aquifer slope 0.5
- Variable thickness range from the static model 80m to 5m
- Porosity 0.1
- Brooks-Corey function parameter (λ) 0.67
- Brine Saturation (S_{lr}) 0.3
- Residual Gas Saturations (S_{gr}) 0.1, 0.2 & 0.3
- Permeability (mD) 30 & 100

9.2.3 Vertical Equilibrium Model:

The Vertical Equilibrium model was used to simulate CO_2 spreading and related pressure increase in the Dalders Monocline and Dalders Structure. The modelling technique assumes a vertical equilibrium pressure (Bear, 1972) in the reservoir and enables modelling of variable density and viscosity properties based on different reservoir pressure and temperature conditions. The VEM methodology is less computationally intensive and permits the integration of cap rock topography information. In the case of both the Dalders Monocline and Dalders Structure this was defined as the extent of the Ordovician Alum Shale above the Middle Cambrian reservoir.

Focussed on the inclusion of CO_2 density and viscosity parameters, this technique allows simulation of the thickness and movement of the CO_2 plume tip during the injection and post injection phases.

The modelling domain reservoir parameters were derived from the static model data as for the Tough 2 modelling and the boundary conditions are the same as those presented in Section 9.2.1. The injection and monitoring simulation parameters for the VEM model are outlined in Table 32 below.

Table 32: VEM Model scenarios and Injection Rates

Model Domain	Description	No. of Injection Wells	Injection Rates Modelled ($MtCO_2$/year)			Injection Location	Injection Time (yrs)	Post Injection Monitoring (yrs)
Southern Dalders Monocline Area	Southern Dalders Monocline Area	1	0.5			Inj_2	50	500
	Southern Dalders Monocline Area - Multiple Well, Simultaneous Injection	3	1	1	1	Inj_1,2&3	50	500
	Southern Dalders Monocline Area - Multiple Well, Simultaneous Injection	3	0.5	0.5	0.5	Inj_1,2&3	50	500
Dalders Structure	Single Well Injection into the lowermost part of the reservoir	1	0.3				50	500

9.3 Dynamic Modelling Results

Several scenarios of dynamic modelling were developed for both the Dalders Monocline and the Dalders Structure. The requirements for CO_2 sequestration based on calculated emission from the industrial sector in the Baltic Sea region suggests that the injection of 50Mt of CO_2 per annum over 25 years is needed.

Initial analytical modelling demonstrates that in order to preserve cap integrity and avoid fault reactivation, injection rates should not exceed 0.5Mt per well per year.

This section summarises and discusses the modelled scenarios of CO_2 injection. More in depth analysis and the results of the individual scenarios modelled are available in the dynamic modelling report include in **Appendix A**.

Results for both the Dalders Monocline and the Dalders structure discussed below are focussed on:

- Pressure regime and overpressure ratio calculated
- CO_2 saturation within the reservoir
- CO_2 dissolution
- CO_2 plume migration
- Mobile CO_2 Plume Thickness

9.3.1 Dalders Monocline

Section 9.2.2 presented several dynamic modelling scenarios for the Dalders Monocline. These involved different injection rates as well as single and multi-well injections. The highest single well injection rate of 3Mt/yr was simulated for the entire Monocline domain

based on the injection well being located in an area of higher reservoir quality where higher porosity and permeability values in the order of 15% and 96mD respectively were estimated. The results of this model show that overpressure of 102% is reached at the injection point following the injection period (50 years) with the development of a CO_2 plume of insignificant size with respect to the Dalders Monocline size (Figure 24).

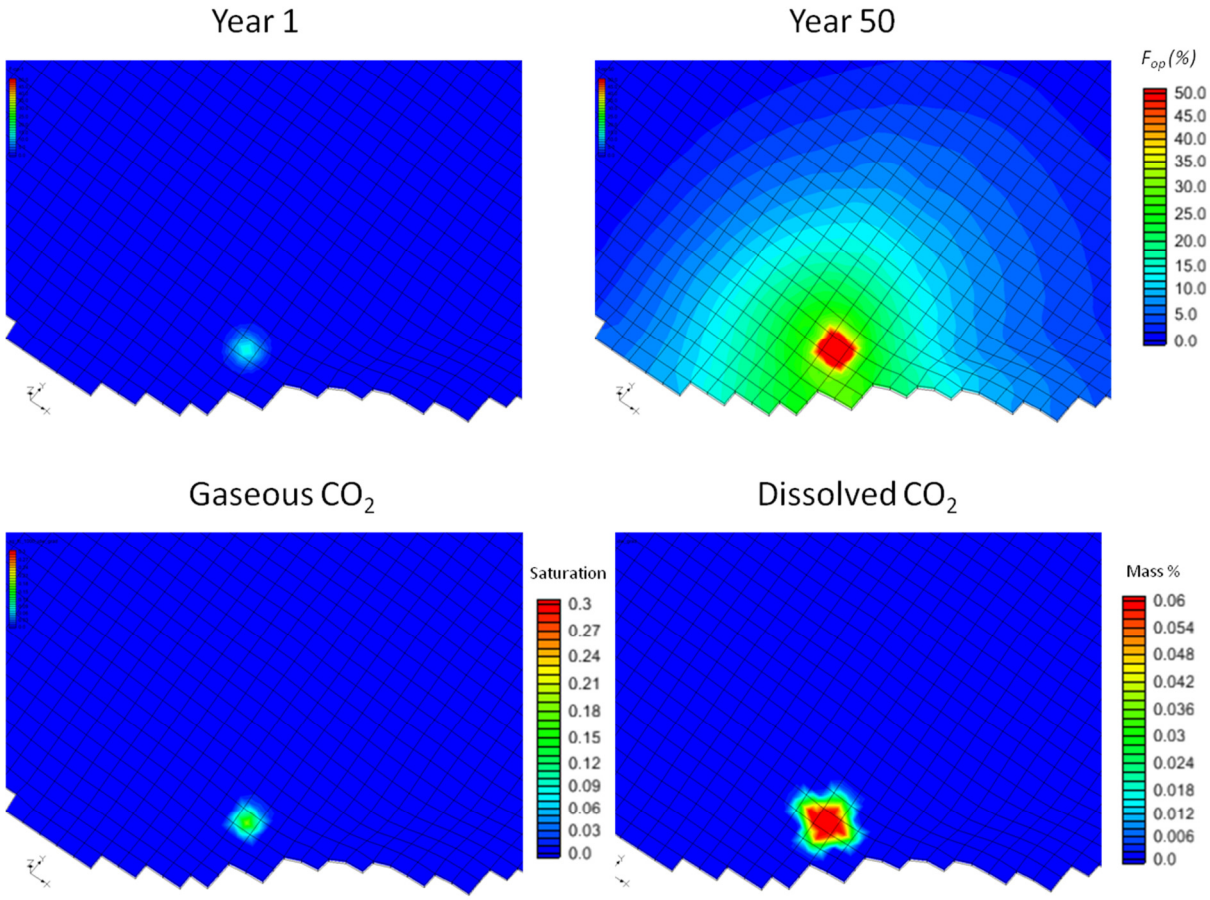

Figure 24 Percentage overpressure (F_{op}) showing pressure build up at years 1 (a) and 50 (b) at the end of injection. CO2 plume (c) and distribution of dissolved CO2 (d) at the end of year 1000.

A limited amount of well data with reservoir petrophysical properties is available for the northern part of the Dalders Monocline where the modelled injection well for this scenario is located. For this reason the results of this model can only be considered indicative.

The southern part of the Dalders Monocline, located in the northern part of the Polish offshore sector and southern Swedish offshore sector, was selected because there is more well data including reservoir and cap rock properties, and fault characteristics based on seismic data from operating hydrocarbon fields. Two dynamic modelling scenarios were run for this area, the results of which are discussed in detail below:

- Single well injection at 1 Mt/ye injection rate
- Multiple well injection from 3 wells

Single Well Injection -1 Mt/yr:

Injection simulation at a rate of 1Mt/yr of CO_2 for a period of 50 years in the southern part of the Monocline from a single well resulted in an overpressure of 150% at the injection point (**Figure 25**a & b).

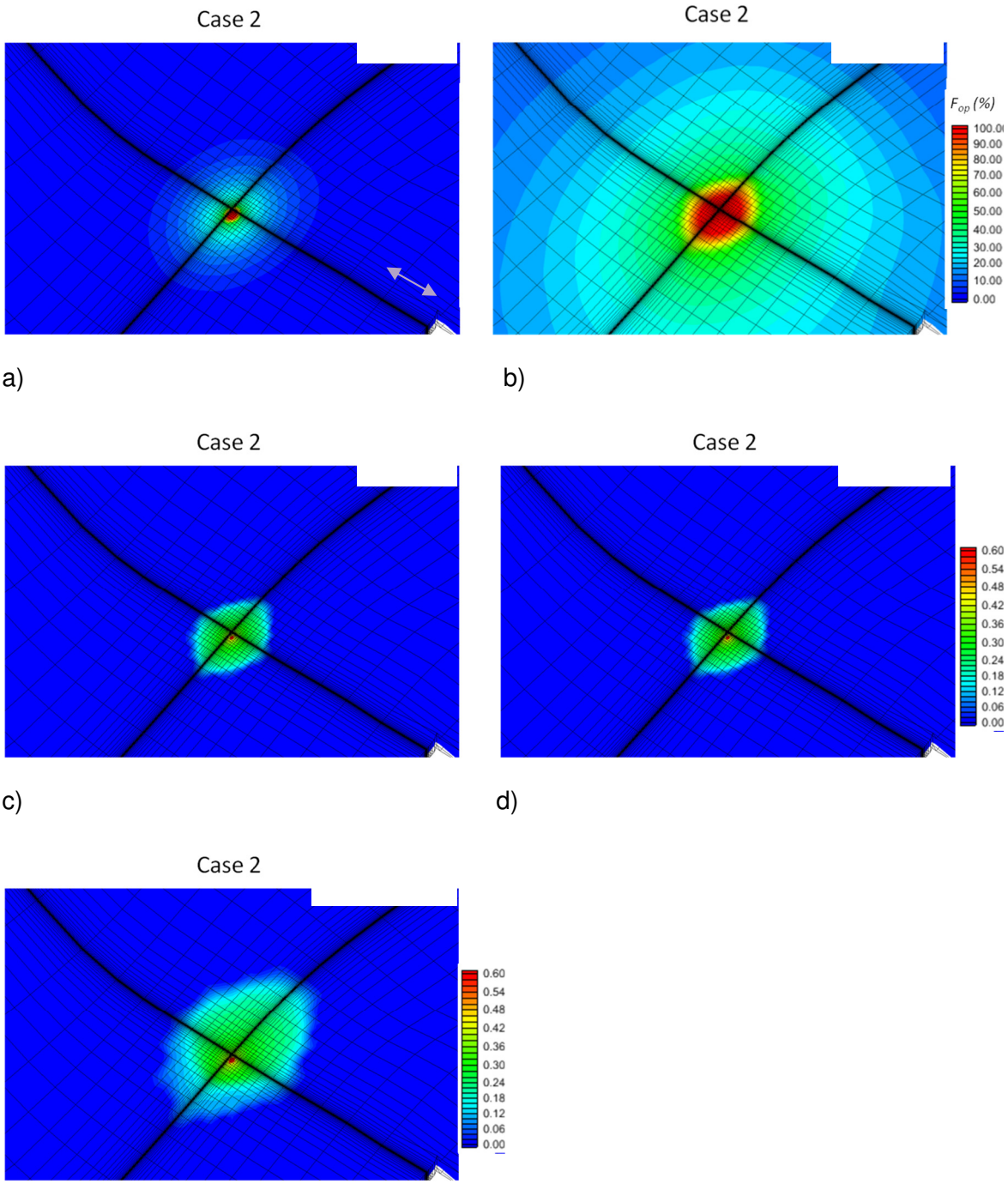

Figure 25: Overpressure after 1 year of CO_2 injection (a) and after 50 years of injection (b). CO_2 saturation after 1 year of CO_2 injection (c) and after 50 years of injection (d) and post injection saturation at year 1,000 (e).

The CO_2 saturation values demonstrate the relatively small size of the CO_2 plume after 50 years of injection (approximately 5km) and the migration of the plume up-dip towards the north east away from the closed south eastern faulted boundary of the Monocline. The

plume size post injection was approximately 18km in length. A similar scenario using a reduced injection of 0.5 Mt/yr for the same well location demonstrated similar results with overpressure build-up of up to 40% at the end of the injection phase with similar up-dip plume migration observed at the end of the modelling phase.

Multi Well Injection

A multi well simulation was carried out for the southern part of the Monocline area to assess the viability of using multiple injection points for CO_2 injection. Both a TOUGH 2 and VE model were run to simulate injection from wells Inj_1, Inj_2 and Inj_3 (refer to Plate 3). The injection rates in the TOUGH 2 model were 0.5Mt/yr for wells 1 and 2 and 0.2Mt/yr for well 3 due to its close proximity to the southern closed, faulted boundary of the Monocline. The VE model simulations used 0.5Mt/yr from three wells in one simulation and 1Mt/yr for the second.

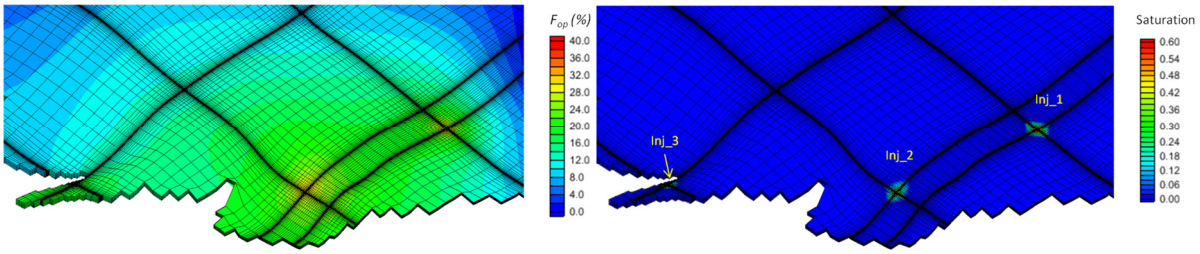

Figure 26 TOUGH2

a) overpressure profile after 50 years of injection.

b) CO_2 saturation after 50 years of injection.

Both methods show that with an injection rate of 0.5Mt/yr modest overpressure develops in the reservoir. Some difference were observed with respect to the absolute values obtained with 40% overall for the TOUGH2 model (Figure 26a) and 70%, 90% and over 200% in the VE model for the Inj_1, Inj_2 and Inj_3 wells respectively (Figure 26a). These results confirm that the highest overpressure is reached in the southern tip of the modelling domain where injection well Inj_3 is located (Plate 3). This injection point is close to the closed, fault bound, southern margin of the Monocline, which explains these high values.

Differences in the results for the two models are as a result of the different modelled injection pressures used in the TOUGH2 simulations. Nonetheless, both models demonstrate that the 0.5 Mt/yr multi well injection scenario results in patchy overpressure responses from each well in the modelling domain during the injection period with a gradual rise in intra-well reservoir pressure reached at the end of the injection period. More significantly the 0.5Mt/yr injection rate does not reach the threshold of 50% overpressure in the reservoir for the TOUGH2 multiwell injection model.

The TOUGH2 and VE models both demonstrate (**Figure 27**a and **Figure 27**b) that the CO_2 plume, generated after 0.5Mt/yr year injection rate for 50 years, is approximately 10km in diameter at each well and there is very limited plume migration and thickness after 500 years.

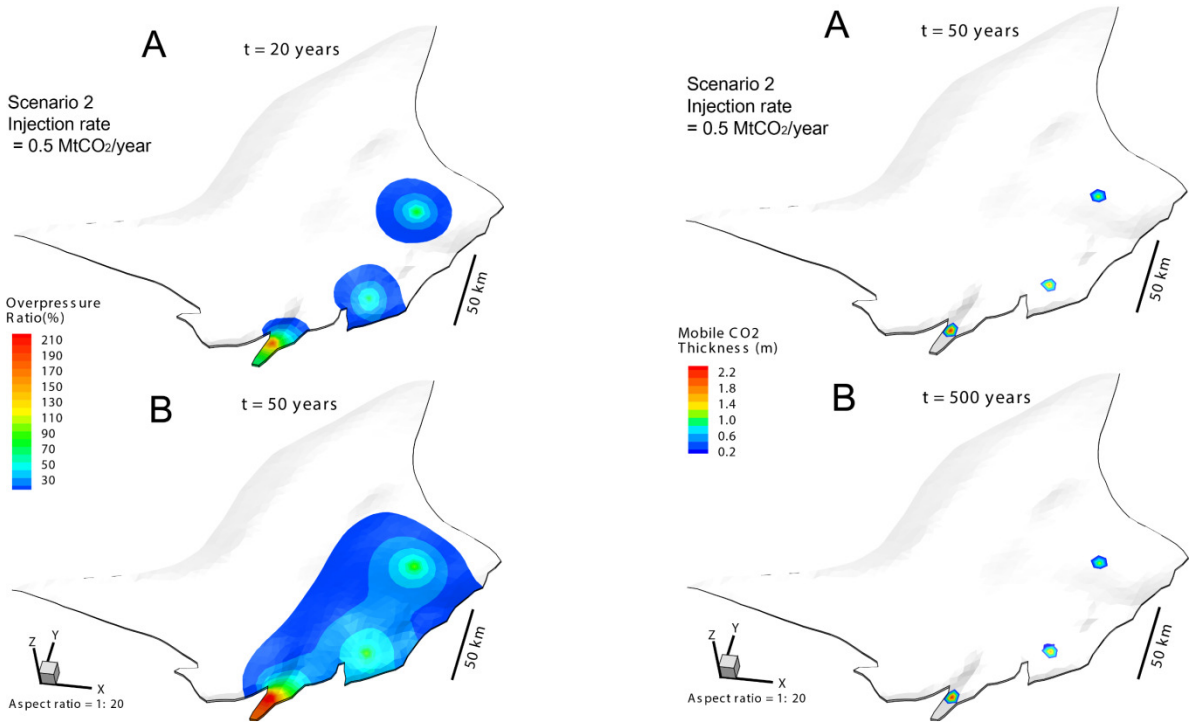

Figure 27: VEM – a) Overpressure ratio with multiple-well injection at a rate of 0.5 Mt CO_2/year per well for 50 years (end of injection at 20 years).

b) Mobile CO_2 plume migration with multiple well injection after 50 years and 500 years.

A second multi well injection simulation using an injection rate of 1MT/yr in each well was carried out using the VE model. The results of this modelling are shown in Figure 28 below.

The overpressure ratio in the reservoir observed as a result of this simulation was recorded as being between 140% and 180%, with the overpressure distribution between the wells increasing more rapidly even after 20 years of injection. This results in a significantly larger overpressure area after 50 years of injection reaching the northern open boundary of the Monocline where values of up to approximately 30% overpressure were recorded.

Figure 28b also shows an increased CO_2 plume thickness of 4m, as well as an increased radius of about 15km observed at each well with a main migration direction remaining towards the north. Despite this increase the size of the plume and its thickness remain insignificant with respect to the regional scale of the Monocline.

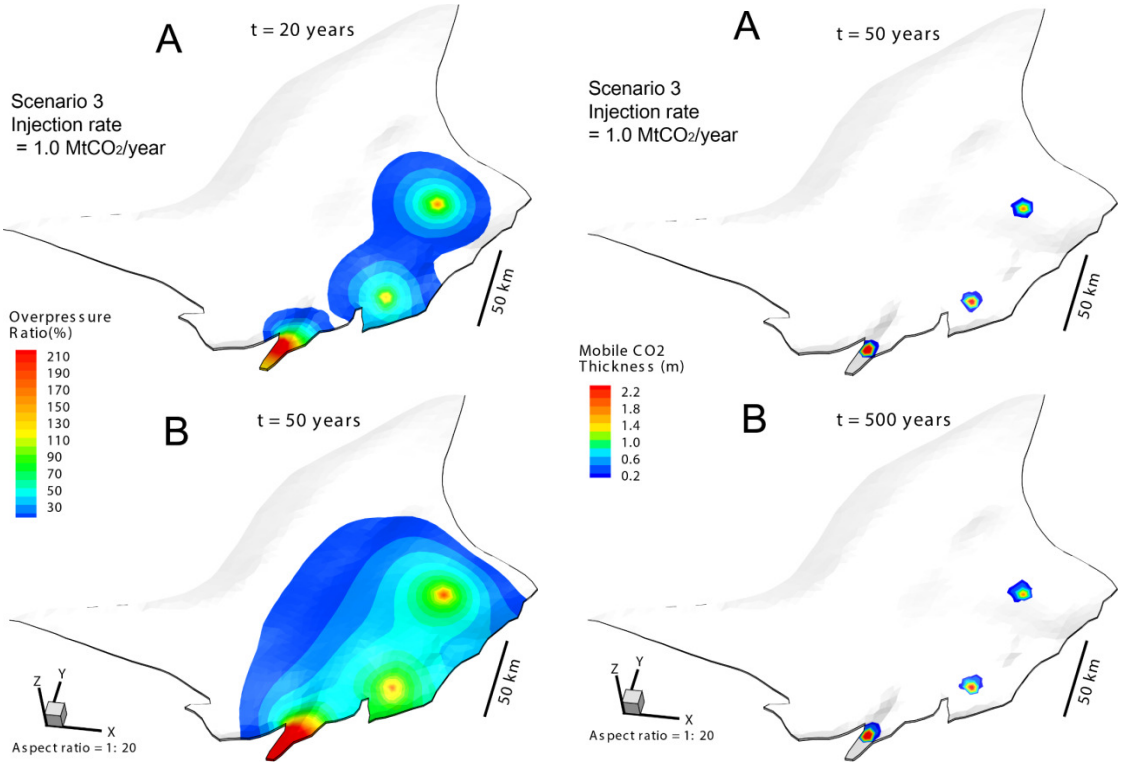

Figure 28: VEM - a) Overpressure ratio with multiple-well injection at a rate of 1 Mt CO_2/year per well for 50 years (end of injection at 20 years). b) Mobile CO_2 plume migration with multiple well injection after 50 years and 500 years.

9.3.2 Dalders Structure

The pressure build-up as a result of TOUGH2 and VEM modelling of injection of CO_2 in the Dalders Structure is displayed in **Figure 29** using the overpressure factor (for definition, see Part B). The TOUGH2 model assumed an injection rate of 0.5Mt per year whilst the VE model assumed an injection rate of 0.3Mt/yr. Both models are in agreement, with low pressure increase of less than 50% overpressure in the case of the TOUHG2 model and 20% in the case of the VE model from the equilibrium formation pressure (**Figure 29**). The pressure response in the reservoir is relatively fast during the injection phase, with the highest pressure increase observed along the closed northern boundary of the structure.

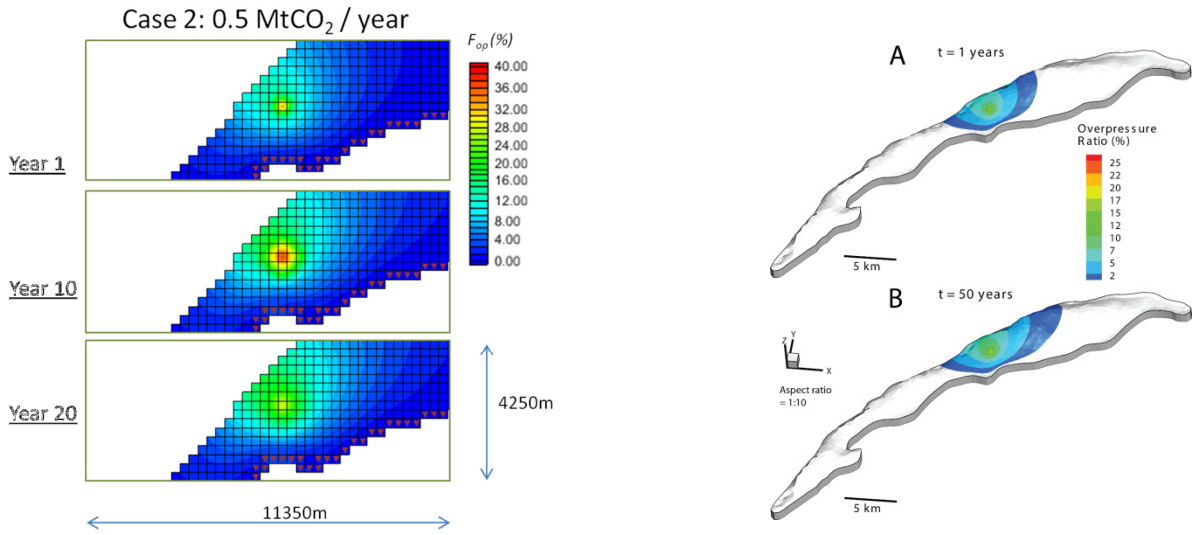

Figure 29 - a). Overpressure ratio by the CO_2 injection. a) overpressure build up for injection rate of 0.5MT/yr at years 1, 10 and 20. Overpressure with injection rate of 0.3 Mt/year for 50 years. (b) 1 year after injection, (c) 50 years after injection.

The CO_2 plume front in the Dalders Structure is modelled as reaching the southern boundary at the end of year 20 of injection. During the post injection phase (between 500 and 1,000 years), the plume continues to move up-dip towards the higher part of the structure towards the north east.

The size of mobile CO_2 plume after 50 years is estimated from the VE model, to be about 3km to 4 km with an overall thickness of between 7 m and 10 m thickness (Figure 30).

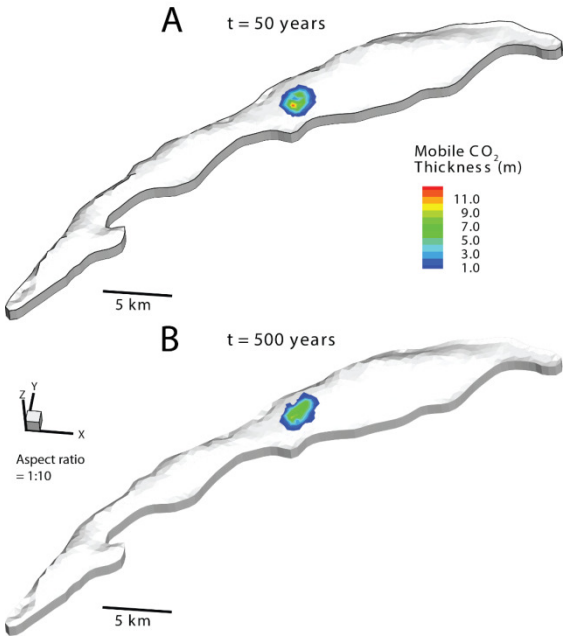

Figure 30. Mobile CO_2 plume migration by the CO_2 injection with the rate of 0.3 Mt CO_2/year for 50 years. (a) 50 years after injection, (b) 500 years after injection.

Both the 0.3Mt/yr and the 0.5Mt/yr injection rate models show that CO_2 reaches the southern boundary of the Dalders Structure by the end of year 50 and escapes the spill point of the structure with 0.00005% and 0.11% of the total CO2 injected escaping through the southern boundary. Post-injection simulation suggests that after 1000 year the total leakage accounts for 0.15% and 1.96% of the CO_2 injected. This is demonstrated in **Figure 31**below that shows the CO_2 saturation in the structure during the injection and post-injection phases.

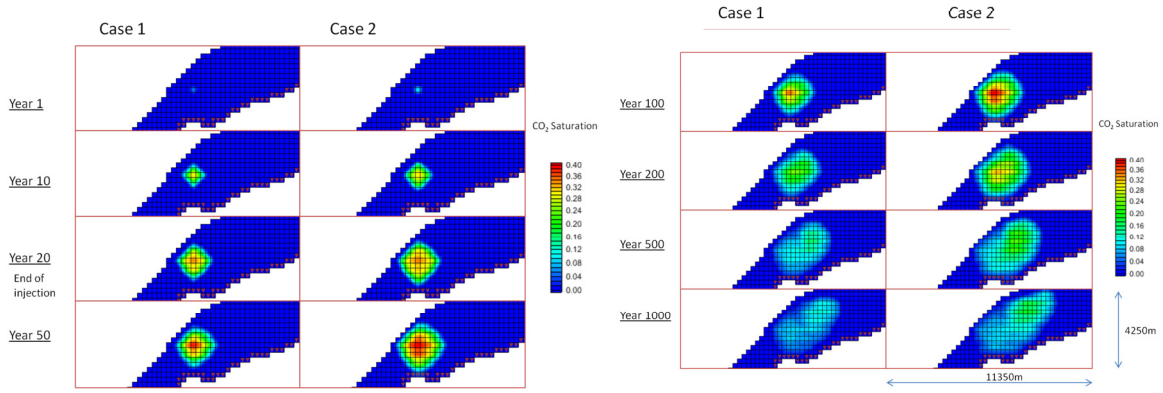

Figure 31. CO_2 Saturation profile in the Dalders Structure at various times. Case 1 injection rate of 0.3Mt/yr. Case 2 injection rate of 0.5Mt/yr. Diagrams show the CO_2 reaching the southern boundary of the structure by year 50.

9.4 Plume Migration

A TOUGH2/EOC2N model was used in the later phases of the dynamic modelling with a view to better understanding CO_2 plume migration patterns and tip migration velocities in the Dalders Monocline.

The results of the modelling show that permeability and gas saturation values significantly influence the migration velocity of the CO_2 plume. A conservative permeability value of 100mD and gas saturation value of 0.2 were assumed for modelling the migration of CO_2 across the entire Dalders Monocline (**Figure 32**).

The modelling results considered a total injected volume of 30Mt of CO2 from one well (mass of 1.7x107 kg) in a reservoir (represented by a 2D slice) with 100mD permeability and a residual gas saturation values of 0.2. If convective dissolution effects are not considered, the potential maximum migration distance of the plume is 50km for an average plume thickness of 15m in a period of 14,000 years. However, given this long time frame, convective dissolution processes can significantly reduce the plume migration distance. The mass that can potentially be dissolved in our modelled area (50 km long 2D slice) is about 9×106 kg, which is more than half of the initial CO2 mass. This means that, in this case, convective dissolution has the potential to significantly drag the plume migration, and that the plume migration distance will be actually much smaller than 50 km.

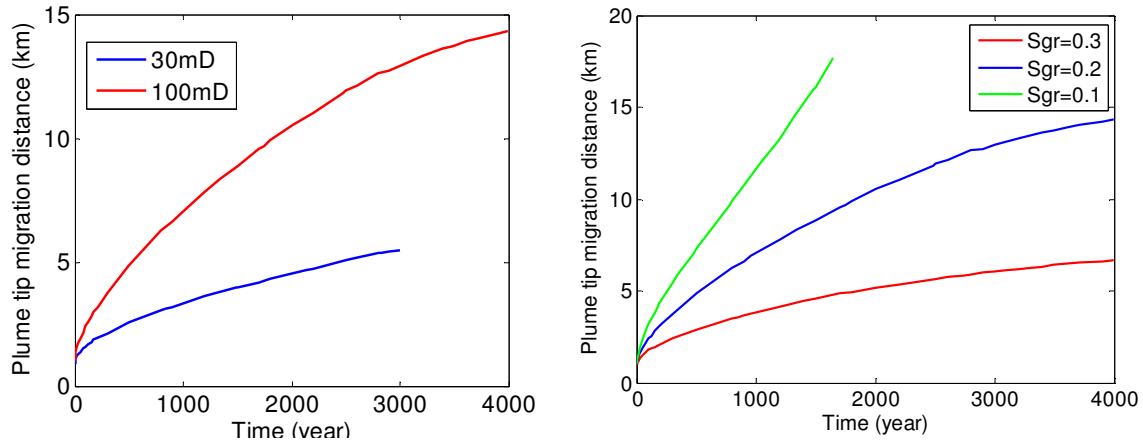

Figure 32: a) CO_2 plume tip migration distance as a function of time for permeabilities 30 and 100 mD. Residual gas saturation is 0.2 for both cases b) CO_2 plume tip distance as a function of time for different residual gas saturation values. Permeability k = 100 mD.

9.5 Discussion

In the above paragraphs and in Appendix A the results from the preliminary dynamic modelling that was carried out for the southern part of the Dalders monocline and the Dalders structure is presented.

The dynamic modelling parameters used to estimate rates of injection of CO_2 in the Dalders Monocline are based on limited well data and reservoir properties, mostly confined to the southern part of the Monocline region within the Swedish offshore sector.

The preliminary simulations indicate for the southern part of the Dalders Monocline a maximum total injection rate of the order of 2.5 Mt/yr if five injection wells are used and assuming a maximum sustainable pressure increase of 50% from the hydrostatic condition. The 50% cutoff value was used as site-specific mechanical data is not available. Increasing the number of wells would allow a larger total injection rate (e.g. 7 wells would allow an injection rate of about 3 Mt/yr) as would reducing the total injection time from 50 years to e.g. 25 years. The maximum injection rate is sensitive to parameters such as formation thickness and permeability, and analysing the effect of their local variability fully does require more detailed modelling than was possible in this preliminary study. In these preliminary simulations impermeable sealing units (cap-rocks) were also assumed and it should be noted that the injection-induced pressure increase could be dissipated by brine displacement through cap-rock if the permeability of the cap-rock is not extremely low and the compressibility of the cap-rock is large. In addition, pore pressure could be further relieved through brine production wells, thus allowing higher injection rates. The role of using horizontal, rather than vertical injection wells should also be investigated. Further modelling studies should address these issues in more detail. Such analyses should optimally be accompanied with additional site-specific data and/or further parameter sensitivity studies where data acquisition is not possible.

The Cambrian reservoir in the southern section of the Monocline has relatively low porosity and permeability values (of the order of 8% to 11 % porosity and 9mD to 70mD permeability respectively) with an improvement of these values towards the north east (Plate 5) where permeability values of up 300mD for the Middle Cambrian sandstones have been documented in exploration wells. The example injection rate of 0.5Mt/yr from 5 wells is conservative and in areas of higher reservoir quality in the northern part it can be expected that higher CO_2 injection rates can be used without the risk of seal failure or fault

reactivation. However, based on the currently limited well data in the northern part of the Monocline, this can only be considered speculative until additional data is obtained.

The dynamic modelling results have assumed a threshold pressure of 50% above the hydrostatic pressure. This assumption was used as lack of formation leak off test data for the monocline area did not allow a more accurate estimate of this threshold. This could have implications for improved injection rates. The leak off test data would also provide thresholds for cap rock integrity and the risk for reactivation of existing fault structures.

The effects on overpressure modelled for higher injection rates suggest that these may be possible for single injection wells in better reservoir quality areas. However the use of CO_2 injection rates higher than 0.5Mt/yr in multiple well injections in the lower quality reservoir is not recommended. Should a grouped well injection methodology using several deviated wells from a central platform be adopted the overpressure and CO_2 plume sizes are likely to be different to the single injection point methodology adopted in this model.

The modelling scenarios considered in this study are, for the most part, based on an injection period of 50 years. This may exceed the infrastructure lifetime and possible timescale of operational CO_2 storage projects.

10.0 TEST INJECTION METHODOLOGY

10.1 Introduction

The results of the dynamic modelling phase have demonstrated that there is potential for injection of CO_2 in the Middle Cambrian sandstone reservoirs within the Swedish offshore sector in the Dalders Monocline and in the Dalders Structure situated in the central part of the Baltic Sea.

To further assess the business case for the injection of CO_2 in the Baltic Sea a more detailed assessment of the reservoir capacity for long term CO_2 storage is required. The compilation of regional reservoir data demonstrates that a proposed test injection methodology needs to be focussed on a number of key objectives to validate the feasibility of injection at the Dalders Monocline and Dalders Structure sites. These include:

- The characterisation of specific reservoir properties at the proposed test site
- Characterisation studies of the cap rock and potential sealing capacity, confirming the findings of the initial sealing integrity assessment
- Pump testing and hydraulic reservoir property estimations
- Residual trapping, CO_2 migration and pressure build up

10.2 Proposed Testing Methodology

The further development of the BASTOR project requires phased test injection methodology to be undertaken in order to prove the viability of injecting CO_2 in the Middle Cambrian sandstone. Existing projects such as the Mustang and Ottway projects have developed testing methodologies that fulfil these requirements. An indicative phased approach is presented below and describes the principal steps to be taken to drill and log a well at a selected target location, carry out formation property testing and carry out pump testing and injection of CO_2. The proposed test injection methodology has been considered in the implementation of an adequate MMV methodology. This is further discussed in Section 11.0 below.

Step 1: Drilling

- Drilling of the borehole(s) (core retrieval at least some length for both the reservoir rock and the cap rock).
- Borehole logging (standard geophysical logging)

Step 2: Pre-injection tests

- Baseline geophysics (borehole and surface)
- Hydraulic characterization tests:
  1) Pumping test to get overall hydraulic conductivity
  2) FFEC test to get vertical variability of hydraulic conductivity
- Fluid sampling of in-situ fluids (and their chemical analysis in the laboratory)
- Tracer tests (especially intra-well tracer transport, if we have two wells)
- Thermal test (to obtain the thermal conductivity)

Step 3: Laboratory tests on rock samples

- Laboratory testing on the cores, including permeability, porosity, mineralogy, relative permeability- gas saturation functions, capillary pressure-gas saturation functions, rock mechanical properties, (behaviour of the rock when in contact with CO_2 and or brine saturated with CO_2)
- To carry out these tests, we need to know the in-situ fluid composition (step 3)
-

Step 4: CO_2 injection tests

- Push-pull test (single well test) to get an understanding of in-situ residual trapping
- Two-well test, to get an understanding on formation heterogeneity, in-situ residual and dissolution trapping
- These tests require instrumentation of the boreholes, include pressure and temperature monitoring, and fluid sampling under high-pressure conditions and obviously surface installations for CO_2 injection

In-situ mechanical testing needs to be carefully coordinated with the other tests to obtain information about the prevailing stress fields.

11.0 MMV PROGRAMME

11.1 Introduction

The dynamic modelling of the Dalders Monocline and the Dalders Structure indicates the need to drill a CO_2 test injection well. This section describes the measurement, monitoring and verification (MMV) monitoring plan based on the results of the sensitivity analysis, the risks identified and the seal integrity assessment.

The EU Directive on the geological storage of Carbon Dioxide (2009/31/EC) outlines the requirements to assess the behaviour of injected CO_2, to prevent any migration or leakage and assess if any identified leaks are potentially damaging to the environment and human health. Based on the data available and results of the dynamic modelling for the Dalders Structure, a monitoring plan has been developed using the International Energy Agency Monitoring Selection Tool for the injection and post injection phases. This model considers the risks identified in the sealing integrity report with respect to potential leakage pathways. However the lack of specific hydrochemical characteristics for the reservoir fluids as well as detailed temperature and pressure conditions for this area will require the monitoring plan discussed below to be reconsidered and redefined once additional well data becomes available.

11.2 Risk Assessment

The findings of the reservoir dynamic modelling and sealing integrity studies for the cap rock formations overlying the reservoir and the fault structures that characterise the Dalders Monocline are presented in sections 8 and 9 of this report. Based on these findings, the potential hazards with respects to leakage of CO_2 from a possible storage complex in the Dalders Monocline are summarised in Table 33 below.

Table 33: CO_2 Storage Risk Identification

Hazard	Characterisation	Risk	Mitigation
Leakage Pathways	Top seal failure - failure or breach of the cap rock	**Low** Significant thickness of Ordovician and Silurian Cap rock across the Monocline	Ensure adequate characterisation of sealing formations at the proposed injection site
	Migration up the bounding fault planes - where fault structures are not sealed and represent a risk of upward migration	**Low** Fault Structures binding the southern and eastern parts of the Monocline juxtapose the reservoir to mostly impermeable shales and siltstones	Detailed structural interpretation from seismic survey data to identify any small scale fault structures in the vicinity of the well bore. Restrict Injection Pressure to limit over pressure build up
	Across fault plane - where the reservoir is juxtaposed against permeable Ordovician Limestones	**Low** Regional Fault Structures binding the southern and eastern parts of the Monocline are characterised as sealed	Reservoir and cap rock characterisation from well data and seismic interpretation
	Existing wells - where the integrity of existing offshore wells casing and cements are compromised	**Low** Cement plug and casing details of existing wells have been verified	Consider possible casing corrosion in advance of injection to verify completion

			Adequate wireline logging of new wells
	Lateral migration up-dip within the reservoir towards the Swedish Coast and Gotland Island.	**Low** Cement plug and casing details of existing wells have been verified	Limit Injection pressure Limit injection rates Restrict injection sites to the eastern part of the Monocline
Parameters Affecting Leakage	Injection Rates - where these generate excessive overpressure in the reservoir	**Moderate**	Keep injection rates below 0.5 Mt/yr in areas of lower reservoir quality
	Reservoir porosity and permeability - areas of better reservoir quality have the potential to reduce reservoir overpressure at the time of injection but could result in greater migration of the CO_2 plume in the post injection phases. Areas where lower porosity and permeability has been observed have an increased risk of overpressure build up and potential for leakage through fault planes and cap rocks.	**Moderate**	Reservoir and cap rock characterisation from any proposed injection site
	Reservoir thickness - variations in reservoir thickness across the Monocline area will lead to potentially different migration pathways of the CO_2 plume, with reduced movement in areas where the reservoir is thickest.		Select injection sites where reservoir thickness is greatest Limit injection pressure in thin reservoir areas
	Cap rock properties - the Ordovician sequence (particularly in the southern part of the Monocline) is characterised by the presence of the Alum Shale that directly overlies the reservoir. Other lithological units including mudstones, siltstones and limestones are characteristic of the Ordovician. Whilst these do not directly overlie the reservoir there is a limited potential for upward migration where values of porosity and permeability are higher.		Cap rock characterisation and mechanical property testing where injection sites are selected
	Fault sealing rates - regional stress system studies suggest that the north east south west regional faults bounding the eastern part of the Monocline and the east west fault in the southern part are sealed. Other smaller scale structures oriented north south are considered potentially open	**Low** Initial Structural assessment suggests that east west and north south trending fault structures are less common in the Monocline area	Characterisation of fault structures that are associated or cross cutting the main bounding faults

	and potential pathways for leakage		
	Injection Strategy - lower injection rates through several wells rather, than individual wells are likely to reduce the risk of excessive pressure build up, cap rock failure and fault re-activation.	Moderate	Strategy should favour injection from multiple wells at lower rates
Secondary Effect of CO_2 Storage	Displacement of brine within the aquifer resulting in brine pressure difference along the onshore extension of the Dalders Monocline	**Low**	
	CO_2 migration into the atmosphere where the middle Cambrian reservoir is at shallow depths	**Low**	Install onshore CO_2 surface detection measures

11.3 Exposure Assessment

To fulfil the objectives of the Measurement, Monitoring and Verification (MMV) plan, all phases of the project pre-injection, injection, post-injection and post-closure need to be considered in the context of the environmentally sensitive domains near to or connected to the storage complex. The successful implementation of the MMV plan can only be achieved against a set of base level data, which will allow accurate accounting of CO_2 stored in the storage complex.

The storage complex is divided up into a number of environmentally sensitive domains. The domains are the geosphere, marine biosphere and atmosphere and shown in Figure 33.

The offshore Dalders Monocline storage site does not include the fresh water domain. Wells are treated as a separate category because key risks are associated with well integrity. This is discussed separately in Section 11.7.

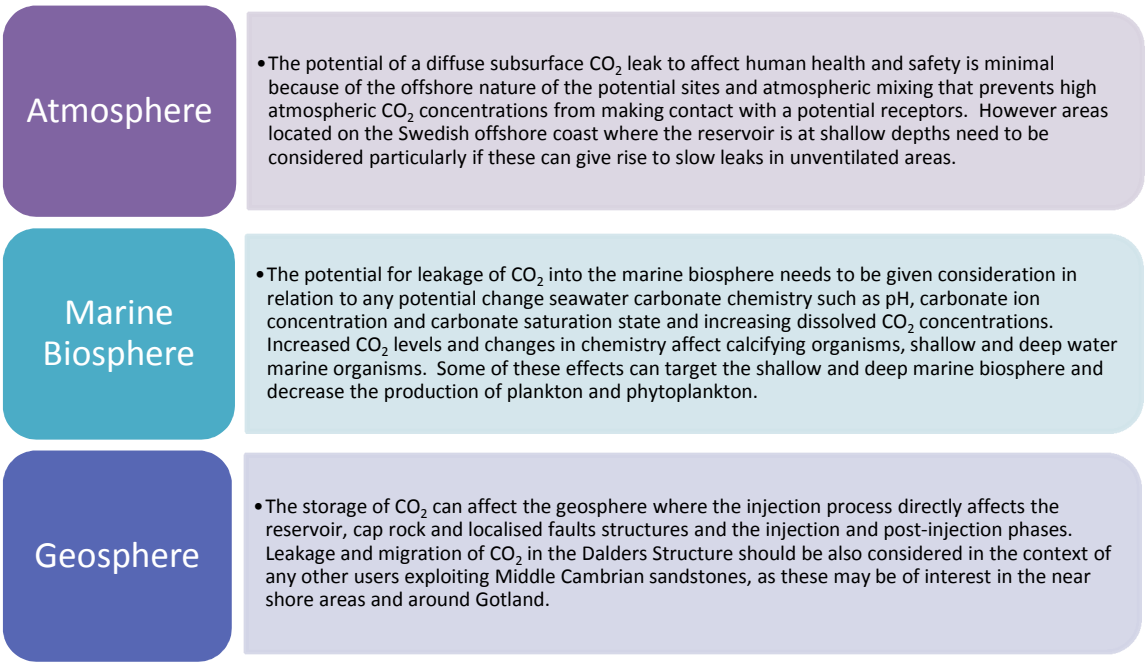

Figure 33: Environmental Domains (adapted from Tucker et. *al*, 2013)

11.4 Monitoring Selection Tool Parameters

The modelling tool parameters selected are based on the sensitivity analysis of the base case parameters outlined in the analytical model described in Section 9.2.1. The following parameters were chosen:

Reservoir Depth (km) 1.5 to 2.5

Reservoir Type Aquifer

Injection Rate 2.5 Mt/yr (based on 0.5Mt/yr injection from 5 wells)

Injection Period 50 years

Monitoring Aim Plume, Top-Seal, Migration, Leakage, Seismicity, Integrity

11.5 Injection Phase

A set of detailed monitoring techniques have been selected to address the risks identified as part of the injection phase of CO_2 Storage in the Dalders Monocline. These are outlined in **Figure 34** below.

Location	Offshore
Depth	500 to 1500 m
Type	Aquifer
Quantity	125.000 Mt (2.500 Mt/yr for 50.0 yrs)
Package	Non-protected+Syn-injection+All

Tool	Rating %	Plume	Seal	Migration	Leakages	Seismicity	Integrity
3D surface seismic	67	4.0	4.0	4.0	1.0	0.0	3.0
Multicomponent surface seismic	62	3.0	4.0	3.0	0.0	2.0	3.0
Microseismic monitoring	46	2.0	2.0	1.0	0.0	4.0	2.0
Downhole pressure/temperature	46	1.0	4.0	1.0	0.0	2.0	3.0
Downhole fluid chemistry	42	1.0	2.0	2.0	3.0	0.0	2.0
Tracers	38	1.0	2.0	2.0	2.0	0.0	2.0
Bubble stream detection	38	0.0	0.0	1.0	4.0	0.0	4.0
2D surface seismic	38	2.0	2.0	2.0	1.0	0.0	2.0
Geophysical logs	38	1.0	2.0	2.0	0.0	0.0	4.0
Long-term downhole pH	29	1.0	2.0	2.0	2.0	0.0	0.0
Seabottom gas sampling	29	0.0	0.0	1.0	4.0	0.0	2.0
Surface gas flux	29	0.0	0.0	1.0	3.0	0.0	3.0
Cross-hole seismic	25	2.0	2.0	1.0	0.0	0.0	1.0
Vertical seismic profiling (VSP)	25	2.0	2.0	1.0	0.0	0.0	1.0
Sidescan sonar	21	0.0	0.0	0.0	3.0	0.0	2.0
Cross-hole EM	21	2.0	1.0	1.0	0.0	0.0	1.0
Multibeam echo sounding	21	0.0	0.0	0.0	3.0	0.0	2.0
Fluid geochemistry	17	0.0	0.0	1.0	2.0	0.0	1.0
Tiltmeters	17	0.0	1.0	0.0	1.0	2.0	0.0
Boomer/Sparker profiling	17	0.0	0.0	1.0	2.0	0.0	1.0
Bubble stream chemistry	17	0.0	0.0	0.0	3.0	0.0	1.0
Cross-hole ERT	17	2.0	1.0	1.0	0.0	0.0	0.0
Seawater chemistry	17	0.0	0.0	0.0	3.0	0.0	1.0
Single well EM	12	1.0	1.0	0.0	0.0	0.0	1.0
High resolution acoustic imaging	12	0.0	0.0	0.0	2.0	0.0	1.0
Surface gravimetry	12	1.0	0.0	2.0	0.0	0.0	0.0
Well gravimetry	12	1.0	1.0	1.0	0.0	0.0	0.0

Figure 34: IEA MMV Selection tool results for the injection phase.

Deployment of all of the monitoring techniques supplied by the IEA Monitoring Selection Tool is unlikely to be realistic, either logistically or financially.The most effective and appropriate monitoring techniques are highlighted in red. These are specifically designed to address site safety issues with regard to public opinion and are based on current demonstration and flagship projects that are referenced on the IEA Greenhouse Gas R&D Programme website.

11.6 Post-Injection Phase

A set of detailed monitoring measures have been selected to address the risks identified as part of the post-injection phase of CO_2 Storage in the Dalders Monocline. These are outlined in Figure 25 below.

Location	Offshore
Depth	500 to 1500 m
Type	Aquifer
Quantity	125.000 Mt (2.500 Mt/yr for 50.0 yrs)
Package	Non-protected+Post-injection+All

Tool	Rating %	Plume	Seal	Migration	Leakages	Seismicity	Integrity
3D surface seismic	67	4.0	4.0	4.0	1.0	0.0	3.0
Multicomponent surface seismic	62	3.0	4.0	3.0	0.0	2.0	3.0
Microseismic monitoring	46	2.0	2.0	1.0	0.0	4.0	2.0
Downhole pressure/temperature	46	1.0	4.0	1.0	0.0	2.0	3.0
Downhole fluid chemistry	42	1.0	2.0	2.0	3.0	0.0	2.0
Tracers	38	1.0	2.0	2.0	2.0	0.0	2.0
Bubble stream detection	38	0.0	0.0	1.0	4.0	0.0	4.0
2D surface seismic	38	2.0	2.0	2.0	1.0	0.0	2.0
Geophysical logs	38	1.0	2.0	2.0	0.0	0.0	4.0
Long-term downhole pH	29	1.0	2.0	2.0	2.0	0.0	0.0
Seabottom gas sampling	29	0.0	0.0	1.0	4.0	0.0	2.0
Surface gas flux	29	0.0	0.0	1.0	3.0	0.0	3.0
Cross-hole seismic	25	2.0	2.0	1.0	0.0	0.0	1.0
Vertical seismic profiling (VSP)	25	2.0	2.0	1.0	0.0	0.0	1.0
Sidescan sonar	21	0.0	0.0	0.0	3.0	0.0	2.0
Cross-hole EM	21	2.0	1.0	1.0	0.0	0.0	1.0
Multibeam echo sounding	21	0.0	0.0	0.0	3.0	0.0	2.0
Fluid geochemistry	17	0.0	0.0	1.0	2.0	0.0	1.0
Tiltmeters	17	0.0	1.0	0.0	1.0	2.0	0.0
Boomer/Sparker profiling	17	0.0	0.0	1.0	2.0	0.0	1.0
Bubble stream chemistry	17	0.0	0.0	0.0	3.0	0.0	1.0
Cross-hole ERT	17	2.0	1.0	1.0	0.0	0.0	0.0
Seawater chemistry	17	0.0	0.0	0.0	3.0	0.0	1.0
Single well EM	12	1.0	1.0	0.0	0.0	0.0	1.0

Figure 35: IEA MMV Selection tool results for the post-injection phase.

The most effective and appropriate monitoring techniques are highlighted in red and are based on current demonstration and flagship projects that are referenced on the IEA Greenhouse Gas R&D Programme website.

11.7 Monitoring Technique Description:

The IEA MMV Selection tools makes recommendations for the deployment of specific monitoring techniques with the objective of assessing which of these are most applicable to the storage site and CO_2 volumes being considered over the duration of a proposed injection period. This section describes the potential risks and receiving environments different techniques that have been identified as strongly recommended (red categories in Figure 34 & Figure 35) and are regarded as key elements in meeting particular monitoring objectives of the MMV programme when considering CO_2 injection at a site in the Dalders Monocline. Exclusion of these essential techniques would reduce the potential for the aim to be achieved. Additional measures classified as 'definitely applicable' by the IEA tools (orange categories - Figure 34 & Figure 35) should be included to meet specific monitoring aims for the injection and storage in the Dalders Monocline.

Specific site conditions will have to be given careful consideration to ensure that they will not undermine the efficacy of each technique, or even preclude its deployment. Based on specific site conditions, the MMV plan proposed should be revised and updated.

The individual Techniques and their potential objectives are further discussed below in Table 34.

Table 34: MMV Technology Review and Potential Deployment phases

Technique	Objectives	Deployment Phases
Multicomponent Surface Seismic	• fluid behaviour monitoring • imaging beneath gas accumulations • discrimination of fluid pressure • saturation changes. monitoring low permeability overburden sequences	Injection and Post Injection
Microseismic Monitoring	• Collection of baseline seismicity • detection, measurement and triangulation of low-level seismic events • fracturing of the reservoir due to injection overpressure or migration of the injected CO_2 • Fault reactivation and cap rock failure	Pre-injection, Injection & Post-Injection phases
Bubble Stream Detection	• Full 3D volumetric sweeps for bubble detection at an offshore storage site (this has already been successfully used in the Polish offshore sector)	Injection & Post Injection
Tracers	• assess and confirm the migration of CO_2 (free and dissolved) within the reservoir • detect migration in overlying and underlying formations; • estimate volume and flow rates of CO_2 within the overlying and underlying formations • detect possible interconnection between reservoir & cap rock	Injection
Long Term Down hole pH	• Monitor CO_2 dissolution into the formation water • Characterise fluid-rock interactions, including mineral trapping. • early indication of CO_2 migration in the overburden	Injection & Post-injection
Surface Gas Flux:	• Measurement of the rate of CO_2 flowing from the ground surface to the atmosphere • Quantifying any mass of CO_2 leaking from a storage site • Compile baseline data from the margins of the Dalders Monocline (onshore Sweden) to identifying natural background variations as a proxy for onshore migration of CO_2 form the reservoir.	Pre-injection Injection Post Injection phases
Vertical Seismic Profiling (VSP)	• Detailed formation characterisation in the near well bore area providing greater certainty of the reservoir and fault characteristics as well as their relationship with the cap rock;	Pre-Injection Injection

	• multiple walkway surveys to characterise plume migration if a multi-well cluster is considered	Post- Injection
Cross Hole Seismic	• measure CO_2 saturations • measure pressure changes during CO_2 injection. • CO_2 plume movement • calibrate seismic data • Early warning of CO_2 leakage	Injection & Post Injection
Cross Hole EM:	• Electrical Conductivity mapping between boreholes • Resistivity contrast mapping of saline aquifer fluids and more conductive CO_2 as an indication for plume migration • changes in CO_2 saturation in the reservoir	Injection and Post Injection
Fluid geochemistry	• fluid chemistry, including pH & bicarbonate concentrations at the well head • detection of CO_2 dissolved in reservoir fluid to assess any migration of CO2 towards onshore Sweden • general information on fluid-rock processes, leakage processes and changes to water quality	Pre-Injection Injection and Post Injection phases
Bubble Stream Chemistry	• Gas composition, flow rate and potential origin *(consideration should be given to the use of a buoy based system such as that trialled in the Gulf of Trieste by the GeoNet2 project if long term monitoring is considered)*	Injection (possible post injection phases)
Tilt Meters	• Baseline rock mechanical properties • Rock mechanical integrity - reservoir and cap rock • changes in strain within the reservoir, caprock or overburden • Storage site deformation sue to high overpressure	Pre-Injection & Injection Phases
Cross Hole ERT	• Resistivity contrasts between the CO_2 and reservoir • monitoring of the approximate distribution of a CO_2 plume between wells. *(subject to confirming borehole spacing and locations based on estimated CO_2 plume and reservoir thickness)*	Injection & Post-Injection
Surface Gravimetry	• Independent verification of changes in the subsurface mass at and post injection • Complementary to seismic monitoring • Estimates of CO_2 dissolution.	Injection and Post Injection phases

11.8 Well Integrity Monitoring:

Additional monitoring measures aimed at addressing the prevention of leakage and CO_2 migration at or near the injection wells are proposed below.

- Pressure testing, at a minimum pressure to be confirmed based on leak off test data, of new wells being considered for injection.
- Caliper survey to measure any potential corrosion of the tubing.
- Corrosion coupons at the injection skid to confirm the dehydration specs are being adhered to and corrosion is not occurring in the pipeline and wellbore completion.
- Routine well maintenance of the wellhead valves and the measurement of the pressure on the different casing annuli.
- Cement Bond Logs, Ultrasonic Casing Logs and Electromagnetic Casing Logs (CBL, MWIT, USIT, EMIT) will verify the initial integrity of the cement bond and well completion along the entire length of each injector.
- Hold Up Depths (HUD) should be measured at every wire-line entry in a well before the CBL/MWIT/USIT/EMIT logs are run, to ensure no plugging exists across the perforation interval. This may have to be repeated at regular intervals as part of the lifetime of the project
- Distributed Temperature Sensing (DTS) along an optical fibre permanently deployed from the surface down to the first seal on the outside of the intermediate casing will provide a continuous means on verifying cement bond integrity and the absence of CO_2 outside the casing. In the unexpected event of a loss of cement bond integrity, any upward migration of CO_2 outside the casing will lower the temperature on the adjacent portion of the DTS fibre due to increased thermal insulation from the in-situ formation temperature provided by the out-of-place CO_2.

12.0 CONCLUSIONS

The principal conclusion from this study is that there is large theoretical storage capacity in the Baltic Sea basin beneath a 900 metre thick impermeable caprock. Ranking of Baltic Sea sub-basins in terms of suitability for CO_2 geological sequestration identified the Slupsk Border Zone as the highest rank. Theoretical storage capacity calculations for the sub-basins indicated more than 100Mt of CO_2 storage capacity in the Dalders Structure within the Dalders Monocline. Preliminary dynamic simulations have been carried out focussing on the southern part of the Dalders monocline offshore Sweden. These suggest that, for example, maintaining the reservoir pressure at 50% above the hydrostatic pressure, would limit the injection rate to 0.5Mt per well per annum over a 50 year period if five injection wells are used. Increasing the number of wells, would increase the total annual rate (e.g. seven wells could correspond to a total rate of about 3 Mt per year) as would reducing the injection time to e.g. 25 years. The maximum injection rate is sensitive to parameters such as formation thickness and permeability, and analyzing the effect of their local variability fully does require more detailed modelling than was possible in this preliminary study. In these preliminary simulations impermeable sealing units (cap-rocks) were also assumed and it should be noted that the injection-induced pressure increase could be dissipated by brine displacement through cap-rock if cap-rock properties are suitable. In addition, pore pressure could be further relieved through brine production wells, thus allowing higher injection rates. The role of using horizontal, rather than vertical injection wells should also be investigated. Further modelling studies should address these issues in more detail. Such analyses should optimally be accompanied with additional site-specific data and/or further parameter sensitivity studies where data acquisition is not possible.

Keeping these reservations in mind, the above numerical values can be considered only indicative.

The results from the data analysis and the preliminary dynamic modelling do, however, indicate that the reservoir quality in the presently modelled area is not suitable to high injection rates and therefore not sufficient for CO_2 storage at the scale of projected emissions around the Baltic Sea. Other areas to the north east of the Monocline, such as offshore Latvia, where limited data is available, could include suitable areas for storage with better reservoir quality and where a higher rate of injection could be achieved.

The regional storage capacity assessment demonstrated that there are sweet spots in the Cambrian reservoir such as onshore Latvia, where there is commercial gas storage, and both onshore and offshore Kaliningrad, where there in ongoing hydrocarbon production.

13.0 RECOMMENDATIONS

The potential to store significant quantities of CO_2 in the Swedish part of the Dalders Monocline appears to be limited based on current data and assumptions of the reservoir and top seal properties used to model potential injection scenarios.

Existing seismic line data covering the Swedish offshore sector of the Dalders Monocline should be calibrated to available well data and re-interpreted to identify any primary and secondary fault structures and map reservoir porosity and permeability variations based on seismic attributes.

Further reservoir characterisation studies such as those discussed above should be combined with improved estimates of seal fracture pressures based on well leak off test data and core sample anaylses.

This would improve the understanding of the connectivity in higher quality intervals of the reservoir and provide a more heterogeneous static model on which further CO_2 injection modelling scenarios could be undertaken.

Future exploration efforts should be focussed on areas where the best reservoir quality and storage potential are likely to be found. This should be done in parallel with more refined dynamic simulations to gain further understanding of the true storage capacity of various parts of the region.

Reservoir formation data from core samples and wire line logs should be obtained from any newly drilled wells in the area to improve the understanding of porosity, permeability and formation pressure values associated with the reservoir across the Baltic Sea region.

As offshore and onshore well data indicate that the north eastern portion of the Dalders Monocline appears to have better reservoir qualities than the current study area, new data covering this area, in particular offshore Latvia, could help to identify more suitable sites for CO_2 storage.

As the regional reservoir quality maps based on limited data indicate that onshore and offshore Kaliningrad would appear to have better reservoir qualities than the current study area, access to additional existing data from this area would help to identify more suitable sites for CO_2 storage

Thus Baltic State cooperation is imperative to ensure the success of any Baltic Sea CO_2 storage initiative. Additional efforts to increase this cooperation between Baltic States should be undertaken to ensure that an effective strategy for CO_2 storage in the Baltic Sea region is adopted.

14.0 BIBLIOGRAPHY

Amoco Latvia Oil Company. 1995. Dalders Prospect, Depth Structure Map, Top Mid-Cambrian Sandstone. Enclosure 21 - Dalders Summary Report. 1996.

Bachu, S. et al. (2007). Estimation of CO2 storage Capacity in Geological Media - Phase 2. Work under auspices of the Carbon Sequestration leadership Forum

Bachu, S. (2003, March). Screening and ranking of sedimentary basins for sequestration of CO2 in geological media in response to climate change. *Environmental Geology* , pp. 277-289.

Bear J (1972) *Dynamics of Fluids in Porous Media*. Dover Publications, Inc., New York.

Brangulis A.P., S. K. (1993). Geology and hydrocarbon prospects of the Paleozoic in the Baltic region. *Petroleum Geology of Northwest Europe: Proceedings of the 4th Conference (Ed J.R. Parker)* (pp. 651-656). London: The Geological Society of London.

Brangulis, A.P., Kanev, S.V., Margulis, L.S., Pomerantseva, R.A (2008).. Petroleum Geology of Northwest Europe: Proceedings of the 4th Conference. 1993 Petroleum Geology. Published by The Geological Society, London, pp 651- 656. Erlstrom, M. *Lagring av koldioxid i djupa akviferer.* Elforsk.

Chadwick, A. (2008). *Best Practice for the storage of CO_2 in Saline Aquifers.* Keyworth: British Geological Survey.

Donoho, D.W., Hart, W.H. 1996. Dalders Summary Report. Amoco.

Erlstrom, M. (2008). Lagring av koldioxid i djupa akviferer. Stockholm: Elforsk.

Erlstrom, M. F., Fredriksson, D. , Juhojuntti, N., Sivhed, U., Wickström, L. (2011). *Lagring av koldioxid i berggrunden.* Stockholm: Sveriges geologiska undersökning.

EU Geocapacity, (2009). WP4 Report - Capacity Standards and Site Selection Criteria. Assessing European Capacity for Geological Storage of Carbon Dioxide. SES6-518318

Favalli, M. and Pareschi, M.T., 2004. Digital elevation model construction from structured topographic data: The DEST algorithm. Journal of Geophysical Research, **109**, F04004.

Grigelis, A. 2011. Research of the bedrock geology of the Central Baltic Sea. *Baltica.* **24.** Issue 1. Pages1-12. Viknius.

Kanev, S., Kushik, E., Peregudov, Y. (2000). A large Ordovician carbonate buildup offshore Latvia. *Latvijas Geologijas Vestis Journal,* 8, 22–23.

Krushin, J. (1994). *A Semi-Quatitaive Analysis of the Sealing Potential for the Middle Cambrian Sandstones, Dalders Prospect, Baltic Sea.* Amoco Production Comapny.

LO&G, 2002. Latvia Offshore, Hydrocarbon Potential of Blocks 1, 2 and 3 offered in Latvia's 1st E&P Licensing Round. Reiterated Opening April – October 2002.

LO&G, 2002. Enclosure 2, Baltic Basin, Top & Base Cambrian Depth Map 1:1M. Latvia Offshore, Hydrocarbon Potential of Blocks 1, 2 and 3 offered in Latvia's 1st E&P Licensing Round. Reiterated Opening April – October 2002.

LO&G, 2002. Enclosure 3, Latvia Licenses 1, 2 & 3 Evaluation Montage. Latvia Offshore, Hydrocarbon Potential of Blocks 1, 2 and 3 offered in Latvia's 1st E&P Licensing Round. Reiterated Opening April – October 2002.

LOTOS, 2010. The Possibility of CCS realisation in LOTOS Group by using oil fields on the Baltic Sea. Presentation to the CCS Workshop, Warsaw.

Mathias, S.A., González Martínez de Miguel, G.J., Thatcher, K.E., Zimmerman R.W. (2011a). Pressure buildup during CO_2 injection into a closed brine aquifer. *Transport in Porous Media*, 89, 383–97.

Mathias, S.A., González Martínez de Miguel, G.J., Hosseini, S.A. (2011b). Role of partial miscibility on pressure buildup due to constant rate injection of CO2 into closed and open brine aquifers. *Water Resources Research*, 47, W12525.

Modliński, Z., Podhalańska, T. (2010). Outline of the lithology and depositional features of the lower Paleozoic strata in the Polish part of the Baltic region. Geological Quaterly, 54, 109-121.

Nilsson, P. A. (2011). *Bastor - Baltic Sea CO2 Storage.* Stockholm.

OPAB (2011). Hagenfeldt, S., E. Dalders, Silurian to Ordovician Source Rocks. Internal Report

OPAB (1990). *Sweden Baltic Sea OPAB Farmout Prospectivity Appraisal.* Amoco Sweden Petroleum Company.

Otmas, A.A. (2011).Development and location of the oil structures in the Kaliningrad region. Thesis. St Petersbourg.

Petroswede Svenska Petroleum Exploration (2010). *Annual Report 2009.* Petroswede AB.

Pruess, K., Oldenburg, C., Moridis, G. (1999). TOUGH2 User's Guide, Version 2.0. Report LBNL-43134. Lawrence Berkeley National Laboratory, Berkeley, California.

Pruess, K., Spycher, N. (2007). ECO2N - A fluid property module for the TOUGH2 code for studies of CO2 storage in saline aquifers. *Energy Conversion and Management* 48, 1761-1767.

Purra, V., Flodén.T. Rapakivi-granit-anorthosite magmatism – a way of thinning and stabilisation of the Sevcofennean crust, Baltic Sea Basin. *Tectonophysics.* 1999. **V 305.** Issue 1-3, Pages 75-92

Qiang Xu, J. (2009). *Reservoir Engineering Aspects in Site Characterization, Short-Term Modelling. and Long-Term Fate of CO_2 in Carbon Dioxide Geosequestration.* Bureau of Economic Geology: The American Association of Petroleum Geologists.

Raukas, A., Teedumäe, A. (eds) (1997). Geology and Mineral Resources of Estonia. Estonian Academy Publishers, Tallinn. 436 pp.

Schuppers, J., D., Holloway, S., May, F., Gerling, P, Bøe, R., Magnus, C. Riis, F, Osmundsen, P. T., Larsen, M., Andersen, P. R. and Hatzyannis, G. (2003). Storage Capacity and quality of the hydrocarbon structures of the North Sea and the Aegian region. TNO-report NITG 02-020-B.

Shogenova, A. S. (2009). The Baltic Basin: structure, properties of reservoir rocks, and capacity for geological storage of CO2. *Estonian Journal of Earth Sciences* , pp. 259-267.

Šliaupa, S., Šliaupiene, R. 2010. Potential of geological storage of CO_2 in Lithuania. CGS Europe, Poster.

Šliaupa, S., Fokin, P., Lazuaskiene, J., Stephenson, R.A. The Vendian Early Palaeozoic sedimentary basins of the East European Craton. *Geological Society of London Memoirs.* 2006, **32**, Pages 449-462

Šliaupa, S. (2009). Potential of geological storage of CO2 in Lithuania. *CO2NET EAST workshop 'CO2 Capture and Storage - Response to Climate Change'*, (p. Poster). Bratislava.

Šliaupa S., Hoth P. 2010. Geological evolution and resources of the Baltic Sea Area from the Precambrian to the Quaternary. In: J. Harff, S. Björck, P. Hoth (eds.). *The Baltic Sea Basin. Springer*. Berlin. 13–51.

Šliaupiene, R., Šliaupa, S. (2010). CO_2 Storage potential of Lithuania. CGS Europe, Poster.

Šliaupiene, R., Šliaupa, S. (2011). Prospects for CO2 geological storage in deep saline aquifers of Lithuania and adjacent territories. Geologija, 53, 121-133.

Šliaupiene, R., Šliaupa, S. (2012). Risk Factors of CO_2 Geological Storage in the Baltic Sedimentary Basins. *Geologija*, 54, 3, 100–123.

Siggerud, E. (2008). *Sedimentology Early to Late Cambrian within the Dalders Prospect, Central Baltic Sea.* In-House Report Svenska Petroleum Exploration AB.

Skirius, C. (1996). Baltic Sea Middle Cambrian Sandstone Analysis, Wells B3-1, B6 and E7-1. Amoco Report. EPTG.

Sokołowski, A., Tęgowski, J. (2012). Cruise Report within EU project ECO2 (B3 field, southern Baltic Sea, Poland). University of Gdańsk, Institute of Oceanography, Gdynia, Poland

Streimikiene, D. 2010. Use of comparative assessment framework for comparison of geological nuclear waste and CO2 disposal technologies. World Energy Congress 2010.

Svenska Petroleum, AB. (1996). Proposal for the Facilities Design, Economics and Work Programme for the Development of the Kretinga and Nausodis Oil Fields. Volume A, Submission to the Licence Committee of Lithuania – Agreement Area Evaluation.

Svenska Petroleum, AB. (1996). The Geophysical, Geological and Development Appraisal of the Kretinga, Nausodis Fields and volumetric Reappraisal of the Genciai Field. Volume B, Submission to the Licence Committee of Lithuania – Agreement Area Evaluation.

Svenska Petroleum Exploration OPAB. (2010). GEOLOGICAL SUMMARY, BALTIC SEA, OPAB PRESENT KNOWLEDGEBASE. *Internal Presentation* .

Tarvis, T. (2007). Geology of the central Baltic Sea and its implication for hydrocarbon potential. Part 1 - Palaeozoic geology and structural evolution of the central Baltic Sea and its hydrocarbon potential. *Unpublished Masters Thesis.* University of Stockholm.

Tucker, O., Garnham, P., Wood, P., Berlang, W., Susnato, I. (2013). Development of an offshore monitoring plan for commercial CO_2 storage pilot. Energy Procedia. **37** (2013). pp. 4317 – 4335.

Ulmishek, G. (1990), The Geological Evolution and Petroleum Resources of the Baltic Basin: Chapter 31: Part II. Selected Analog, Interior Cratonic Basins: Analog Basin. AAPG Special Volumes, M51: Interior Cratonic Basins, Pages 603-632

Ūsaitytė, D. (2000) The geology of the southeastern Baltic Sea: a review. *Earth Science Reviews,* 50**,** 137-225

VTT. (2010). *Potential for carbon capture and storage (CCS) in the Nordic region.* VTT

Wójcicki, A., Paczesna, J. (2012). CO2 storage potential in the Polish part of the Baltic Sea. Stockholm.

Woodcock, N. and Stracken, R. (2000). Geological History of Britain and Ireland. Blackwell Science Ltd.

Zytner Y.I., Fenin G.I., Chibisova V.S. and Rovinskaya E.L. (2009). Mineral resources of hydrocarbons and the licensing status Baltic oil province (Kaliningrad). Petroleum geology. Theory and practice, v4-4. http://www.ngtp.ru/rub/6/44_2009.pdf - in Russian.

15.0 CLOSURE

This report has been prepared by SLR Consulting Limited with all reasonable skill, care and diligence, and taking account of the manpower and resources devoted to it by agreement with the client. Information reported herein is based on the interpretation of data collected and has been accepted in good faith as being accurate and valid.

This report is for the exclusive use of Elforsk; no warranties or guarantees are expressed or should be inferred by any third parties. This report may not be relied upon by other parties without written consent from SLR.

SLR disclaims any responsibility to the client and others in respect of any matters outside the agreed scope of the work.

Plate 1 – Baltic Sea Map

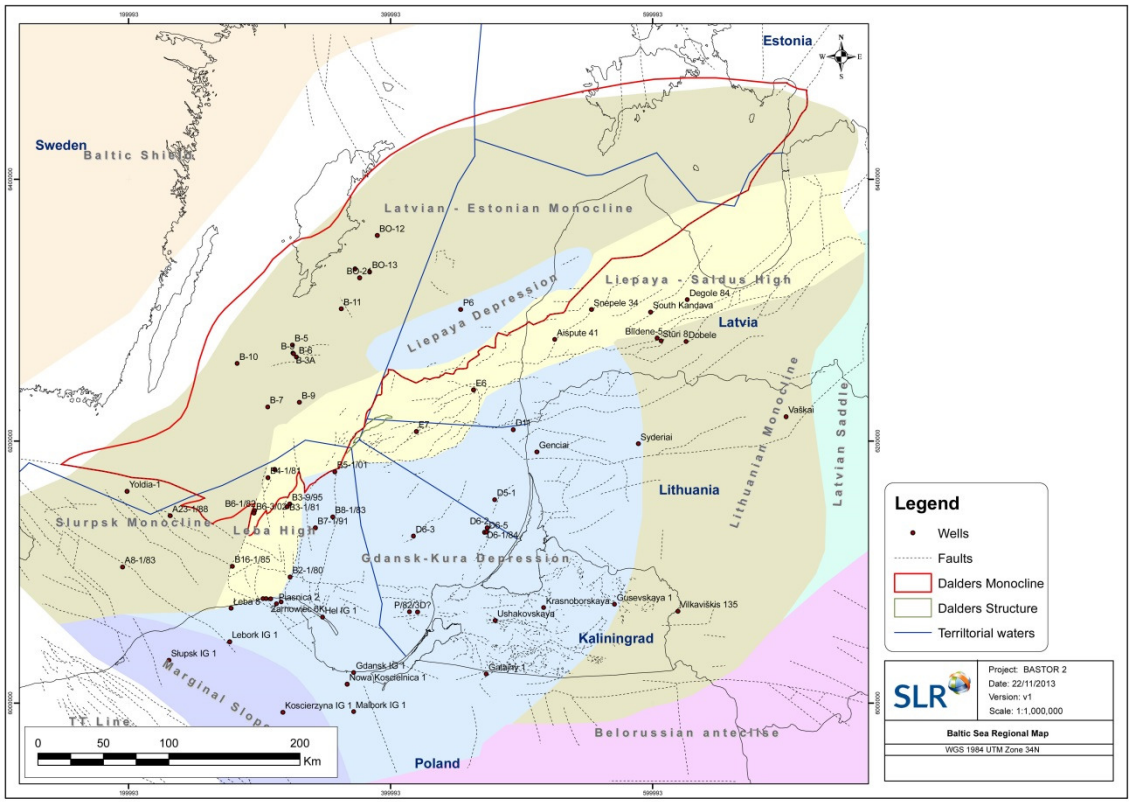

Plate 2 – Structures

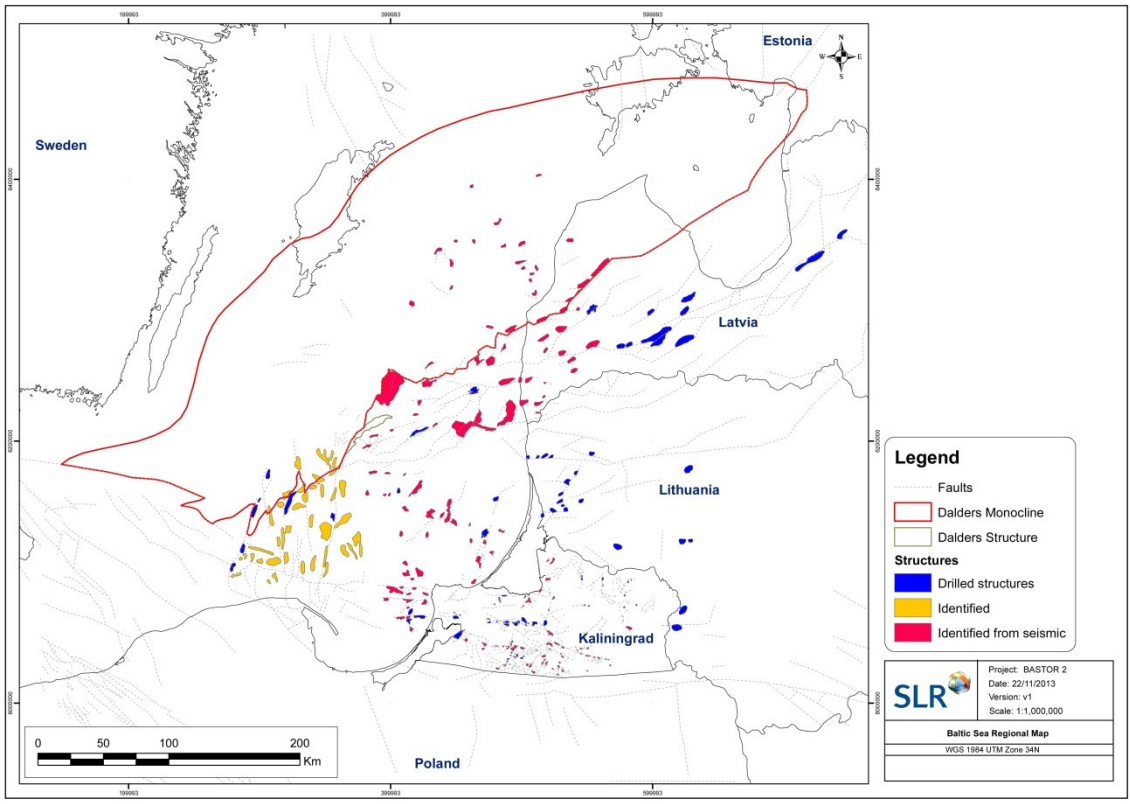

Plate 3 – Alum Shale and Injection Locations (OPAB, 2011)

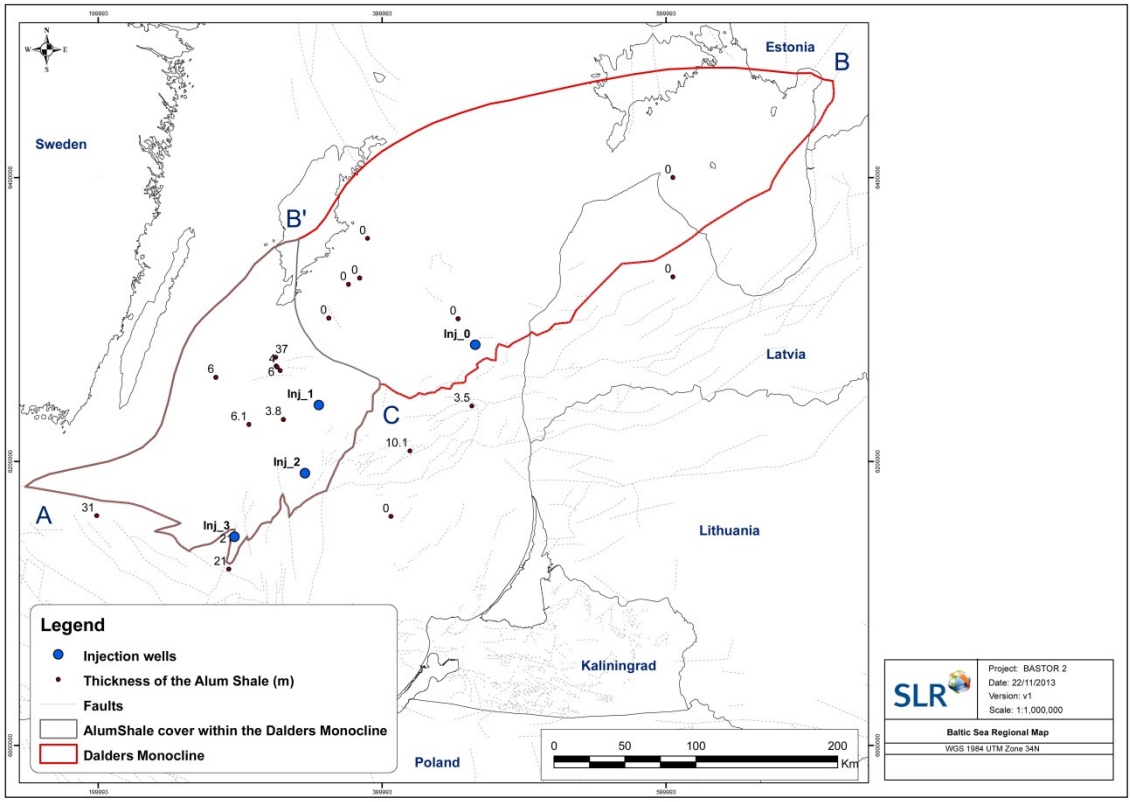

Plate 4 – Ordovician Thickness

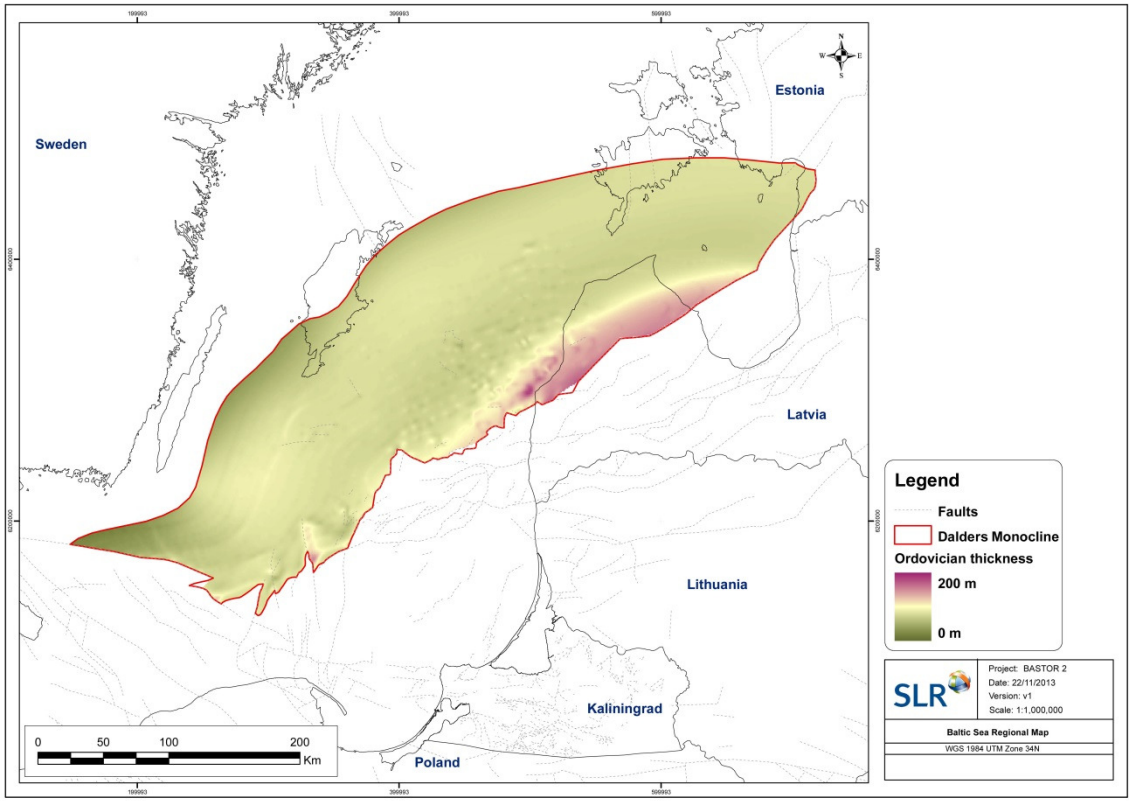

Plate 5 – Permeability and Porosity

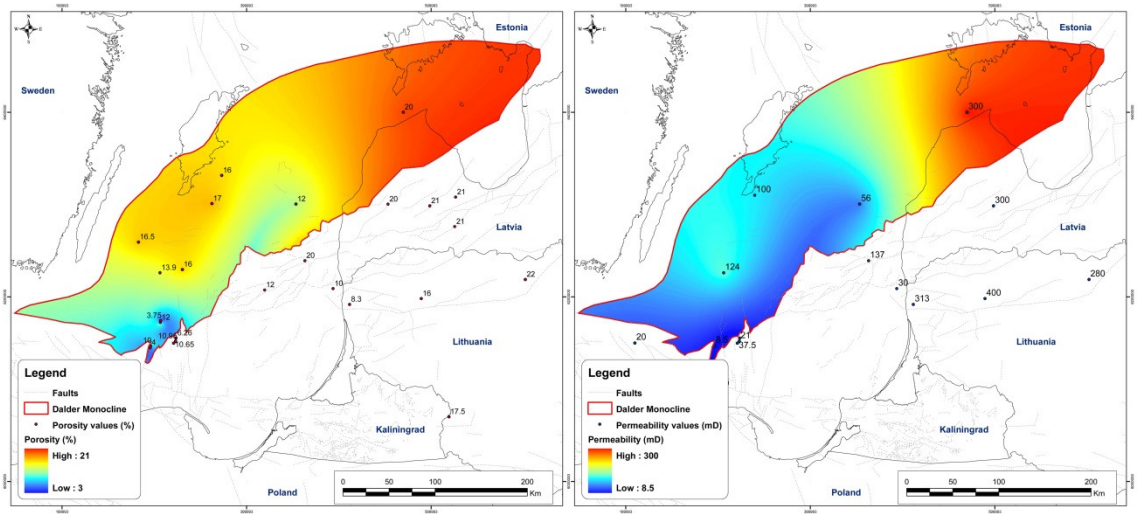

Appendix A - Modelling of CO_2 spreading and related pressure response in Dalders Monocline and Dalders Structure – Uppsala University, Department of Earth Sciences

16.0 MODELING OF CO_2 SPREADING AND RELATED PRESSURE RESPONSE IN DALDERS MONOCLINE AND DALDERS STRUCTURE

Auli Niemi, Zhibing Yang, Liang Tian, Byeongju Jung, Fritjof Fagerlund, Saba Joodaki

Uppsala University, Department of Earth Sciences

We have carried out preliminary modeling of CO_2 injection into selected parts of the Dalders Monocline and Dalders structure, in order to estimate the feasibility of these formations for industrial scale CO_2 injection. This Appendix presents the results of this study, this Chapter 16 presents the summary of the results and Chapters 17 to 21 present the underlying work.

The approach taken in the modeling has been to use different modeling approaches parallel, thereby increasing the confidence and reliability of the predictions, given the data available at the present moment. The modeling approaches used are 1) preliminary determination of the injection rates by means of analytical solution; 2) Numerical modeling of CO_2 plume spreading and related effects effects with TOUGH2 model and 3) vertical- equilibrium (VE) model. We have also estimated the long-term CO2 transport by means of analytical and TOUGH2 models. The objective of this preliminary study is to get order-of-magnitude estimates of the behavior of the formations during the CO_2 injection and subsequent storage periods under specific injection scenarios. Below we will first discuss the results of the major formation, the Dalders Monocline and then proceed to the considerably smaller formation, the Dalders Structure. In the case of the Dalders Monocline, the focus is in the southern part of this domain (see Figure 4 in Part B) where there is high confidence in the characteristics of the overlying cap-rock.

The data and static geological models for these simulations have been provided by SLR and are presented elsewhere in this report. For the numerical models (TOUGH and VE models) the permeability and porosity maps presented in the static model were directly used (Figures 13 a and b) as input and for the analytical models single homogeneous values were used and varied within the realistic range.

16.1 Dalders Monocline

The target area modeled for the CO_2 injection is the deep (southernmost) part of the Dalders Monocline. The modeled units are the lower and middle Cambrian units, which have relatively high permeability and porosity, and are mostly continuous within the monocline area. From above the aquifer is sealed by thick Ordovician units and Alum shale that can work as excellent cap-rocks. The thickness of Cambrian units varies depending on locations, but generally the structure become thinner and pinches out by moving northward. The overall thickness in the deepest part is about 100 m. The southern side of the monocline is bounded by a fault zone, and the sedimentary units

in the northern side are exposed in the submarine/atmosphere. We assume the southern boundary of the modeling domain to be closed (but a sensitivity study considers an open condition here as well) and the northern boundary to be open. The hydrogeological parameters used in the model were obtained from several boreholes spread over the monocline.

As the first model (Part A) we use an analytical solution by Mathias et al. (2011a,b), to get an initial estimate of what CO_2 injection rates can be used, in order not to cause pressure increases resulting in unacceptable mechanical effects. As site-specific mechanical information is presently lacking, we use a commonly applied estimate of 1.5 times the initial hydrostatic pressure as a preliminary pressure cutoff criterion. The analytical model assumes homogeneous and uniform medium properties. It takes into account the injection well interference with other wells. Using the mean values of the formation as the base case, and assigning a maximum allowed pressure of 180 bars, then the maximum injection rate is about 0.5 Mt/yr per well when injecting simultaneously from five wells for fifty years. This would correspond to 2.5 Mt/yr in total for five wells and the area considered is the southern part of the Dalders Monocline. Figures 1 to 3 of Part A allow inspecting how varying different factors, such as layer thickness and permeability, influences the maximum allowable injection rate. Figure 3 also shows the effect of the number of injection wells, where it can be seen that distribution of the injection to a larger number of wells reduces the injection pressure.

The base-case result of 0.5 Mt/year per well was used as a starting point in the subsequent numerical simulations, where numerical simulations with TOUGH2 and TOUGHMP (PART B) and VE-models (PART E) were used for more detailed analyses. With these numerical models the local variations in material properties, thickness etc., as well as processes like CO_2 dissolution can also be taken into account.

The TOUGH2 simulations (PART B) were carried out by gradually increasing the complexity of the model, starting from coarse 2D models (or ‘pseudo 3D’ models where layer thickness was varied while keeping the model 2D) and proceeding to finer discretization and fully 3D models (Table 2 of Part B). Also here the focus is on the southern part of the Dalders Monocline. The most interesting results are those from the full 3D cases (Cases 4 and 5) where fine discretization was used near the injection wells and the domain was vertically discretized, to allow a realistic interpretation of the buoyancy flow. In the single well injection case, where 0.5 Mt/year is injected in the centrally located well (inj_02; Figure 4, Part B) the maximum overpressure is about 60% (Figure 12). The plume spreading (in the uppermost layer where the spreading has reached farthest, due to buoyancy, see Figure 11) can be seen in Figure 13, from which it can be seen that the spread of the plume is about 7 km at the end of the 50 years injection. After the end of the injection, when the injection pressure driving force is removed the plume advancement is slow and after 158 years (Figure 14) the plume still has moved to less than 8 km from the injection well.

In the case of the multiple well injection, where 0.5 Mt/yr was injected from the middle and eastern wells and 0.2 Mt/yr from the southernmost well situated in the vicinity of the closed lower boundary (Figure 4, PART B). A smaller injection rate was used in the southernmost well as the results from the VE-model (Part D) had shown unacceptably high pressure increases in case the 0.5 Mt/yr rate was used from this well also. In this case the plume spreading pattern is similar to that in the Case

4 single-well injection, and even the maximum pressure increase in the well where results could be compared (central well, Figure 16). Also in this case the highest overpressure in the central injection well was of the order of 60% (as in the single well scenario), which is also in good agreement with the analytical solution of PART A. In the southernmost well close to fault zone the pressure increases were higher, as can be expected.

The vertical equilibrium model is a simplified, yet powerful approach used quite extensively in large scale modeling predictions of CO_2 injection. It is especially used in the academia and considered as one of the main alternative approaches for full 3D numerical simulations. The results (Figure 6, Part D) are in good agreement with TOUGH simulations in terms of the spreading of the CO_2 plume. The extent of the plume is less that 10 km at the end of the injection and the movement after the end of injection slow. It should be noted that here the plume of certain thickness is shown, not the CO_2 saturation like in the case of TOUGH2 simulations. The predicted pressure distribution also matches well with the results from other methods, with overpressures of about 90% at injection wells (A and C) in case of 0.5 Mt/year injection per well for 50 years (Figure 5, Part D). The higher pressure in the multiple-well scenario can be partly explained by the extreme pressure response at the southernmost well (Well B in Figure 5, Part D) that is very close to the fault zone.

Finally, the CO_2 migration time after the end of the injection is considered in Part E. Also here the TOUGH2 simulations are used as the simulation method. Assuming the prevailing formation slope and other best estimate properties, the plume migration distance as function of the time for two different permeabilities can be seen in Figure 8. Figure 9 shows the effect of residual saturation on this distance. The results indicate that it would take for the tip 4000 years to travel 14 km. If we consider a total amount of 30 Mt injected CO_2 for one injection well, with Sgr= 0.2, a simple volumetric calculation may yield a potential maximum migration distance of about 50 km, taking into account the plume shape and equilibrium dissolution within the plume. According to the average speed of migration (Figure 9, Part E) a migration distance of 50 km would take about 14000 years. Given this distance and the especially long time, we can also calculate the dissolution trapping capacity. The mass that can potentially be dissolved in our considered system can be estimated to half of the initial CO_2 mass. This means that, in this case, convective dissolution has the potential to significantly drag the plume migration, and that the plume migration distance will be actually much smaller than 50 km in 14 000 years. This can be compared to the 120 km distance between the point of injection and Gotland Island.

16.2 Dalders Structure

This much smaller area is an anticline structure attached to the southern part of the Dalders monocline, consisting of Cambrian sedimentary units. Thick low-permeable Ordovician sequences and shale layers provide a good sealing capacity. The depth ranges 1.3 ~ 1.4 km below sea level, and the physiographic map shows three high locations suitable for commercial size CO_2 injection operation. The northern boundary of the structure is a closed fault zone and considered a closed

boundary in these simulations. The southern boundary is a spill point, and assumed as an open boundary.

The location of the injection well was chosen in the middle of the structure where the depth is relatively deep; hence we can easily observe the overpressure development and migration induced by the CO_2 injection. The injection rate and period applied to one well (Figure 1, Part C and Figure 9, Part D) are 0.3 Mt/year and 0.5 Mt/yrs for 50 years for TOUGH2 model and 0.3 Mt/year for 50 years for the VE-model. With the TOUGH2 model the vertical layering was taken into account (Figure 1, Part C) while with the VE-model the layering was ignored due to the character of the model. With the TOUGH2 model both the 0.3 Mt and 0.5Mt injection scenarios showed moderate pressure increase of less than 50% compared to the in-situ hydro-equilibrium pressure (Figure 2, Part C). Similar pressure increases were observed with the VE-model (Figure 10, Part D).

Based on the TOUGH simulations low CO_2 saturations reach the model boundaries prior to end of injection, which is obviously not desirable. Estimates of this leakage are also given. Similar plume spreading is observed with the VE-model but as here the CO_2 thickness is given rather than CO_2 saturations, the effect of reaching the model boundaries is not as obvious from the Figures. After the end of the injection the plume is migrating up-dip and getting diluted, due to residual trapping and dissolution. These preliminary results indicate that while the pressure increase induced by the injection is acceptable, the location of the well(s) should receive more attention or more detailed calculations to address the question of the plume reaching model boundaries prior to the end of the 50 years injection.

16.3 Concluding remarks

To summarize, the preliminary modeling presented here indicates for the southern part of the Dalders Monocline a maximum total injection rate of the order of 2.5 Mt/yr, assuming a maximum sustainable pressure increase of 50% from the hydrostatic condition, injection from five wells and a homogeneous permeability of 40mD with layer thickness of 50m. This maximum injection rate is sensitive to parameters such as formation thickness, permeability as well as number of wells. Sensitivities to these parameters are shown in Figures 1 to 3 in Chapter 17, indicating how increasing the number of wells would allow a larger total injection rate and how an increase/decrease in permeability influences the maximum injection rate. Reducing the total injection time from 50 years to e.g. 25 years, would also allow increasing the injection rate, as the pressure increase due to injection increases with time. The above results come from the preliminary analytical models but are supported by the results from the numerical models.

In these preliminary simulations the model parameters were taken from the static model as such. For the numerical models the properties were spatially varying while for the analytical models single homogeneous values were used and varied within the realistic range. It should be pointed out that in future studies more comprehensive sensitivity and uncertainty analyses could and should be carried out to test the sensitivity of the numerical models to uncertainties in the input parameter values.

It should also be pointed out that in these preliminary simulations we have assumed impermeable sealing units for the storage formation. The injection-induced pore pressure could be dissipated by brine displacement through cap-rock (pressure 'bleed-off') if the permeability of the cap-rock is not extremely low and the compressibility of the cap-rock is large (see e.g., Chang et al. 2013). In addition, pore pressure could be further relieved through brine production wells. The role of using horizontal, rather than vertical injection wells could also be investigated. Finally it should be noted that the assumed 50% sustainable pressure increase is a reasonable assumed value based on literature, as site-specific mechanical information is presently lacking. Further studies should address these issues in more detail. Such analyses should also be accompanied with additional site-specific data.

Finally, it should be pointed out that in future studies more detailed models describing the behavior near the borehole could be used, including simulators with specific wellbore modules that allow detailed gridding near the borehole.

PART A

17.0 PRELIMINARY DETERMINATION OF MAXIMUM INJECTION RATE BY MEANS OF ANALYTICAL SOLUTION

Zhibing Yang, Auli Niemi

17.1 Introduction

Effective implementation of CO_2 sequestration involves injection of large volumes of CO_2 which causes pressure perturbation in the storage formations. The increase in pore pressure due to injection induces changes in the stress field. This generally increases the risk of shear and tensile failure (which jeopardizes the integrity of the storage reservoir) as well as reactivation of pre-existing faults. In this part of the work, we evaluate the injection induced pore overpressure for the Dalders Monocline via the state of the art analytical model developed for CO_2 storage by Mathias et al. (2011a, b). We investigate the dependence of the formation pressure buildup on the CO_2 injection rate for different parameters such as layer thickness, permeability, number of injection wells. This can be used to preliminarily determine the maximum injection rate if a maximum allowable pressure increase is given.

17.2 Modeling approach

In this section, we briefly introduce the analytical solution developed by Mathias et al. (2011a, b). Under reservoir conditions, supercritical CO_2 can partially dissolve into brine and at the same time water can partially vaporize in the presence of CO_2. This partial miscibility gives rise to complex flow regimes and dynamics for the evaluation of pressure response. For a typical industrial-scale CO_2 injection scenario, there exist a dry-out zone (free of water) around the injection well. In this dry-out zone all water has been either displaced outwards or vaporized into the CO_2 rich (gas) phase and the salt that was originally dissolved in the brine has precipitated. The radius of dry-out zone is typically on the scale of 10^2 meters at the end of the injection period (say e.g. 50 years). Surrounding the dry-out zone is a region where the gas phase and the aqueous phase coexist. The radius of this two-phase flow region is typically several kilometers at the end of the injection period. Outside of the two-phase region only brine exists with single phase brine flow. Assuming vertical pressure equilibrium, constant fluid properties, negligible capillary pressure and equilibrium dissolution between CO_2 and water, Mathias et al. (2011b) solved the relevant (radially symmetric) governing equations describing the above flow characteristics. It is possible to obtain closed-form solutions for the gas saturation and pressure for the case with linear relative permeability functions.

For nonlinear relative permeability functions, numerical evaluation of the gas saturation at the leading shock front needs to be used, and the solution becomes semi-analytical.

The analytical model of Mathias et al. (2011b) can be applied to both open and closed aquifers. It can be summarized as:

$$\Delta P = P - P_{ini} = \frac{M_0}{4\pi\rho_g Hk}\begin{cases}\mu_g q_{D1}\ln(z_T/z)/k_{rs} + \mu_g q_{D2}F_2(z_T) + \mu_b q_{D3}F_1(z_L), & 0 \le z < z_T \\ \mu_g q_{D2}F_2(z) + \mu_b q_{D3}F_1(z_L), & z_T \le z < z_L \\ \mu_b q_{D3}F_1(z), & z \ge z_L\end{cases} \quad (1)$$

where ΔP is the pressure build-up,

P is the vertically averaged pressure,

P_{ini} is the initial pressure (vertically averaged),

M_0 is the mass injection rate of CO_2,

ρ_g is the density of CO_2,

μ_g is the viscosity of CO_2,

k is the permeability of the formation,

H is the thickness of the formation,

k_{rs} is the permeability reduction factor due to salt precipitation,

μ_b is the viscosity of the brine,

q_{D1}, q_{D2}, and q_{D3} are the dimensionless, piecewise total fluxes, which can be obtained from Equations (27) and (28) in Mathias et al. (2011b),

z is the similarity transform variable for time t and radial distance r

$$z = \frac{\pi\phi\rho_g Hr^2}{M_0 t},$$

and z_T and z_L are locations of the trailing and leading shocks in similarity space, which can be evaluated from Equations (30-35 and 53) in Mathias et al. (2011b).

In Equation (1),

$$F_1(z) = \begin{cases}(\alpha z_E)^{-1} - \frac{3}{2} + \ln\left(\frac{z_E}{z}\right) + \frac{z - z_L}{z_E}, & z_E < \frac{0.5615}{\alpha} \\ E_1(\alpha z), & z_E > 0.5615/\alpha\end{cases}$$

with $\alpha = \dfrac{M_0 \mu_b (c_r + c_b)}{4\pi \rho_g H k}$,

$$F_2(z) = -\frac{1}{\mu_g} \int_z^{z_L} \left(\frac{k_{ra}}{\mu_b} + \frac{k_{rg}}{\mu_g} \right)^{-1} \frac{1}{z} dz$$

where ρ_b is the density of the native brine,

ϕ is the porosity,

z_E is similarity transform for the radial extent of the formation r_E,

k_{ra} and k_{rg} are the relative permeabilities of the aqueous phase and gas phase, respectively,

and c_r and c_b are the compressibilities of rock and brine, respectively.

For more details of the analytical model, see Mathias et al. (2011b).

17.3 Modeling scenario and parameters

We perform modeling for a domain consisting of the southern part of the Dalder Monocline. The modeling domain covers an area of about 22260 km^2 (see Figure 3 and 4 in PART B for maps). The storage formation is idealized into a layer with uniform thickness and homogeneous permeability and porosity. The domain is bounded by faults in the south (boundary AC in Figure 4 in PART B) which may be considered as impermeable. The other boundaries can be considered open. The overlying and underlying formations are assumed to be impermeable. Since we are considering multiple injection wells distributed over the modeling domain, the pressure perturbation from each well will interfere with that from the surrounding wells. As a result, the wells that are not close to the open domain boundaries will effectively behave as if they were surrounded by a no-flow boundary. Therefore, in the modeling of pressure buildup in the vicinity of the injection well, we consider a closed domain for each individual injection point with domain radial extent r_E determined by the domain area A and the number of injection wells n_w, that is, $r_E=(A/2\pi n_w)^{0.5}$.

Base case parameters used for the pressure analysis are given in Table 1 (based on the averaged values of property maps given by SLR for the Dalders Monocline). The fluid properties depend on the pressure and thus cannot be known beforehand. Therefore, we use iterative procedures to find the pressure and at the same time the fluid properties such as densities, viscosities, dissolved mass fractions of CO_2 in water and water in CO_2.

Table 1. Base-case modeling parameters for pressure buildup at the injection wells.

Parameter	Value and unit
Initial pressure P_{ini}	120 bars
Number of wells n_w	5
Permeability k	40 mD
Thickness H	50 m
Porosity φ	0.12
Injection time t	50 years
Rock compressibility c_r	4.5×10^{-10} Pa^{-1}
Brine compressibility c_b	3.54×10^{-10} Pa^{-1}

17.4 Estimation for maximum injection rates

We model the pore pressure at the injection well for a series of injection rates. Sensitivity of the injection rate – pressure dependence to the modeling parameters is explored for formation thickness, permeability and number of wells.

Results (Figure 1-3) suggest that pore pressure (and thus pressure buildup) increases approximately linearly with injection rates. They also show that the pore pressure increase is very sensitive to the chosen parameters (formation thickness, permeability and number of wells).

In order to estimate the maximum injection rates, we need to know the sustainable pressure buildup that a given storage system is expected to tolerate without geomechanical degradation (such as microfracturing and/or fault reactivation) for the sealing structures (Rutqvist et al., 2007; Zhou et al., 2008). However, the sustainable pressure buildup should be obtained on a site-by-site basis since it is depending on the in situ stress field and the geomechanical properties of the rock units. Due to the lack of detailed measurements of geomechanical properties of the sealing structure and in situ stress condition in our case here, we assign a maximum pressure increase of 50% from the initial hydrostatic pressure. This corresponds to a maximum pore pressure of 180 bars (or maximum pressure buildup of 60 bars) close to the injection well. The threshold pressure increase of 50% is in accordance with Zhou et al. (2008). We note that the sustainable pressure buildup should be reevaluated once site-specific information on in situ stress and geomechanical properties is obtained.

According to the base case result (the green curves in the following figures), if we assign a threshold pore pressure of 180 bars, then the maximum injection rate is about 0.5 Mt/yr per well. This would correspond to 2.5 Mt/yr in total for five wells.

Figure 1 shows how decreasing/increasing layer thickness influences the maximum injection rate (e.g., increasing the thickness from 50 m to 60 m would increase the injection rate per well to about 0.7 Mt/year). Figure 2 in turn shows the large effect of formation permeability. For example, increasing the permeability to 80 mD would increase the allowed injection rate to over 0.8 Mt/year. Finally, Figure 3 shows the effect of number of injection wells, where it is clear that distribution of the injection to a larger number of wells reduces the injection pressure.

The base-case result of 0.5 Mt/year was used as starting point in the subsequent numerical simulations (PART B and D) with TOUGH2 and VE-models, where local variations in material properties, thickness etc., time-dependent behavior and variable boundary conditions could be taken into account more accurately.

17.5 Discussion

We have performed analytical modeling of pressure buildup for the southern part of the Dalders Monocline using a recently developed semi-analytical solution. For the base-case parameters we obtained a maximum total injection rate of 2.5 Mt/yr, assuming a maximum sustainable pressure increase of 50% from the hydrostatic condition. Sensitivity study results indicate that the maximum injection rate can be sensitive to parameters such as formation thickness, permeability and number of wells.

It is worth noting that the 2.5 Mt/yr (multiplied by 50 years) should not be directly used for pressure-limited capacity estimation. In our case here, we have assumed impermeable sealing units for the storage formation. The injection-induce pore pressure could be dissipated by brine displacement through caprock if the permeability of the caprock is not extremely low and the compressibility of the caprock is large (see e.g., Chang et al. 2013). In addition, pore pressure could be further relieved through brine production wells. However, the technical and economic feasibility should be evaluated for this option.

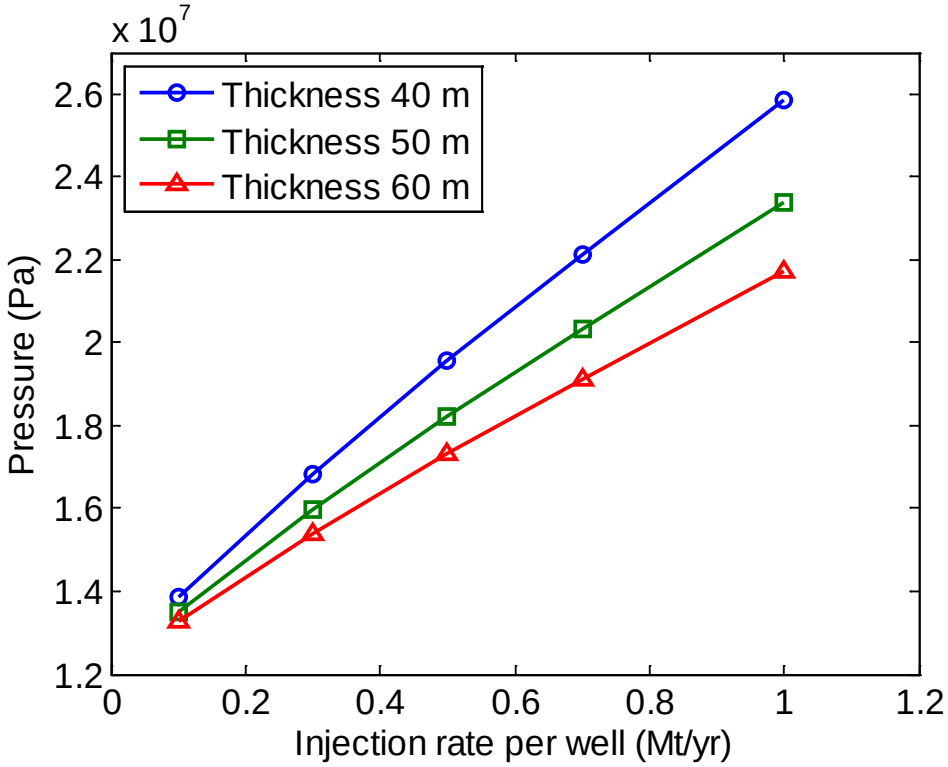

Figure 1. Sensitivity of injection pressure to injection rate for different layer thicknesses.

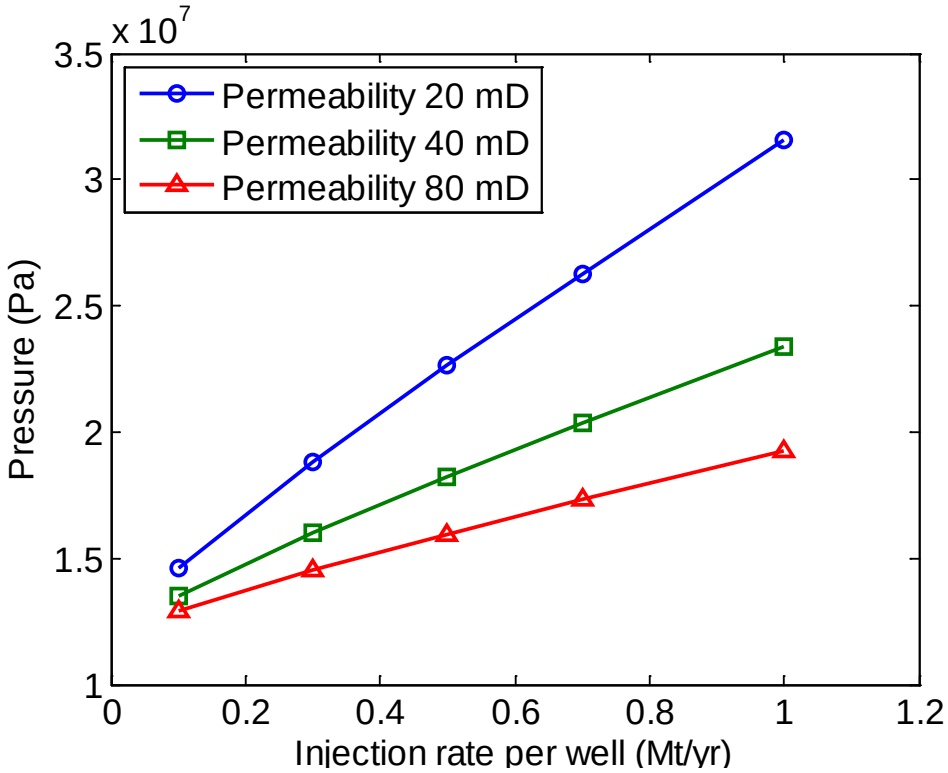

Figure 2. Sensitivity of injection pressure to injection rate for different layer permeabilities. Injection pressure is very sensitive to formation permeability.

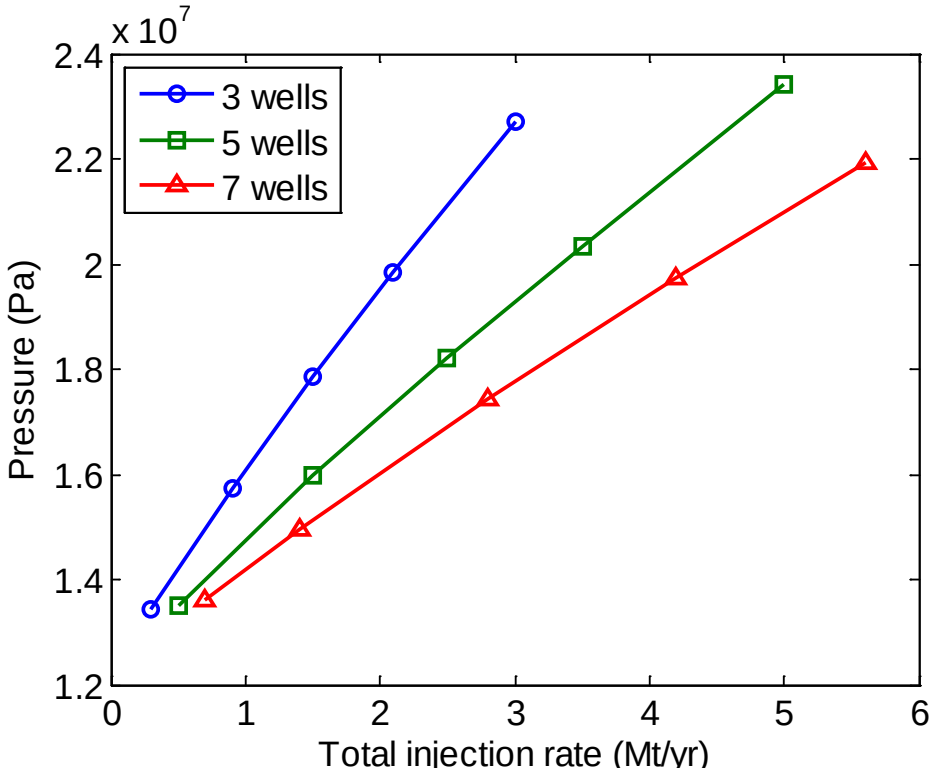

Figure 3. Sensitivity of injection pressure to injection rate for different number of wells.

17.6 References

Chang KW, Hesse MA, & Nicot JP (2013) Reduction of lateral pressure propagation due to dissipation into ambient mudrocks during geological carbon dioxide storage. *Water Resour. Res.* **49**, 2573-2588, doi:10.1002/wrcr.20197.

Mathias SA, González Martínez de Miguel GJ, Thatcher KE, & Zimmerman RW (2011a) Pressure buildup during CO_2 injection into a closed brine aquifer. *Transport in Porous Media* **89**, 383–97.

Mathias SA, Gluyas JG, González Martínez de Miguel GJ, & Hosseini SA (2011b) Role of partial miscibility on pressure buildup due to constant rate injection of CO_2 into closed and open brine aquifers. *Water Resources Research* **47**, W12525.

Rutqvist J, Birkholzer JT, Cappa F, & Tsang CF (2007) Estimating maximum sustainable injection pressure during geological sequestration of CO_2 using coupled fluid flow and geomechanical fault-slip analysis. *Energy Convers. Manag.* **48**, 1798–1807, doi:10.1016/j.enconman.2007.01.021.

Zhou Q, Birkholzer JT, Tsang CF, and Rutqvist J (2008) A method for quick assessment of CO_2 storage capacity in closed and semi-closed saline formations, *Int. J. Greenh. Gas Control*, **2**, 626–639, doi:10.1016/j.ijggc.2008.02.004.

PART B

18.0 SIMULATION OF CO2 SPREADING AND RELATED PROCESSES WITH TOUGH2 MODEL – DALDERS MONOCLINE

Liang Tian, Fritjof Fagerlund and Auli Niemi

18.1 Dalders Monocline - Model description

18.1.1 Digital elevation model (DEM) and SLRs static model

The modeled region is centered at the Baltic Sea basin (Figure1). The subsurface topography is described by 1000 m grid Digital Elevation Model (DEM). A three- dimensional geological structure model is constructed for an area of dimensions 549 km x 369 km among which the Dalders Monocline static model is mapped covering an area of 72,168 km^2. Table 1 summarizes the geo-hydrological properties of the static model. All the information concerning the static model and related parameter values for this modeling work have been obtained from SLR.

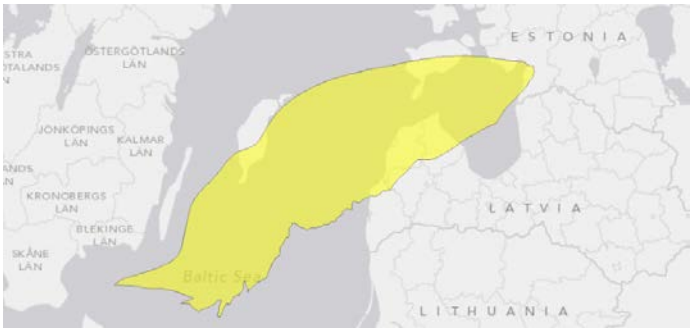

Figure 1. Map view of the modeling region highlighting the Mid-Cambrian (Dalders Monocline)

Table 1. Summary of the geo-hydrological properties mapping from the static model

Data Resolution	1000m		
Porosity	4,30%	-	20,60%
permeability	8,5 mD	-	300 mD
formation top	-225 m	-	-1756 m
Thickness	0 m[#]	-	82 m

#note: the formation pinches out at the edge of the reservoir which results in zero thickness.

18.1.2 Conceptual model and numerical grid

For the purpose of numerical modeling with the TOUGH2 code (Pruess, 1999) several conceptual models and numerical grids were considered. The first coarse model considered the entire region of interest and was a 'psuedo-3D' model consisting of one layer of variable thickness in the vertical direction, and a 2D plane with uniform size grid blocks of dimension 5000 x 6000 m (Figure 2). The permeability, porosity, top and bottom elevations were retained by linear interpolation from the information provided by SLR. No vertical discretization was included in this first model. As can be seen in Figure 2, the formation is deepest in the South-Eastern part and gradually becomes thinner and shallower towards North-West.

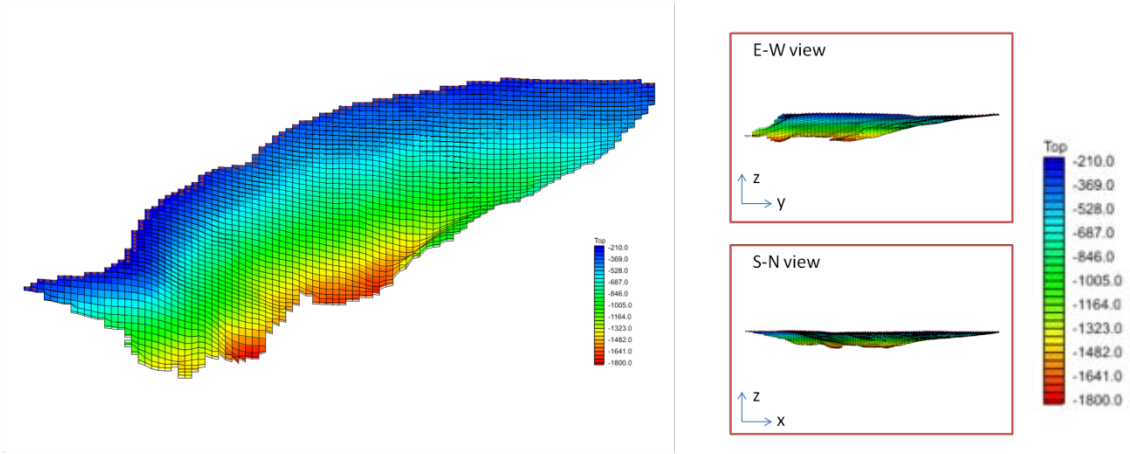

Figure 2. Coarse model for the Dalders Monocline - the color indicates the elevation of the formation top (from the mean sea level in units of m).

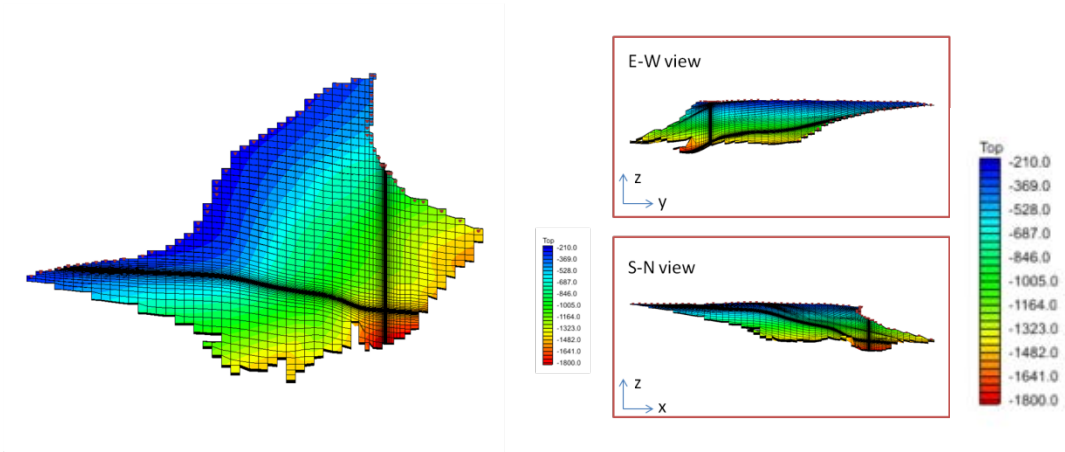

Figure 3. Model for the Southern Dalders Monocline - the color indicates the elevation of the formation top (from the mean sea level in units of m). Finer discretization in the vicinity of the injection well.

A second model was created focusing only on the southern half of the Dalders Monocline static model where the cap-rock integrity is most confidently identified. In this model also a more refined grid is used in the vicinity of the injection well, by using a gradual refinement method. For this second domain both 'pseudo-3D' and a full 3D models were considered. In the full 3D case the model was vertically discretized into 7 element layers. As insufficient information was available concerning the local heterogeneity in the vertical direction, permeability and porosity were assumed vertically homogeneous. No permeability anisotropy was considered. The vertical discretization does still allow a more realistic evaluation of the buoyancy flow of the upwards migrating CO_2.

An example discretization of the model for the southern part is shown Figure 3. In this example only one injection well is shown. All the simulation scenarios considered will be summarized in detail in section 1.4.

18.1.3 Initial and boundary conditions

The initial condition for pressure is obtained by assuming a gravity equilibrium condition. Salinity is assumed constant in the entire modeling domain and to be 11.54% (wt. NaCl based on data from well E7-1). Due to lack of thermal information, isothermal condition is considered with a constant temperature of 50℃.

In these simulations the overlying cap-rock is assumed impermeable and closed boundary conditions are used both at the top and bottom of the modeling domain. For the lateral boundaries the following boundary conditions are used (Figure 4.): in the north-east and north (A-B'-B) the boundary is open (constant pressure boundary), in the south and south-east side (A-C-B), there is uncertainty in the character of the boundary condition and therefore both open and closed conditions are considered. When focusing only at the southern Dalders Monocline the east side boundary (B'-C) is set open, allowing fluid to enter the north-eastern part of the formation.

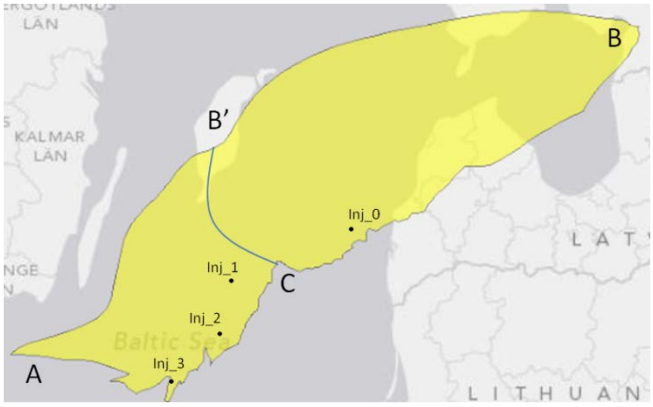

Figure 4. Boundary condition locations and locations of the injection wells.

The injection of CO_2 takes place through one or several vertical injection wells. The locations of the injection wells are presented in Figure 4 as well. The injection rate was initially determined by the semi-analytical calculations presented in Part A. The supercritical CO_2 is injected continuously for 50 years. Then the post-injection development is monitored for 950 years. The total simulation covers 1000 years.

18.1.4 Model Scenarios

The model scenarios are summarized in Table 2.

Table 2. Model scenarios

Case	Model domain	Conceptual Model	Boundary conditions		Injection Rate ($MtCO_2$/year)			
			A-B'-B (A-B')	A-C-B(A-C)	inj_0	inj_1	inj_2	inj_3
1	Dalders Monocline	Psuedo 3D	Open	Closed	3,0	-	-	-
2	Southern Dalders Monocline (Case 2-5)	Psuedo 3D	Open	Closed	-	-	1,0	-
3		Psuedo 3D	Open	Open	-	-	1,0	-
4		3D	Open	Closed	-	-	0.5	-
5		3D	Open	Closed	-	0,5	0,5	0,2

The purpose of Case 1 is to obtain a first estimate of the general CO_2 migration pattern. Cases 2 to 4 are designed to test specific assumptions, namely boundary conditions and the effect of vertical discretization. Case 5 is designed to test a specific injection strategy of three wells instead of one well, like in the other cases.

18.2 Numerical Simulations

TOUGH2/ECO2N simulator is used to simulate the migration of CO_2 in the formation. (Pruess et.al, 1999; Pruess, 2005) TOUGH2MP, a massive parallel version of TOUGH2 is used for the more computational demanding 3D simulations. (Zhang et.al, 2008). The two-phase flow characteristic functions are the van Genuchten model (van Genuchten, 1980) for the capillary pressure–saturation function and the van Genuchten–Mualem model (Mualem, 1976; van Genuchten, 1980) for the relative permeability functions. To simulate the CO_2-brine two-phase flow in the heterogeneous medium, the Leverett scaling (Leverett, 1941) is applied, i.e. capillary entry pressure (P_c) is scaled in relation to the permeability according to

$$P_c = P_{c,ref}\sqrt{\frac{k_{ref}}{k}}$$

The parameters used for the simulations are listed in Table 3. These parameters are chosen as typical literature values due to a lack of relevant data. They fall into the range of parameters used by, for example, Doughty (2007) and Zhou et al. (2010). The choice of parameters will have an impact on the simulation results. For overpressure estimation, the impact of capillary pressure would be negligibly small (Mathias et al., 2011), while the relative permeability parameters may have a sensible effect. However, the uncertainty in estimating overpressure due to unknown relative permeability parameters will likely be less significant than that resulted from other parameters such as permeability, porosity etc. Nevertheless, it would be beneficial for modeling if more field data and core measurements especially regarding two-phase flow properties can be obtained in the future.

Table 3. Parameters used in the simulations

Parameters	*Values*
Irreducible water saturation, $S_{l,r}$ [-]	0.300
Residual gas saturation, $S_{g,r}$ [-]	0.050
Van-Genuchten parameter, m [-]	0.457
Reference for Leverett scaling on capillary pressure, P_{ref} [Pa]	1.98×10^{4}
Reference permeability, k_{ref} [mD]	100
Pore compressibility [Pa^{-1}]	$4.5x10^{-10}$

The Ground Water Modeling system (GMS, Aquaveo, LLC) is used to create the integral finite difference method grids. A modified version of TMT2 (Borgia et.al, 2011) is used to convert the Modflow 2000 grid to TOUGH2 format. The grid block information is summarized in Table 4.

Table 4. Numerical grids used in the different cases

	Modeling Domain	Vertical Section(s)	Grid refinement			Number of grid elemets	Case
			Min (m)	Max (m)	Bias		
1	Dalders Monocline	1	-	-	-	7 154	1
2	Dalders Monocline Southern	1	10	5000	1.1	4 968	2,3
3	Dalders Monocline Southern	7	10	5000	1.1	34 776	4
4	Dalders Monocline Southern	7	50	5000	1.3	73 794	5

18.3 Results and discussion

18.3.1 Case 1

A coarse grid is used for a preliminary injection simulation run with an injection rate of 3MtCO_2 / year. To be able to describe the pressure build up, an overpressure factor (F_{op}) is defined as

$$F_{op} = (P - P_{hydro\text{-}initial}) / P_{hydro\text{-}initial} \times 100\%$$

where the P is the injection pressure during the simulation run and $P_{hydro\text{-}initial}$ is the initial pressure.

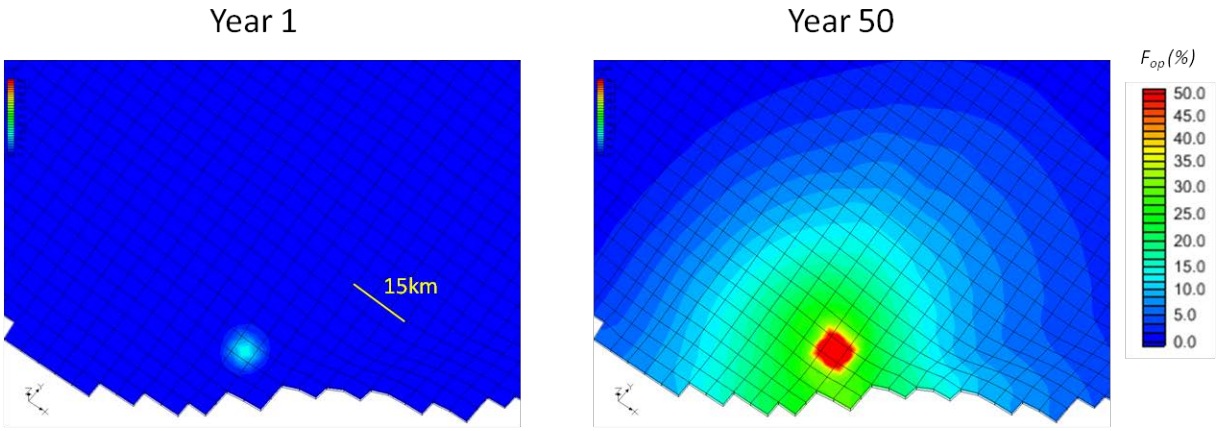

Figure 5. Case 1 - The over pressure factor F_{op} shows the pressure build up at year 1 and year 50 (end of injection).

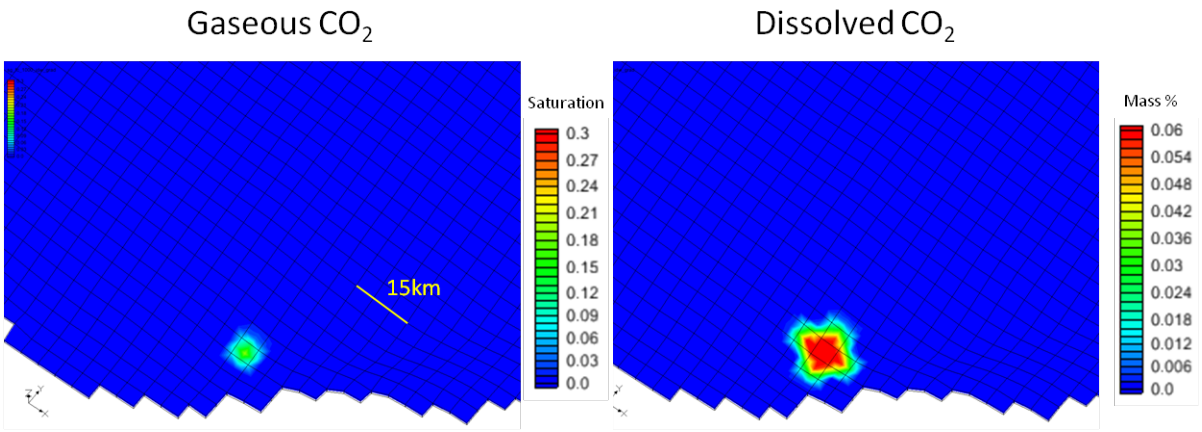

Figure 6. Case 1 - CO_2 plume and distribution of dissolved CO_2 (as mass fraction) at the end of year 1000.

The results show that the spreading of the CO_2 plume only takes place in a few grid blocks in the vicinity of the injection well. A pressure build-up (F_{op}) of 102% is observed at the injection grid at

the end of year 50. It should be pointed out that the grid is very coarse and the results can only be taken as indicative. The large grid size used for the injection region in this case will lead to an underestimation of the maximum overpressure at the injection location. In the subsequent cases, we have refined the grid to have cell sizes of 10-50 meters at the injection locations. This is deem adequate to yield reasonable estimates of maximum overpressure, given that the pressure drop across a radial distance of 50 is small compared to the overpressure at the injection location (This is due to the development of dry out zone with fully saturated low viscosity CO_2).

18.3.2 Case 2 and Case 3

Studies of the cap-rock characteristics, presented elsewhere in this report indicate best cap-rock integrity in the southern part of the domain. Therefore this domain was selected for the subsequent modeling studies. A finer grid was created using gradual grid refinement at the vicinity of the injection well. The first cases for this domain, Cases 2 and 3, only considered one variable thickness layer in the vertical direction. The difference between the cases was the character of the lower boundary that was closed in Case 2 and open in Case 3.

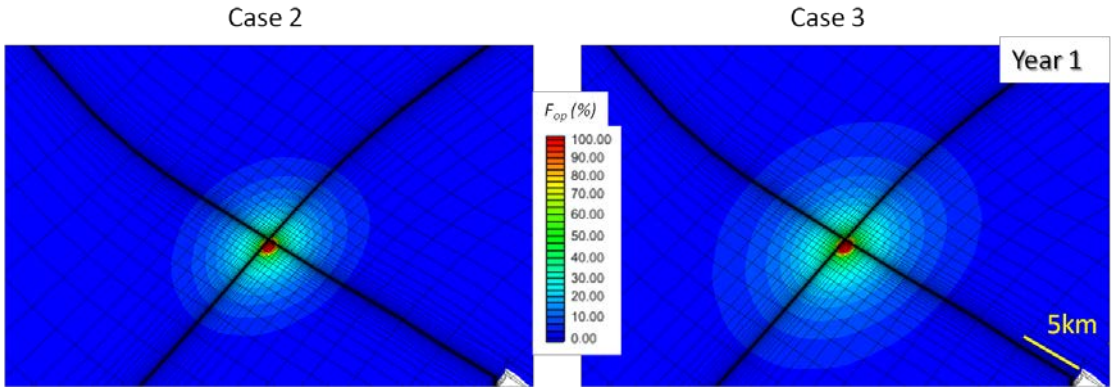

Figure 7. Cases 2 and 3 - Pressure build-up, presented as the overpressure in relation to the original in-situ pressure, after 1 year CO_2 injection.

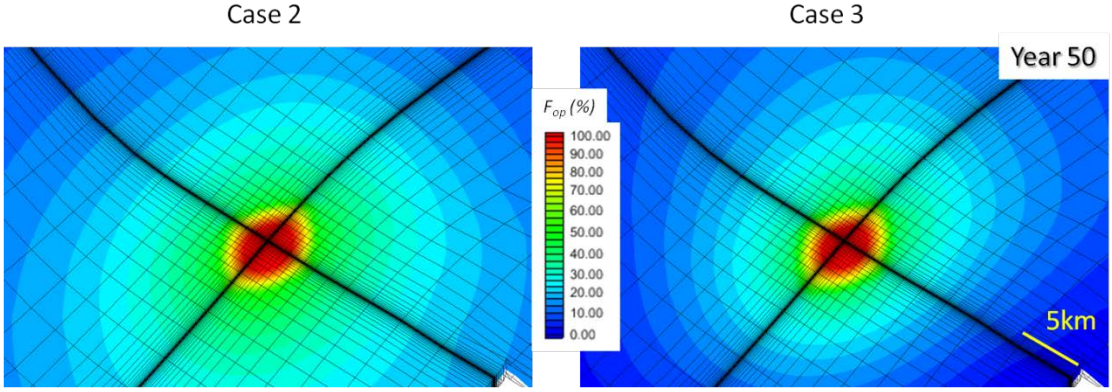

Figure 8. Cases 2 and 3 - Pressure build-up, presented as the overpressure in relation to the original in-situ pressure, after 50 year CO_2 injection.

Simulated pressure evolution, presented as overpressures in relation to the original in-situ pressure are shown in Figures 7 and 8. The pressure plumes from both cases are identical at the beginning of the injection (at year 1). Over pressure factors, F_{op} of 150% and 148% are observed at the injection blocks for Case 2 and Case 3, respectively.

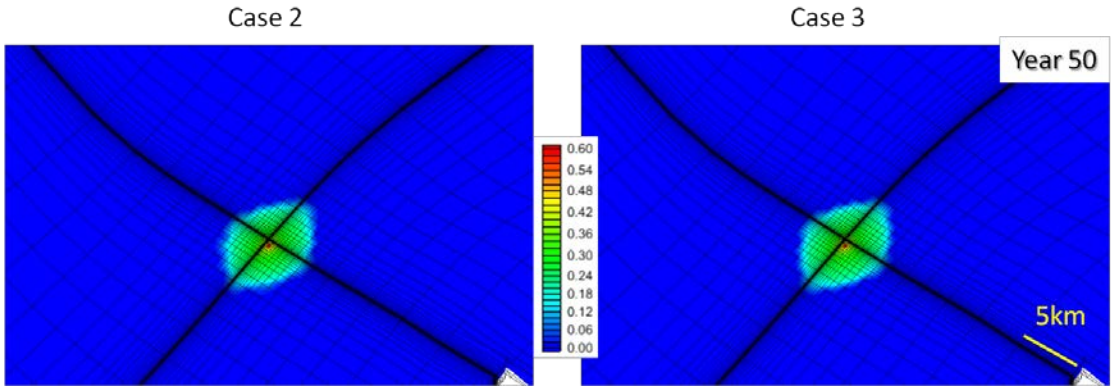

Figure 9. CO_2 saturation at the end of injection (year 50).

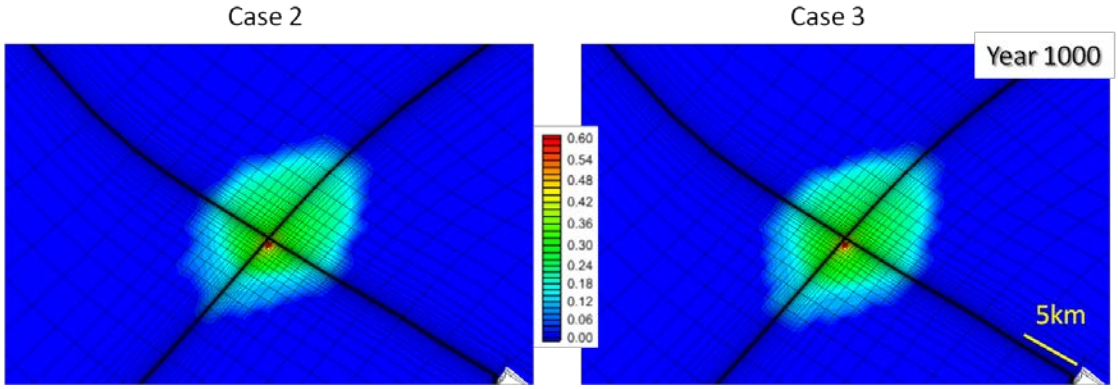

Figure 10. CO_2 saturation at the end of simulation (year 1000).

Identical CO_2 plumes are observed for Case 2 and Case 3 at the end of injection. At the end of simulation (year 1000) the up-dip CO_2 migration is observed for both cases but the trend is more obvious in Case 2. This is caused by the close boundary (A-C). Overall, the differences in these simulations due to the different lower boundary conditions are very small.

18.3.3 Case 4

Due to the significant pressure build-up observed in previous simulation runs, the injection rate was halved to 0.5 Mt CO_2 per year (at Inj_2) in the further simulations. A closed boundary condition at A-C (as in Case 2) was identified as a more conservative assumption, and thus again considered in Case 4.

In order to better resolve the migration pattern of the injected CO_2, a vertical discretization was also implemented. The modeling domain was divided equally in the vertical direction into seven layers. The injection well was perforated in the bottom-most section where the CO_2 injection is assumed to take place.

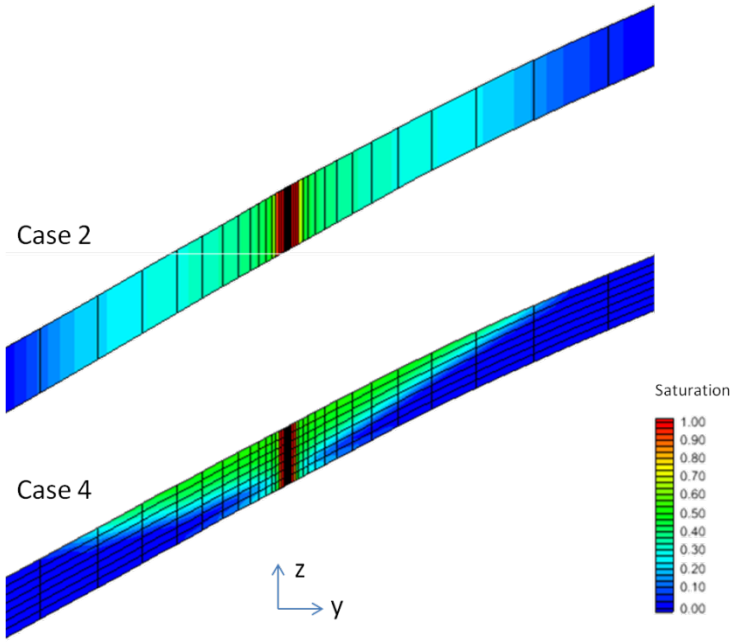

Figure 11. Case 4 - CO_2 saturation at the end of injection (Year 50). The figures show east-west view at the cross section of the injection block. (Exaggeration in z by 25)

It can be observed that the injected gaseous CO_2 migrates into the upper part of the aquifer as the gaseous phase CO_2 is lighter than the formation brine. As CO_2 migrates preferably in the uppermost layer, less formation volume is used by the CO_2 and this leads to a larger plume size compared to Case 2. The size of CO_2 plume in Case 4 is similar to that observed in Case 2 even though the injection rate is halved in Case 4 in comparison to Case 2. Some CO_2 spreading in the bottommost section is also observed in Case 4. This phenomenon is likely related to the still relatively coarse discretization. Further studies could address this, but the results shown in Figure 11 are nevertheless deemed to give a good estimation of overall plume spreading.

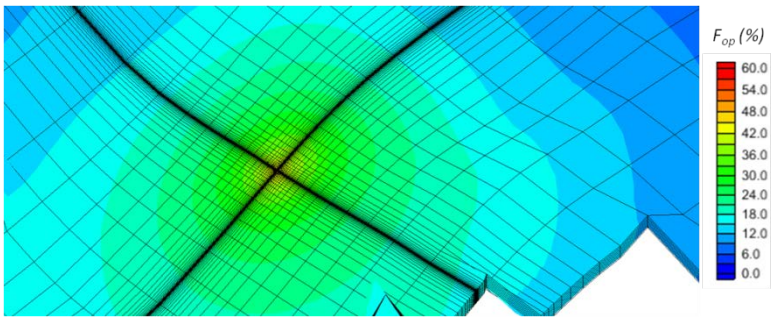

Figure 12. Case 4 - Pressure profile at the end of injection (top section, Year 50).

Maximum observed pressure build-up observed in the vicinity of the well was 59% (Figure 12). It should be pointed out that even though the injection location is in the bottom section of the well, the pressure profile does not vary significantly in the vertical direction.

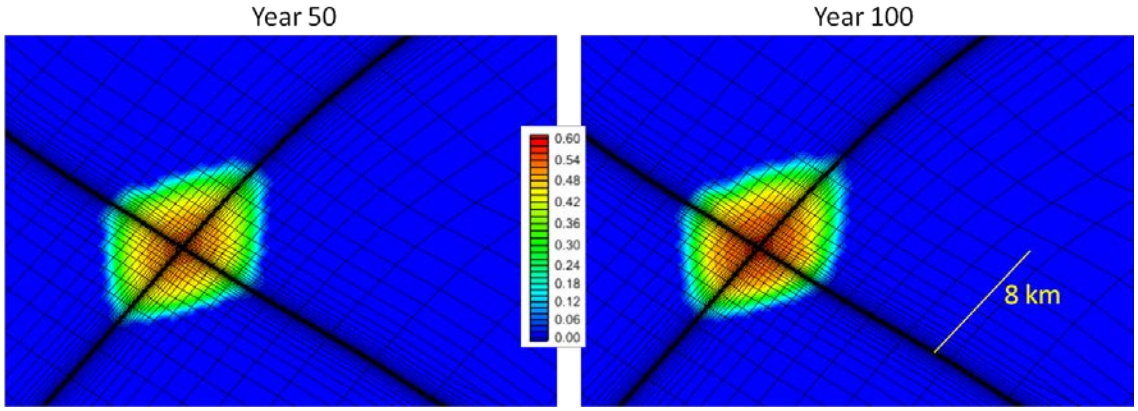

Figure 13. Case 4 - CO_2 saturation at the end of 50-year injection (left panel) and at the end of year 200 (right panel). Note that only the top section is shown in these figures.

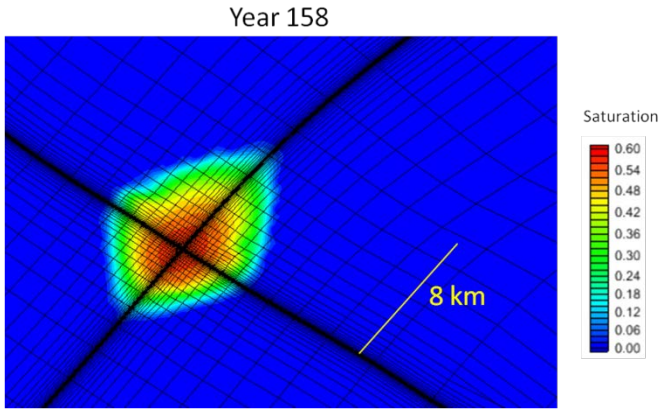

Figure 14. Case 4 - CO_2 saturation at end of year 158.

Figures 13 and 14 show the CO_2 plume spreading at the end of injection (50 years) and at 100 and 158 years. These TOUGH2MP runs were stopped at year 158 due to the time limits of the computation. The results show that during the last 100 year period the plume front has moved less than the length of one grid block in the up-dip direction. The plume front at the end of simulation is less than 8 km up-dip from the injection well. The dilution of the plume can also be observed, caused by the residual trapping and dissolution into formation water.

18.3.4 Case 5

Three injection wells were considered in this last scenario. The model used in Case 4 was modified by adapting grid refinements in the vicinity of all three injection wells. The initial and boundary conditions were the same as the ones used in Case 2. The following are preliminary results from the TOUGH2MP simulation runs, showing the pressure and CO_2 saturation evolution at the end of the 50 years injection. Due to the extensive character of these simulations, the evolution after the end of the injection are not included into the present report but will be presented in subsequent works.

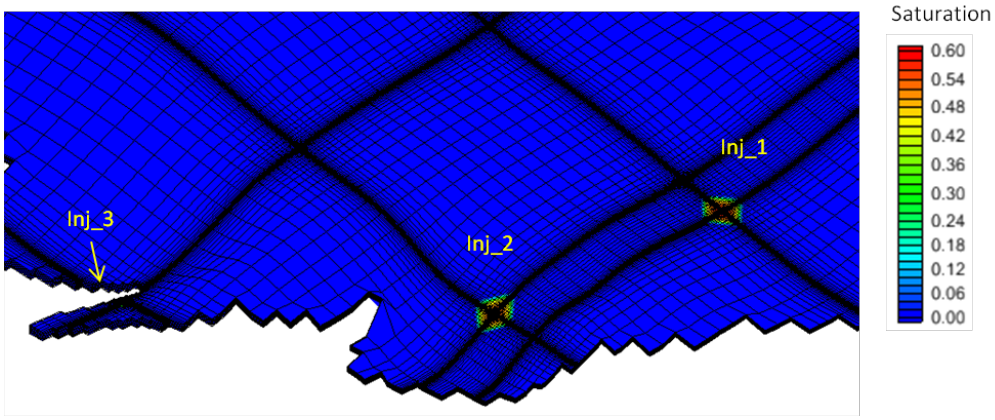

Figure 15. Case 5 - CO_2 saturation at the end of 50-year injection (top section).

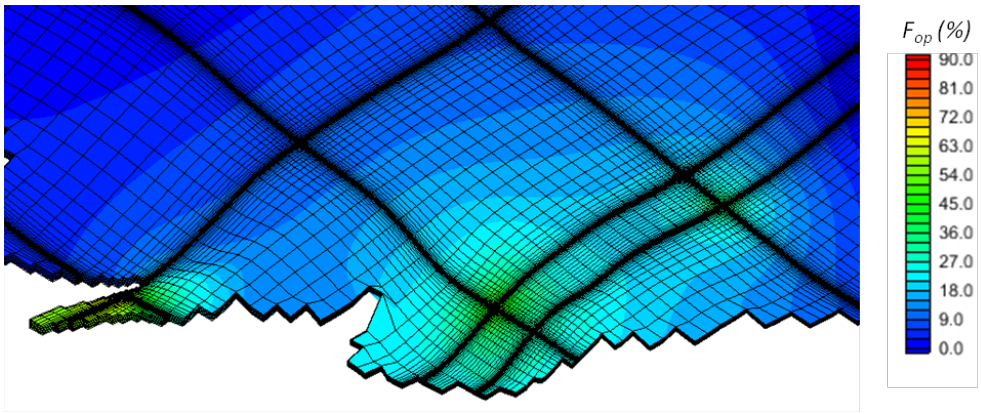

Figure 16. Case 5 - Pressure profile at the end of 50-year injection (top section).

The plume shape at the central injection well (inj_2) is similar to the one observed in Case 4. A pressure buildup of about 60% is observed at inj_2. This is in line with the analytical solution from Part A .When comparing with the results of Case 4, it can be seen that the influence from nearby injection well to the maximum pressure is quite small, which is due to the relative large distance (about 47 km) to the nearest injection well, inj_1. The maximum pressure increase is about 88%

(averaged in the vertical direction) at inj_3 where the lowest permeability is identified among the three injection wells.

18.4 Concluding remarks

The strengths of the TOUGH2/ECO2N model include well-developed equations of state (EOS) for the CO_2-brine system, the ability to account for both dissolution of CO_2 into brine and evaporation of brine into the CO_2-rich phase as well as capability to handle complex geometries in a flexible manner. In the previous chapters the complexity of the modeling is gradually increased starting from coarse 2D and pseudo-3D simulations and proceeding to full 3D models. In terms of detailed CO_2 migration pattern, one has to rely on a full 3D model (TOUGH2MP), while the earlier versions allow preliminary estimates concerning the effects of boundary conditions etc. It should be mentioned that due to the still relatively coarse discretization the numerical dispersion effect will likely cause overestimation of CO_2 dissolution. Further studies should involve even more extensive grid refinement/grid convergence studies, which were beyond the scope and time limitations of the present study.

A very conservative residual gas residual saturation (S_{gr}= 0.05) was used in all the previous simulations. It is likely that the residual gas saturation will be larger, thus further reducing the plume spreading. All models were built assuming smooth caprock topography and impermeable cap-rock. Including a low-permeability cap-rock in the models would likely reduce the pressure increase while still not causing any undesired CO_2 transport to upper layers. Finally, isothermal conditions are assumed in all simulations. Thermal conditions do influence some of the relevant processes such as CO_2 dissolution into the formation brine, and non-isothermal conditions could be considered in future work when more data are available.

18.5 References

Borgia A, Cattaneo L, Marconi D, Delcroix C, Rossi EL, Clemente G, Amoroso CG, Lo Re F, & Tozzato E (2011) Using a MODFLOW grid, generated with GMS, to solve a transport problem with TOUGH2 in complex geological environments: The intertidal deposits of the Venetian Lagoon. *Comput. Geosci*. **37**, 783-790.

Doughty, C. (2007), Modeling geologic storage of carbon dioxide: Comparison of non-hysteretic and hysteretic characteristic curves, *Energy Convers. Manag.*, *48*(6), 1768–1781.

Leverett MC (1941) Capillary behaviour in porous solids. *AIME Trans*. **142**, 152-169.

Mathias SA, González Martínez de Miguel GJ, Thatcher KE, & Zimmerman RW (2011) Pressure buildup during CO_2 injection into a closed brine aquifer. *Transport in Porous Media* **89**, 383–97.

Mualem Y (1976) New Model for Predicting Hydraulic Conductivity of Unsaturated Porous-Media. *Water Resour. Res.* **12**, 513-522.

Pruess K, Oldenburg C, & Moridis G (1999) *TOUGH2 User's Guide, Version 2.0.* Report LBNL-43134, Lawrence Berkeley National Laboratory, Berkeley, California.

Pruess K & Spycher N (2007) ECO2N - A fluid property module for the TOUGH2 code for studies of CO_2 storage in saline aquifers. *Energy Conversion and Management* **48**, 1761-1767.

van Genuchten MT (1980) A Closed-Form Equation for Predicting the Hydraulic Conductivity of Unsaturated Soils. *Soil Science Society of America Journal* **44**, 892-898.

Zhang K, Wu Y, & Pruess K (2008) *User's Guide for TOUGH2-MP A Massively Parallel Version of the TOUGH2 Code*, Report LBNL-315E, Lawrence Berkeley National Laboratory, Berkeley, California.

Zhou, Q., J. T. Birkholzer, E. Mehnert, Y.-F. Lin, and K. Zhang (2010), Modeling Basin- and Plume-Scale Processes of CO2 Storage for Full-Scale Deployment, *Ground Water*, *48*(4), 494–514.

PART C

19.0 SIMULATION OF CO2 SPREADING AND RELATED PROCESSES WITH TOUGH2 MODEL – DALDERS STRUCTURE

Liang Tian, Fritjof Fagerlund and Auli Niemi

19.1 Model description

19.1.1 Description of the Dalders Structure

As for the Dalders Monocline, for Dalders Structure the static geological model and model parameter information for the simulations were provided by SLR. For the Dalders structure there was information available for vertical layering, for which reason the following layers (Table 1) were included into the simulation model.

Table 1. Sub-layer description

Layer	Thickness (m)	Lithology
Mid_Camb_1	56	Sandstone with shale influence
Mid_Camb_2	10	Sandstone
Mid_Camb_3	7	Sandstone with silt/shale
Mid_Camb_4	9	Sandstone
Mid_Camb_5	18	Sandstone with high shale content

Table 2. Summary of the averaged geohydrological properties for the layers

	layer 1	layer 2	layer 3	layer 4	layer 5
Porosity (%)	7,8	12,3	11,7	13,2	5,9
permeability (mD)	19,8	3	24,4	30,9	16,8
layer top (m)	-1425	-1470	-1480	-1487	-1496

19.1.2 Conceptual Model

A 3D model was built based on the 250m x 250 grid of the static model. For the numerical grid, the Mid_Camb_1 layer was further divided in the vertical direction into five sub-layers. Similar, the Mid_Camb_5 layer was divided into two sub-layers. The discretization resulted in a uniform grid of 250m × 250m grid blocks in the horizontal plane and a total of 10 sub-layers in the vertical direction (Figure 1). The total number of grid elements was 17490. The permeability, porosity, top elevation and bottom elevation were retained for each layer by linear interpolation from the static model provided by SLR

19.1.3 Initial and boundary conditions and simulation scenarios

The model domain is initialized by calculating a gravity equilibrium ambient condition. Salinity is assumed constant at 11.54% (wt. NaCl) in the whole domain. Isothermal condition is considered with a constant temperature of 50℃.

Impermeable top and bottom (closed boundary) condition are used as the boundary conditions for the top and bottom of modeling domain. For the lateral boundaries, the northern boundary (B-A-B') is identified coincides with fault lines and considered closed. The southern boundary (B-A'-B') is identified as spill point where the formation continues outside the modeling domain thus set open across all the sub-layers.

The injection of CO_2 is through one vertical well located in the middle, as shown in Figure 1. The well is assumed to be perforated in the bottommost section, where the injection takes place. Supercritical CO_2 is injected continuously for 20 years. The total simulation period is 1000 years. 0.3 $MtCO_2$ / year and 0.5 $MtCO_2$ / year are the two injection rates simulated, based on the semi-analytical calculations in Part A.

19.2 Numerical simulations

TOUGH2/ECO2N model is used to simulate the CO_2 injection and migration in the modeling domain (Pruess et.al, 1999; Pruess, 2005). A description of the modeling tool is given in Part B in connection to the simulations for the Dalders Monocline. The same Leverett scaling of capillary entry pressure is used here also. (Leverett, 1941)

19.3 Results and discussion

Figures 2 to 4 show the simulated pressure increase, CO_2 saturation and mass fraction of dissolved CO_2 at various times for the two injection rates.

Pressure build-up induced by the CO_2 injection is displayed using the overpressure factor (for definition, see Part B). Both 0.3 Mt and 0.5Mt scenarios show moderate pressure increase of less than 50% compared to the in-situ hydro-equilibrium pressure. The pressure increase is more prominent in the 0.5 Mt/year injection case and in both cases the pressure increase reaches the closed northern boundary, even though at low level.

The CO_2 plume front in Case 2 reaches the southern boundary at the end of Year 20. For Case 1 (0.3Mt / year), CO_2 plume front reaches the southern boundary at the end of Year 50. At the end of the 1000 years, the plumes from both cases have moved up-dip while remaining within the 11 km x 4 km observation window.

In Case 1 approximately 0.00005 % of the total CO_2 injected had escaped the model domain through the southern boundary by the end of year 50. In Case 2 the corresponding number is 0.11% of the total injected CO_2. At the end of the 1000 year simulation, the total migration over the formation boundary accounts for 0.15% in Case 1 and 1.96% in Case 2. This is an indication that the proposed injection location should be relocated or less CO_2 should be injected at this location. Further simulations are needed to assess the optimal location for injection wells in the Dalders structure. With an open boundary over which CO_2 migration should be avoided, the effective storage capacity here is limited by the amount that can be stored without migration over the boundary.

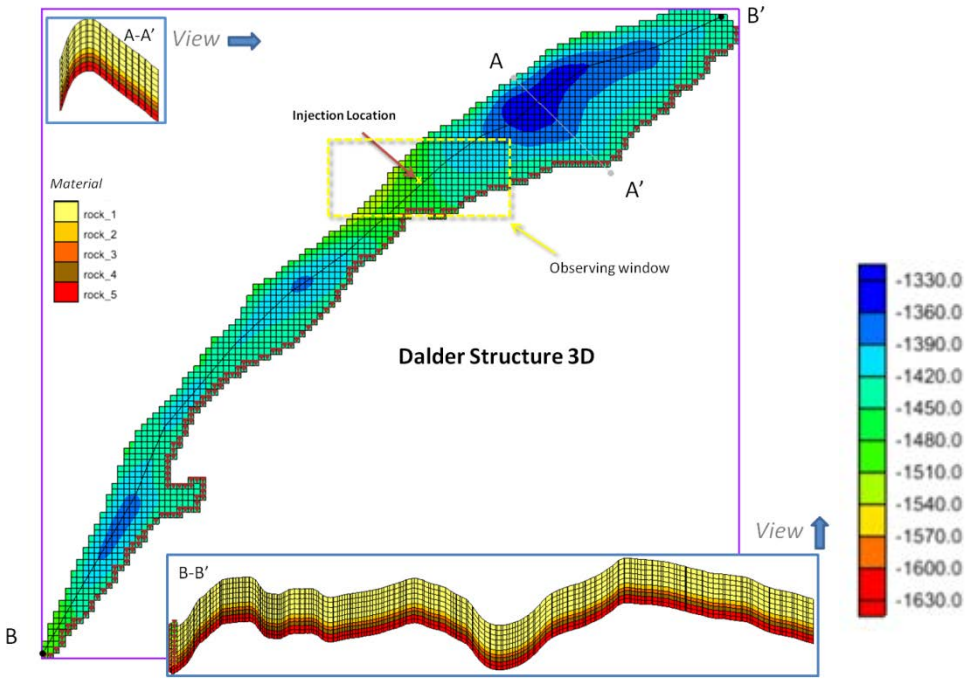

Figure 1. Dalders Structure - Conceptual model, grid and location of the injection well. Colors indicate the depth as expressed in meters in mean sea level.

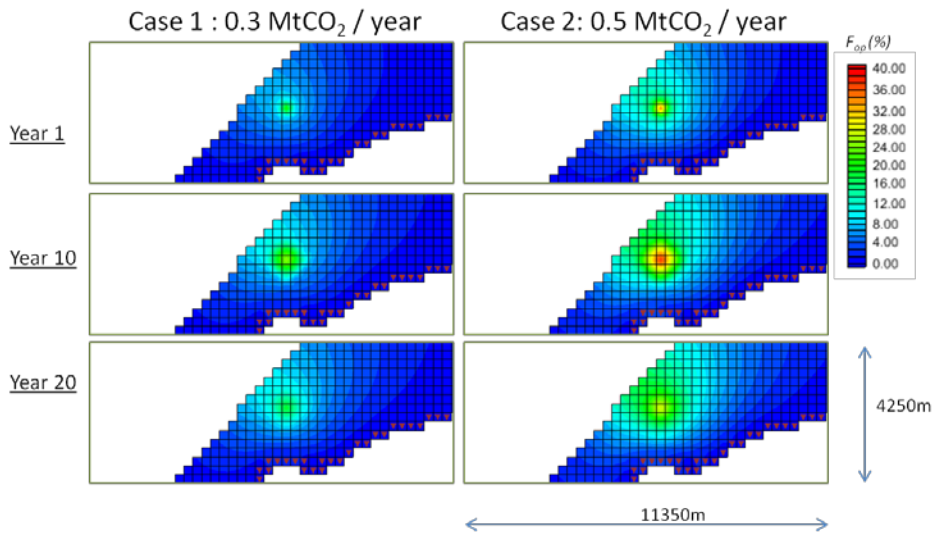

Figure 2. Pressure build-up (bottommost layer). The definition to F_{op} is given in section for Dalders Monocline model.

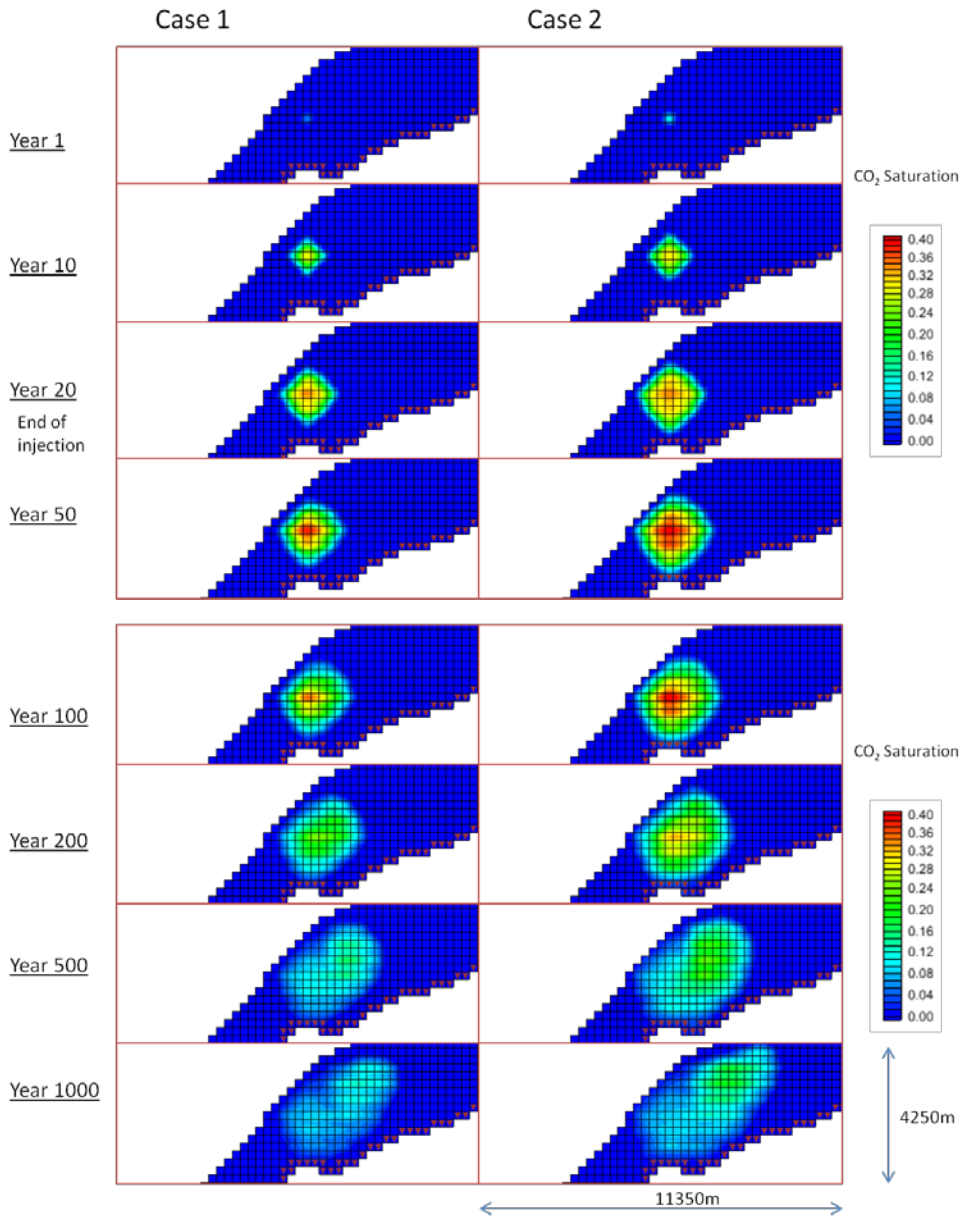

Figure 3. Saturation profile (top layer) at various times. Purple dots show the southern open boundary.

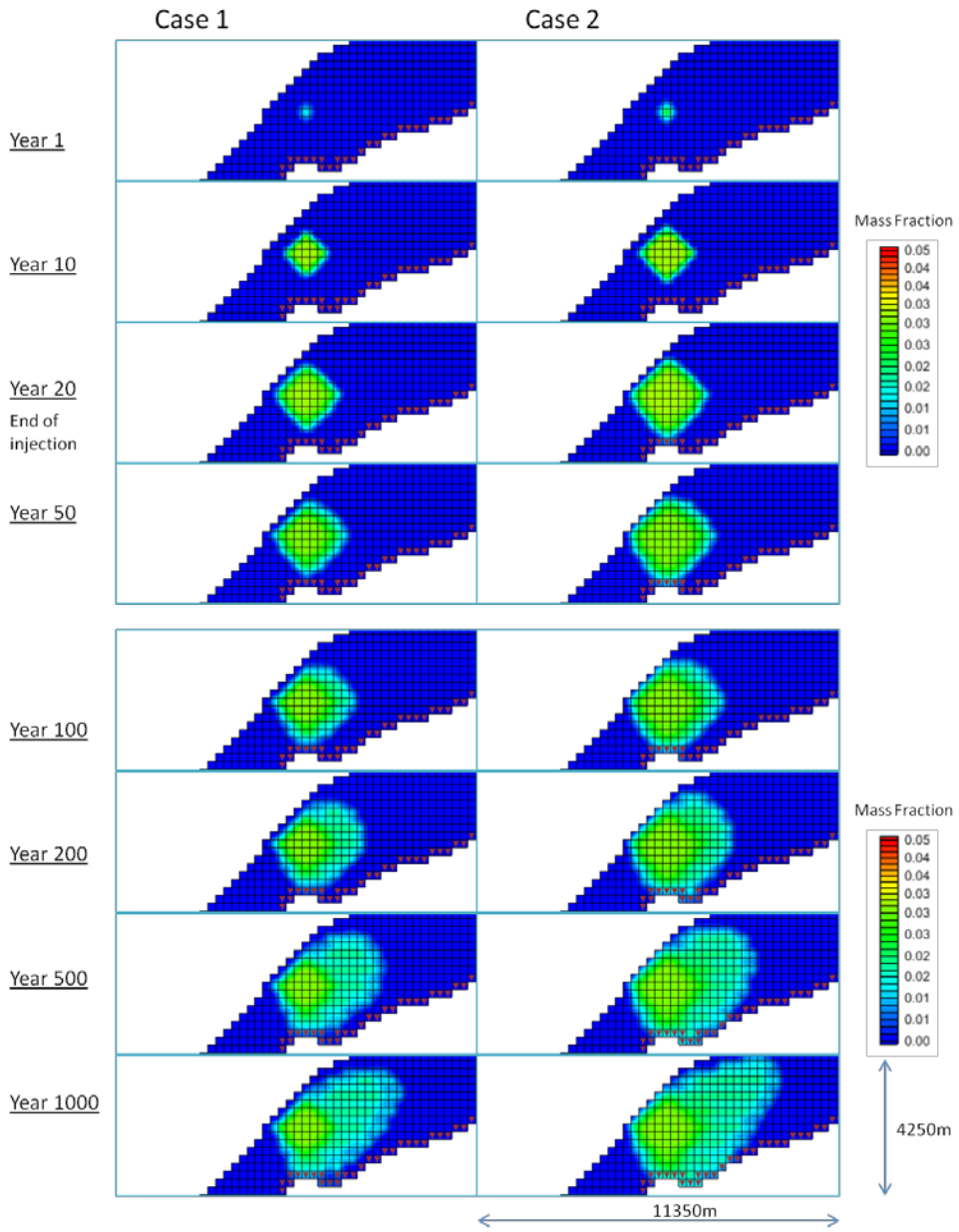

Figure 4. CO_2 dissolution (top layer) at various times. Purple dots show the southern open boundary.

19.4 References

Leverett MC (1941) Capillary behaviour in porous solids. *AIME Trans*. **142**, 152-169.

Pruess K, Oldenburg C, & Moridis G (1999) *TOUGH2 User's Guide, Version 2.0.* Report LBNL-43134, Lawrence Berkeley National Laboratory, Berkeley, California.

Pruess K & Spycher N (2007) ECO2N-A fluid property module for the TOUGH2 code for studies of CO_2 storage in saline aquifers. *Energy Conversion and Management* **48**, 1761-1767.

PART D

20.0 TOPOGRAPHIC EFFECTS OF CO_2 PLUME MIGRATION AND INJECTION PRESSURE ESTIMATION: APPLICATION OF VERTICAL EQUILIBRIUM MODEL TO DALDERS MONOCLINE AND DALDERS STRUCTURE IN BALTIC SEA

Byeongju Jung and Auli Niemi

20.1 Introduction

In this Chapter we present results from so-called vertical equilibrium model as applied to investigate CO_2 spearing and related pressure increase in the Dalders monocline and Dalders structure in Baltic Sea. For this we developed a computational model based on our earlier numerical modes. Our model assumes vertical equilibrium of pressure (Bear, 1972) and enables to consider variable density and viscosity depending on pressure and temperature. The vertical equilibrium approach was originally developed to predict regional groundwater movements in unconfined aquifers, but later extensively used by oil industry due to its accuracy and computational simplicity (Gray *et al.* 2012). Recently, this method is spotlighted again and used for CO_2 injection projects based on the similarity of physical properties of supercritical CO_2 phase and liquid petroleum in a certain condition (Gasda *et al.* 2009; Szulczewski & Juanes 2009; Juanes *et al.* 2010; Gasda *et al.* 2012a; 2012b). The approach implemented in our numerical model follows these CO_2 application approaches.

20.2 Vertical Equilibrium Model for CO_2 Migration

One of the merits using vertical equilibrium approach is the computational efficiency compared to a full 3D model, such as the TOUGH2 simulations presented in Parts B and C of this report. The VE model can, however, include enough complexity to produce more accurate solutions than the available analytical approaches, including the topographic information of the caprock and variable fluid density and viscosity depending on P-T conditions. These factors are important for predicting the fate of the injected CO_2 due to the importance of the buoyancy forces for CO_2 migration.

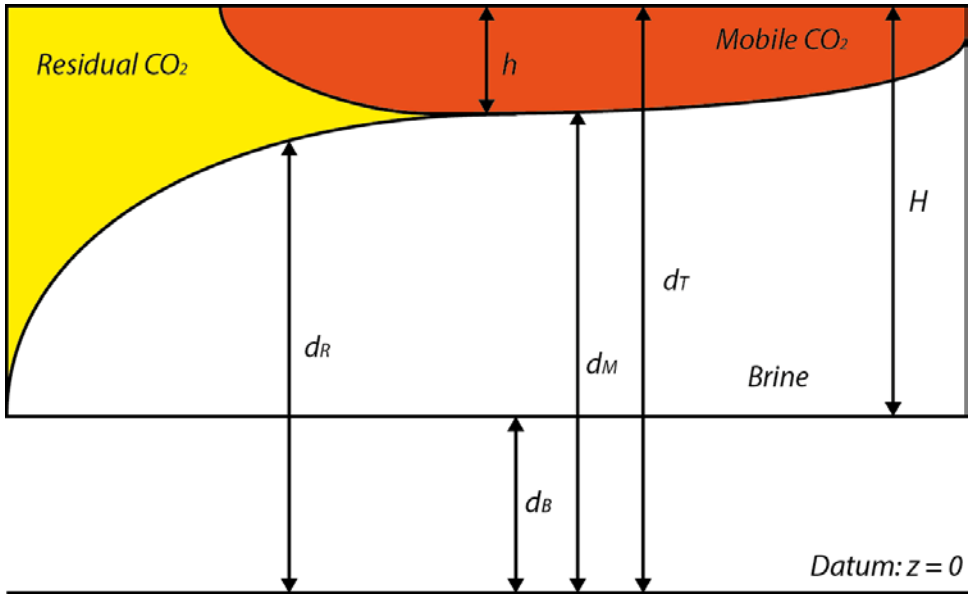

Figure 1. Schematic diagram showing the vertical structure of migrating CO_2 plume after injection (modified from Gasda et al., 2009). H is the confined aquifer thickness, d_T is the distance between the datum to the top of the aquifer, d_B is the distance to the bottom, d_M and d_R represent the distances from the datum to mobile and residual CO_2 plume.

To use the VE approach for dynamic modeling of CO_2 spreading, hydrogeological parameters including permeability, porosity, and compressibility need to be averaged over aquifer thickness. Also, the target aquifer needs to be assumed vertically homogeneous and confined. The capillary pressure between phases and the dissolution of CO_2 were not considered in this study.

To derive the governing equations, we start with the 3D system with two separate phases, which are the non-wetting (CO_2-rich) phase (c) and the wetting (brine) phase (b), having a sharp interface in the confined aquifer of thickness H. The distances between the datum to the top of the aquifer is d_T, and to the bottom is d_B. d_M and d_R represent the distances between the datum and the mobile and residual CO_2 plumes, respectively. Thus, the depth of mobile CO_2 plume, $h = d_T - d_M$ (Fig. 1).

Beginning with the conservation of mass for each phase (α) in the system, where $\alpha = b, c$, we can write (Bear, 1972)

$$\frac{\partial(\phi\rho_\alpha S_\alpha)}{\partial t} = \nabla \cdot (\rho_\alpha \mathbf{q_\alpha}) = \rho_\alpha F_\alpha \qquad (1)$$

where ϕ is the porosity, S_α is the saturation, ρ_α is the density of fluid, F_α is the source and sink term (volume per time), and $\mathbf{q_\alpha}$ is the volumetric flux.

After the standard vertical averaging procedure, we can write (Gasda *et al.* 2009),

$$\phi\rho_b\bar{\beta}_b(H-h)\frac{\partial p_b}{\partial t}+\phi\rho_b(1-S_{res}^b)\frac{\partial(H-h)}{\partial h} \quad (2)$$

$$+\nabla\cdot\rho_b\bar{\mathbf{q}}_\mathbf{b}-\rho_b q_b|_{d_T}-\rho_b q_b|_{d_B}=\int_{d_B}^{d_M}\rho_b F_b dz$$

$$\phi\rho_c\bar{\beta}_c h(1-S_{res}^b)\frac{\partial p_c}{\partial t}+\phi\rho_c(1-S_{res}^b)\frac{\partial h}{\partial t} \quad (3)$$

$$+\nabla\cdot\rho_c\bar{\mathbf{q}}_\mathbf{c}+\rho_c q_c|_{d_T}-\rho_c q_c|_{d_B}=\int_{d_M}^{d_T}\rho_c F_n dz$$

In above equations, $\bar{\beta}_\alpha$ is the vertically-averaged bulk compressibility of phase α and porous media, and S_{res}^b is the residual wetting phase saturation. The vertically-averaged volumetric flux, $\bar{\mathbf{q}}_\boldsymbol{\alpha}$ can be calculated using Darcy's law as below

$$\bar{\mathbf{q}}_\boldsymbol{\alpha}=-\frac{H\bar{\mathbf{k}}_{\mathbf{r}\boldsymbol{\alpha}}\,\mathbf{k}}{\mu_\alpha}\nabla p_\alpha \quad (4)$$

where $\bar{\mathbf{k}}_{\mathrm{r}\alpha}$ is the pseudo relative permeability obtained from the phase average over the thickness of phase α, and **k** is the vertically averaged intrinsic permeability.

20.3 Model - Dalders Monocline

20.3.1 Model Settings

The target area modeled for the CO_2 injection is the deep part of the Dalders monocline (Fig. 2). The modeled units are the lower and middle Cambrian units, which have relatively high permeability and porosity, and are mostly continuous within the monocline area. From above the aquifer is sealed by thick Ordovician units and Alum shale that can work as excellent caprocks for the injected CO_2 plume. The thickness of Cambrian units varies depending on locations, but generally the structure becomes thinner and pinches out by moving northward. The overall thickness in the deepest part is about 100 m.

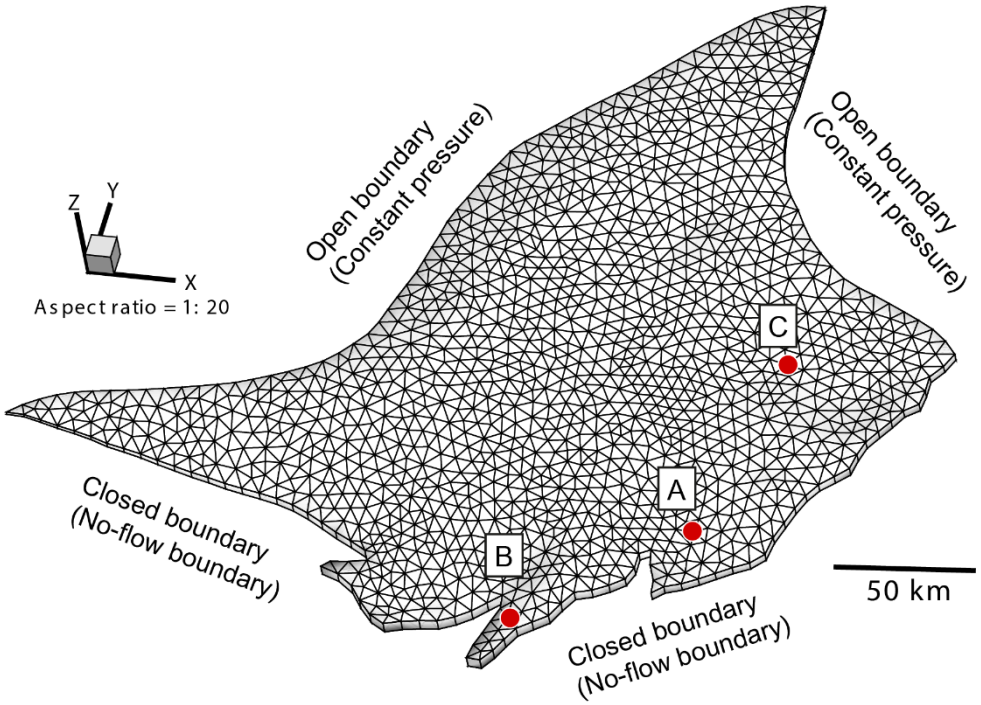

Figure 2. Numerical grid used in the simulation. The CO_2 injection wells are marked in red circles near the southern boundary.

The southern side of the monocline is bounded by a fault zone, and the sedimentary units in the northern side are exposed in the submarine/atmosphere. We assume the southern boundary of the modeling domain to be closed (no-flow boundary condition) and the northern boundary to be open (constant-pressure boundary condition). The hydrogeological parameters (e.g. permeability, porosity) used in the model were obtained from several boreholes spread over the monocline. The permeability ranges tens to one hundred millidarcy. An isothermal temperature ~ 50˚C was assumed for the whole area, and CO_2 density and viscosity were calculated using given pressure and temperature. Relative permeability functions used in the model is linear with respect to vertically averaged saturation (Gasda et al. 2009). Irreducible CO_2 saturation (Sgr) was set to 0.2.

Three different scenarios were tested to investigate the pore pressure development and the CO_2 plume migration during and after the injection: (1) *Scenario 1* – Single-well injection to well A with the rate of 0.5 Mt CO_2/year, (2) *Scenario 2* – Multiple-well injection to wells A, B, and C with the rate of 0.5 Mt CO_2/year, and (3) *Scenario 3* – Multiple-well injection to wells A, B, and C with the rate of 1.0 Mt CO_2/year. The injection periods for all scenarios are 50 years.

20.3.2 Pressure Distribution and CO_2 Plume Migration - Dalders Monocline

Single-well Injection (Scenario 1)

The overpressure ratio was used for plotting fluid pressure increase due to the CO_2 injection.

$$\lambda(\%) = \frac{P_F - P_H}{P_H} \times 100 \quad (5)$$

where λ is overpressure ratio in percentage, P_F is pore fluid pressure, and P_H is hydrostatic pressure.

During the CO_2 injection (0 ~ 50 years), pore fluid pressure around the injection well increases gradually (Fig. 3). The overpressure ratio reaches at the injection well A reaches a maximum value of 89%, after 50 years of injection. The overpressured area also increases with the injection time, and the diameter of 50% overpressured zone becomes about 20 km after 50 years. The shape of the influencing zone is roughly concentric circles bounded by the fault zone.

Overall CO_2 plume diameter is less than 10 km and shows no significant movements during relatively long recovery period after the end of injection (~ 500 years) (Fig.4). The thickness of mobile CO_2 is about 2.0~2.2 m around the injection well and gradually decreases with increasing distance from the center. A small migration of the plume toward the north is detected, but could be considered minor regarding the size of the monocline structure.

Multiple-well Injection (Scenarios 2 and 3)

In these scenarios we simultaneously injected CO_2 into three wells with the rate of 0.5 Mt/year for 50 years (Scenario 2), which are the same rate and period than in the previous single-well scenario (Scenario 1). During the injection, the overpressured areas first (at 20 years) appear as isolated patches, and then (at 50 years) becoming combined into a broader area of overpressure, with higher overpressure ratio in each of the injection wells (Fig. 5). The overpressure ratio in wells A and C is after 50 years ~90% and in the area between the wells is in the order of 20~30%. The injection well C shows a clearly higher overpressure ratio, due to its location close to the closed fault zone and low permeability. In the well C, the maximum overpressure ratio is 230% after 50 years of injection.

The CO_2 plumes created by the multiple-well injection are similar to that by the single-well (Fig. 6). The diameter of each plume is less than 10 km. The thickness of mobile CO_2 plume in the well C is deeper than other two wells because of the low permeability and porosity values of the targeted aquifer. Significant migration was not observed after a relatively long time period after the end of injection (~ 500 years).

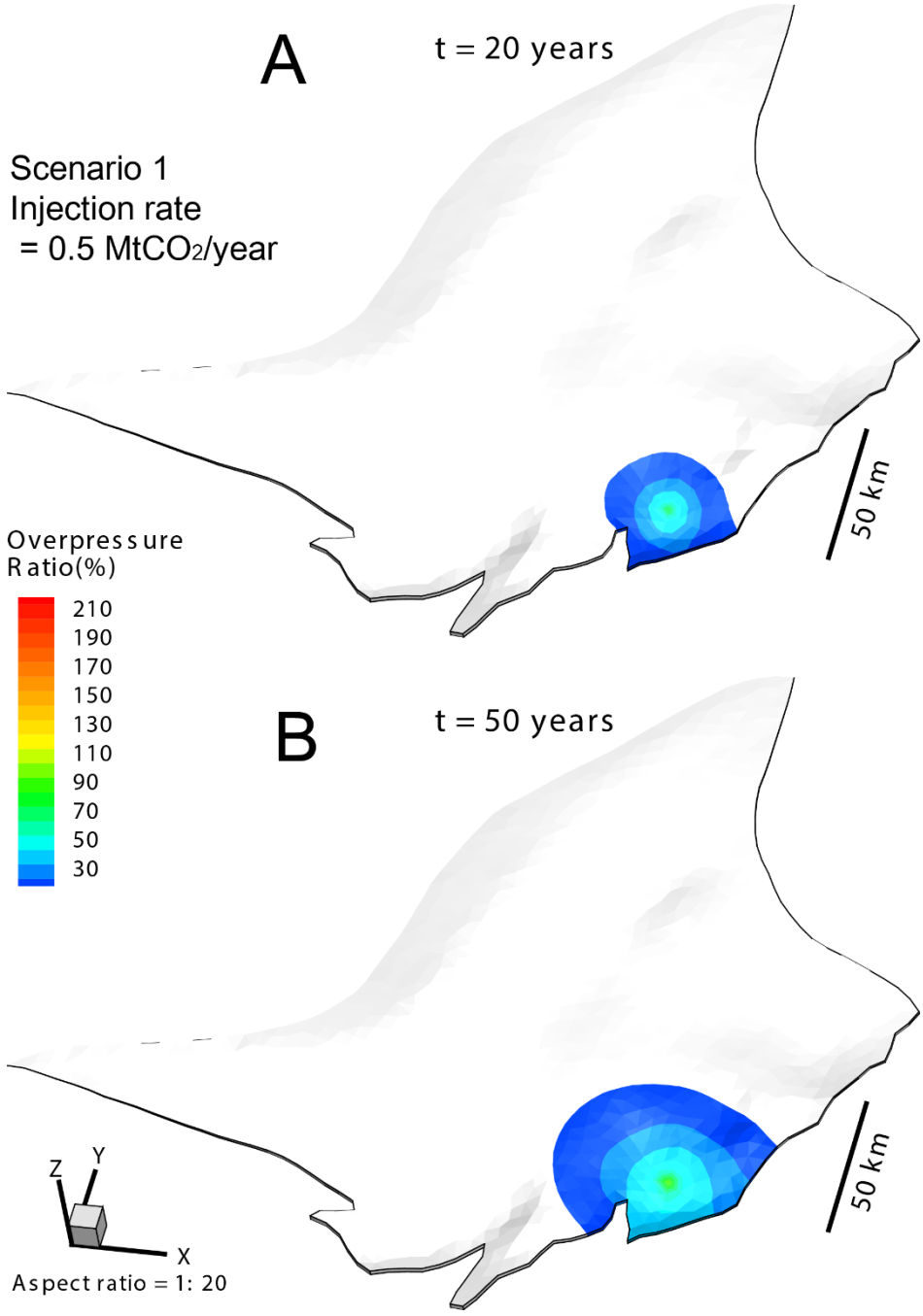

Figure 3. Scenario 1 - Overpressure ratio by the single-well CO_2 injection with the rate of 0.5 Mt CO_2/year for 50 years (Scenario 1). (a) 20 years after injection, (b) 50 years after injection.

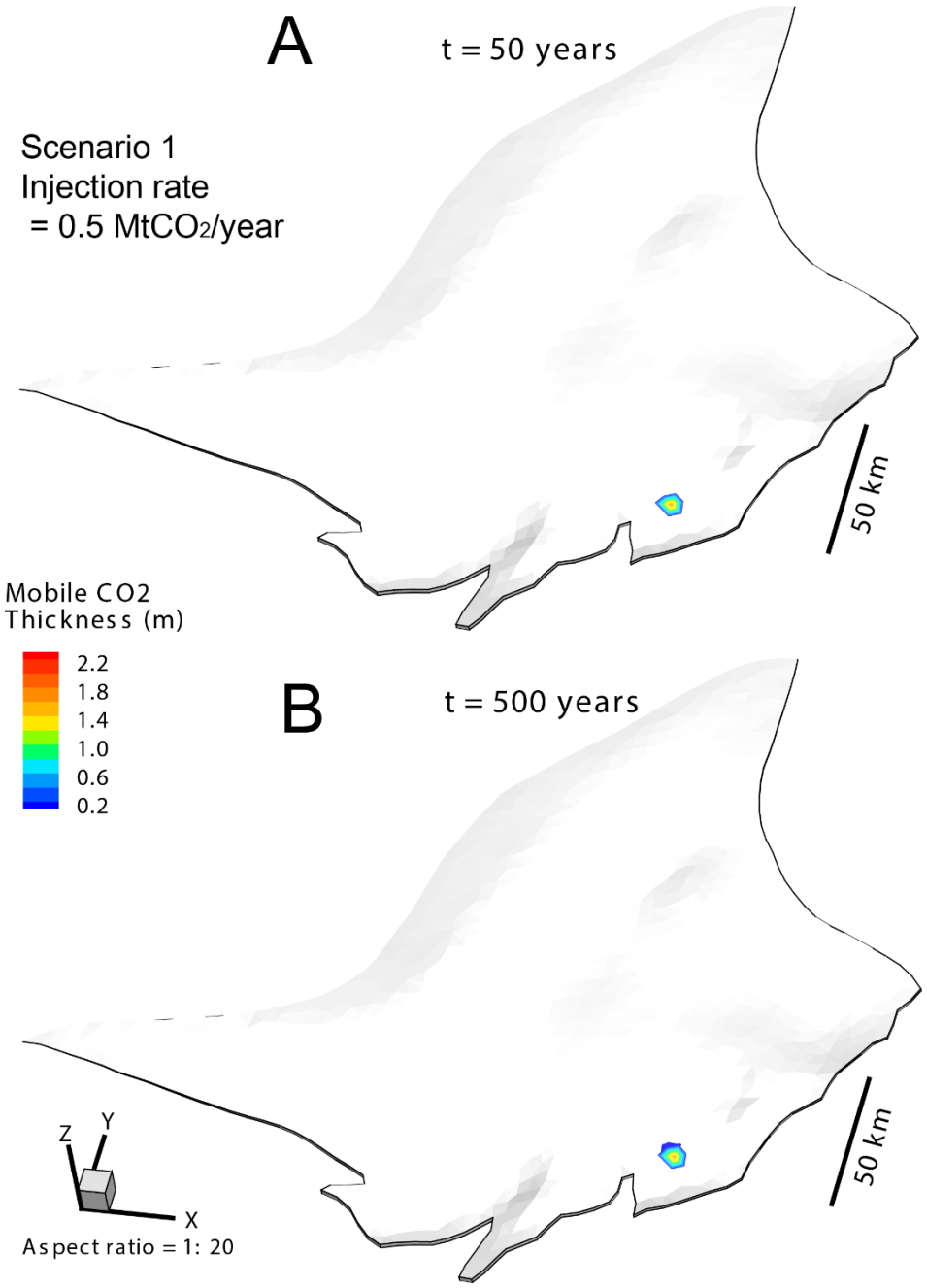

Figure 4. Scenario 1 - Mobile CO_2 plume migration by the single-well injection with the rate of 0.5 Mt CO_2/year for 50 years (Scenario 1). (a) 50 years after injection, (b) 500 years after injection.

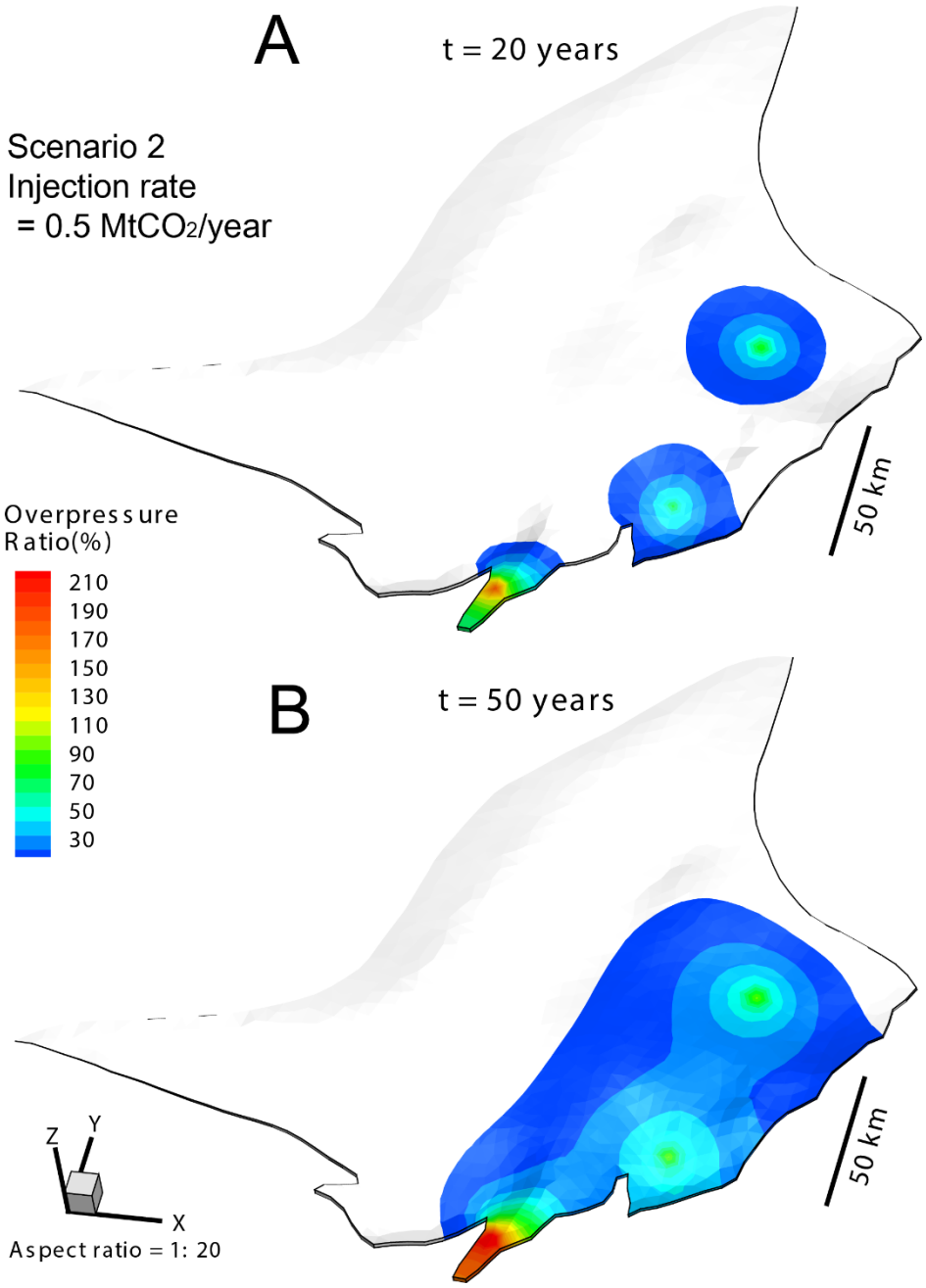

Figure 5. Scenario 2 - Overpressure ratio by the multiple-well CO2 injection with the rate of 0.5 Mt CO2/year per well for 50 years (Scenario 2). (a) 20 years after injection, (b) 50 years after injection.

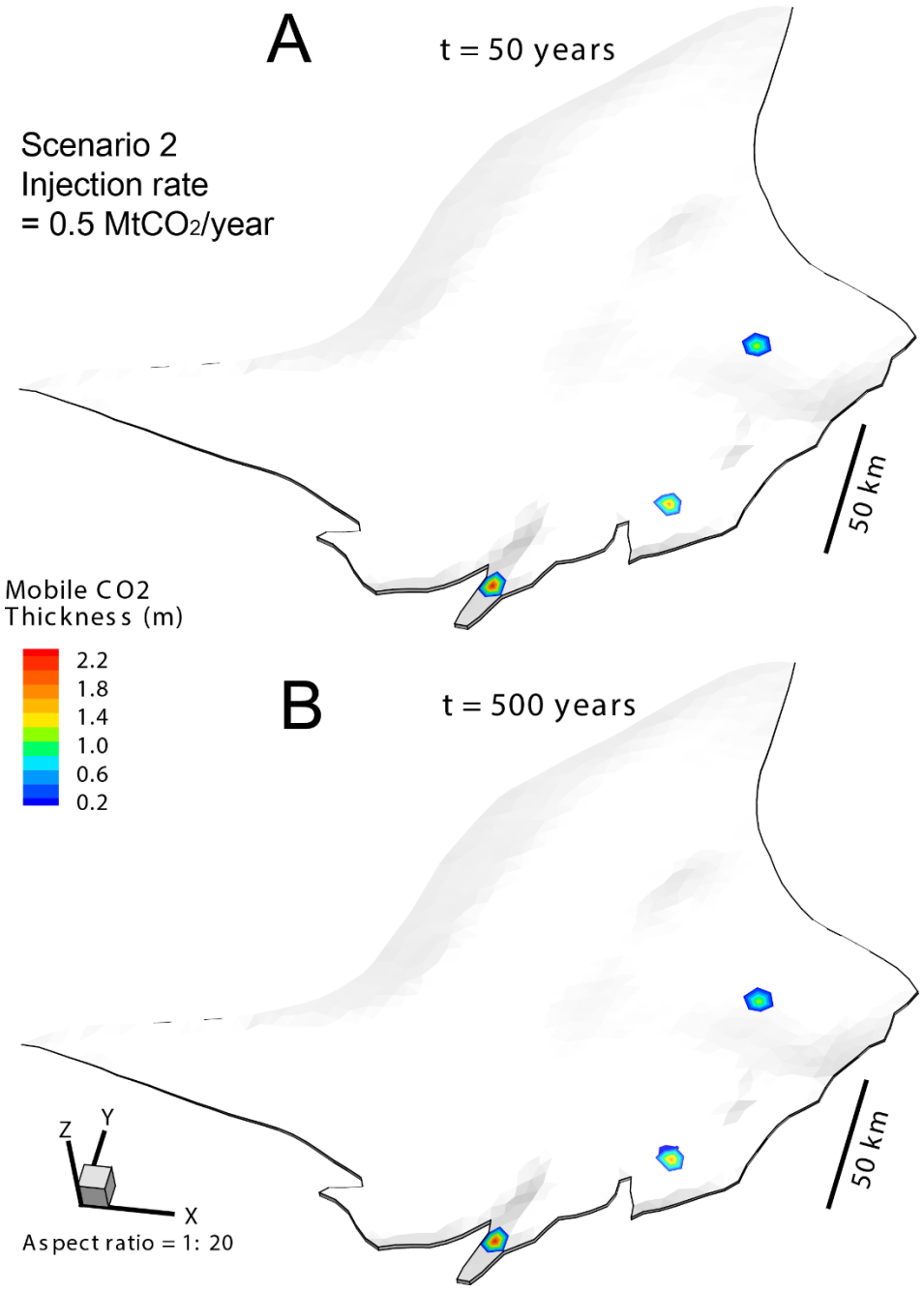

Figure 6. Scenario 2 - Mobile CO2 plume migration by the multiple-well CO2 injection with the rate of 0.5 Mt CO2/year per well for 50 years (Scenario 2). (a) 50 years after injection, (b) 500 years after injection.

In Scenario 3, the injection rate for all three wells is increased to 1.0 Mt/year. The overpressure ratio at the injection wells increased to ~180% (A and C) and the influence area was wider compared to the overpressure distribution from Scenario 2 (Fig. 7). Highly overpressured area around the well C was also expanded in case of the increased injection rate and the maximum value was over 300%.

Increasing the injection rate also influences the size of the CO_2 plume. The maximum thickness of the plume increased to about 4.0 m, and the diameter of the area also increased to about 15 km (Fig. 8). Much more prominent plume migration is observed compared to that from the Scenario 2, although it is still not significant considering the scale of the monocline structure. The overall direction of migration is from south to the north, due to topographic reliefs of the monocline.

20.4 Model - Dalders Structure

20.4.1 Model Settings

This area is an anticline structure attached to the southern part of the Dalders monocline, consisting of Cambrian sedimentary units (Fig. 9). Thick low-permeable Ordovician sequences and shale layers generally provide a good sealing capacity for the CO_2 storage. The average thickness of lower to middle Cambrian sandstone is about 1 km. The depth ranges 1.3 ~ 1.4 km below sea level, and the physiographic map shows three high locations suitable for commercial size CO_2 injection operation.

The northern boundary of the structure is a closed fault zone and considered a closed boundary (no-flow boundary condition). The southern boundary is a spill point, and assumed as an open boundary (constant pressure boundary condition). The location of the injection well (D) was chosen in the middle of the structure where the depth is relatively deep; hence we can easily observe the overpressure development and migration induced by the CO_2 injection. The injection rate and period applied to the well D are 0.3 Mt/year for 50 years.

20.4.2 Pressure Distribution and CO2 Plume Migration: Dalders Structure

The overpressure ratio at the injection well is about 20%, and the influencing area is extended along the northern boundary due to the sealing effect by the closed fault (Fig. 10). The pressure response is relatively fast during the injection due to relatively high permeability of this region (50~80 md).

The size of mobile CO_2 plume after 50 years is about 3~4 km with 7.0 ~ 10.0 m thickness, and the plume slowly moves towards the higher elevation due to the buoyancy (Fig. 11). After 500 years, the plume has migrated further to the north (topographically higher location) and elongated along the center line of the structure.

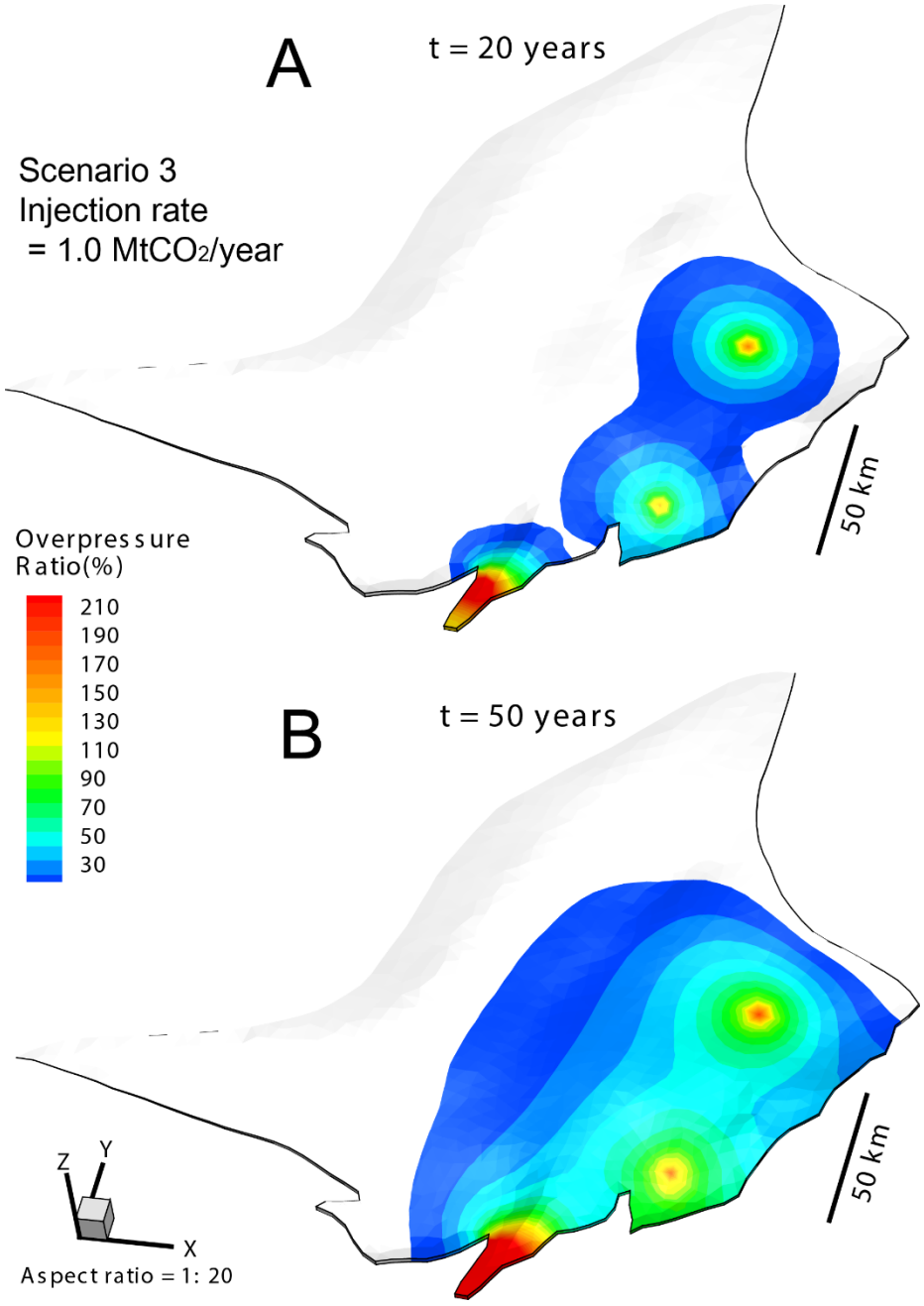

Figure 7. Scenario 3 - Overpressure ratio in the multiple-well CO_2 injection with the rate of 1.0 Mt CO_2/year per well for 50 years (Scenario 1). (a) 20 years after injection, (b) 50 years after injection.

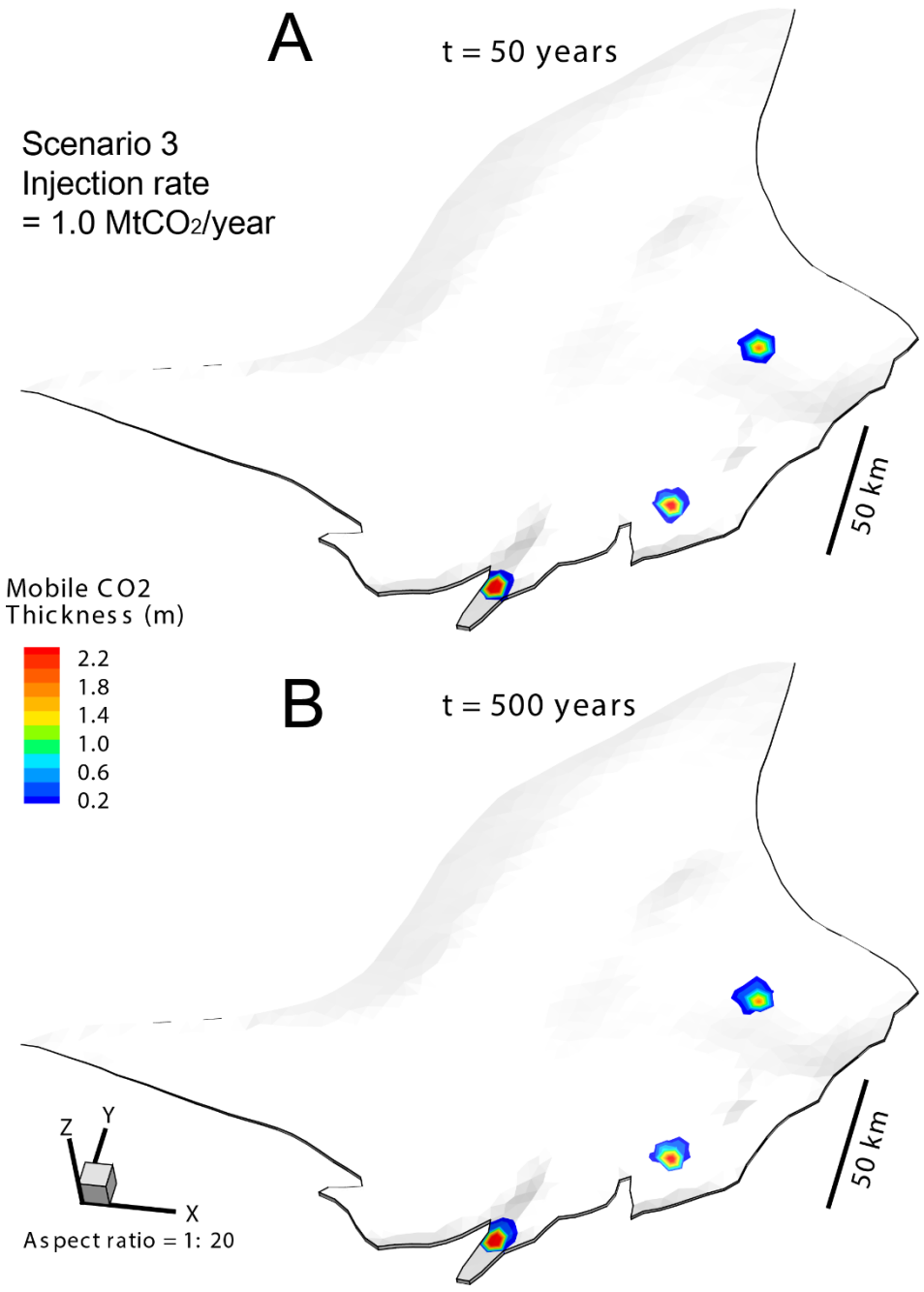

Figure 8. Scenario 3 - Mobile CO2 plume migration by the single-well CO2 injection with the rate of 1.0 Mt CO2/year per well for 50 years (Scenario 1). (a) 50 years after injection, (b) 500 years after injection (post-injection phase).

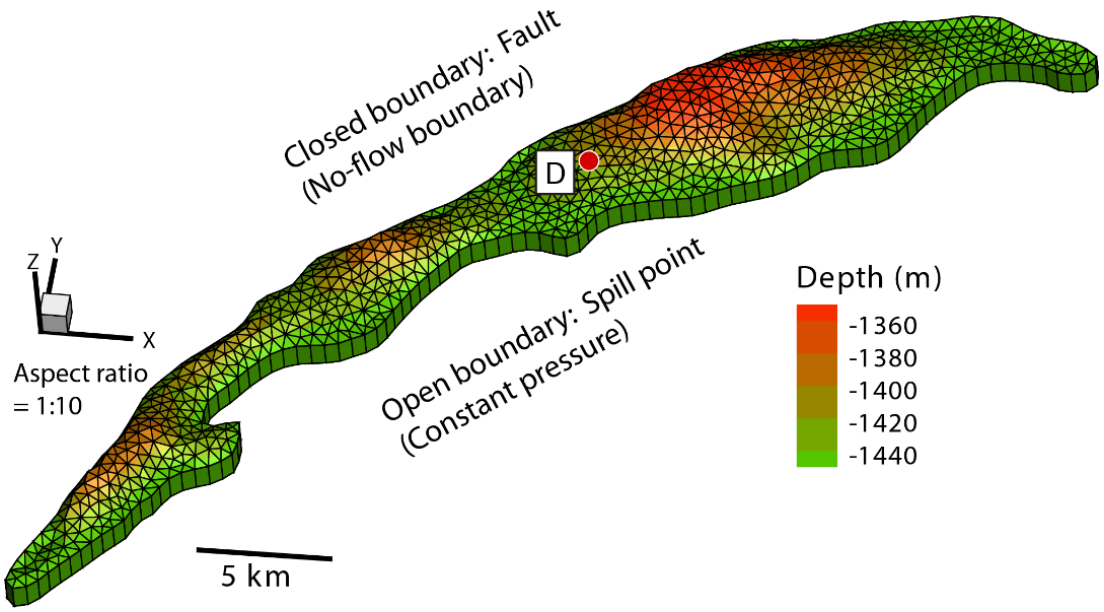

Figure 9. Numerical grid used in the dynamic modeling of the Dalders structure. The CO_2 injection well is marked by the red circle in the center of the structure.

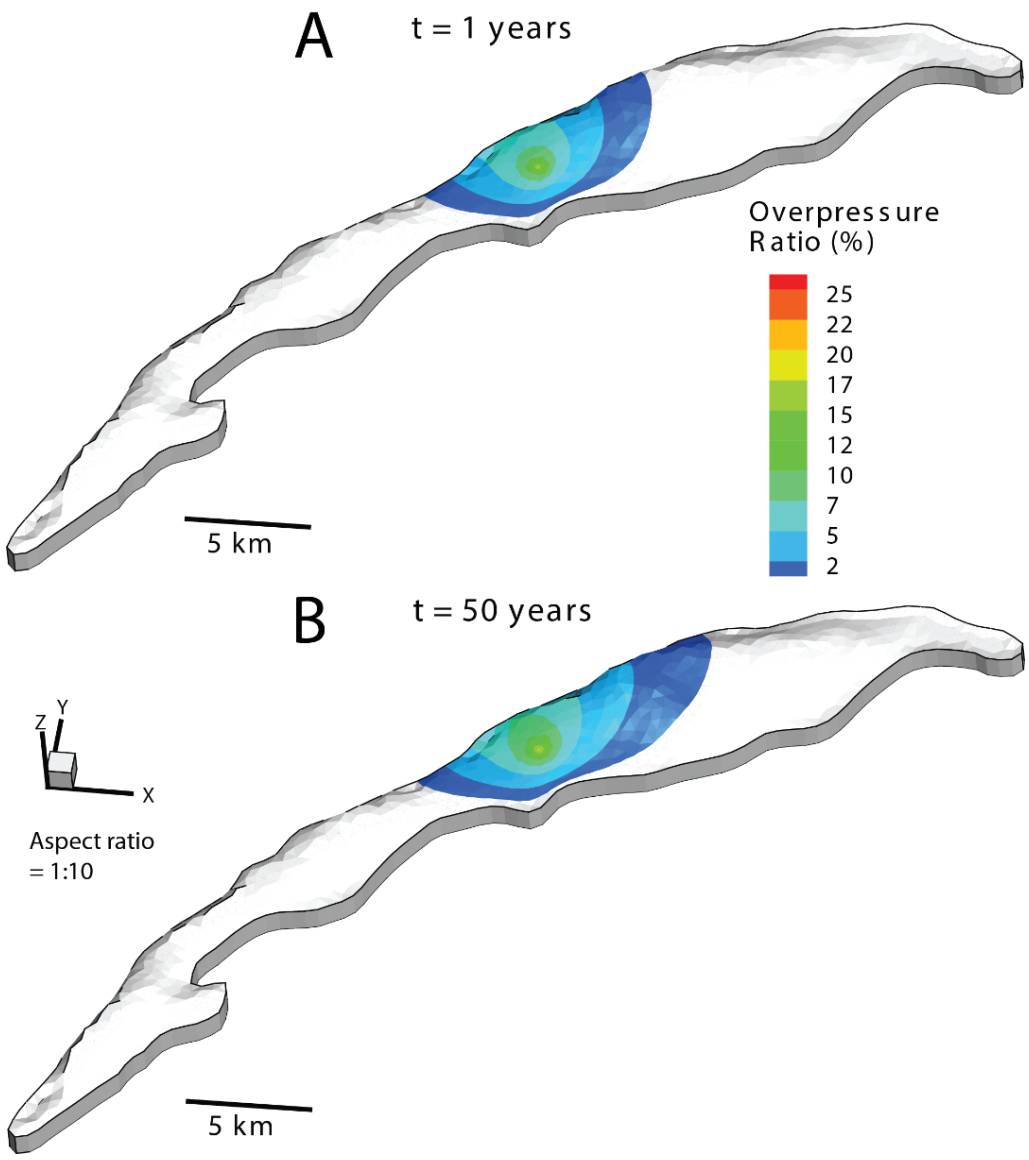

Figure 10. Overpressure ratio by the CO_2 injection with the rate of 0.3 Mt CO_2/year for 50 years. (a) 1 year after injection, (b) 50 years after injection.

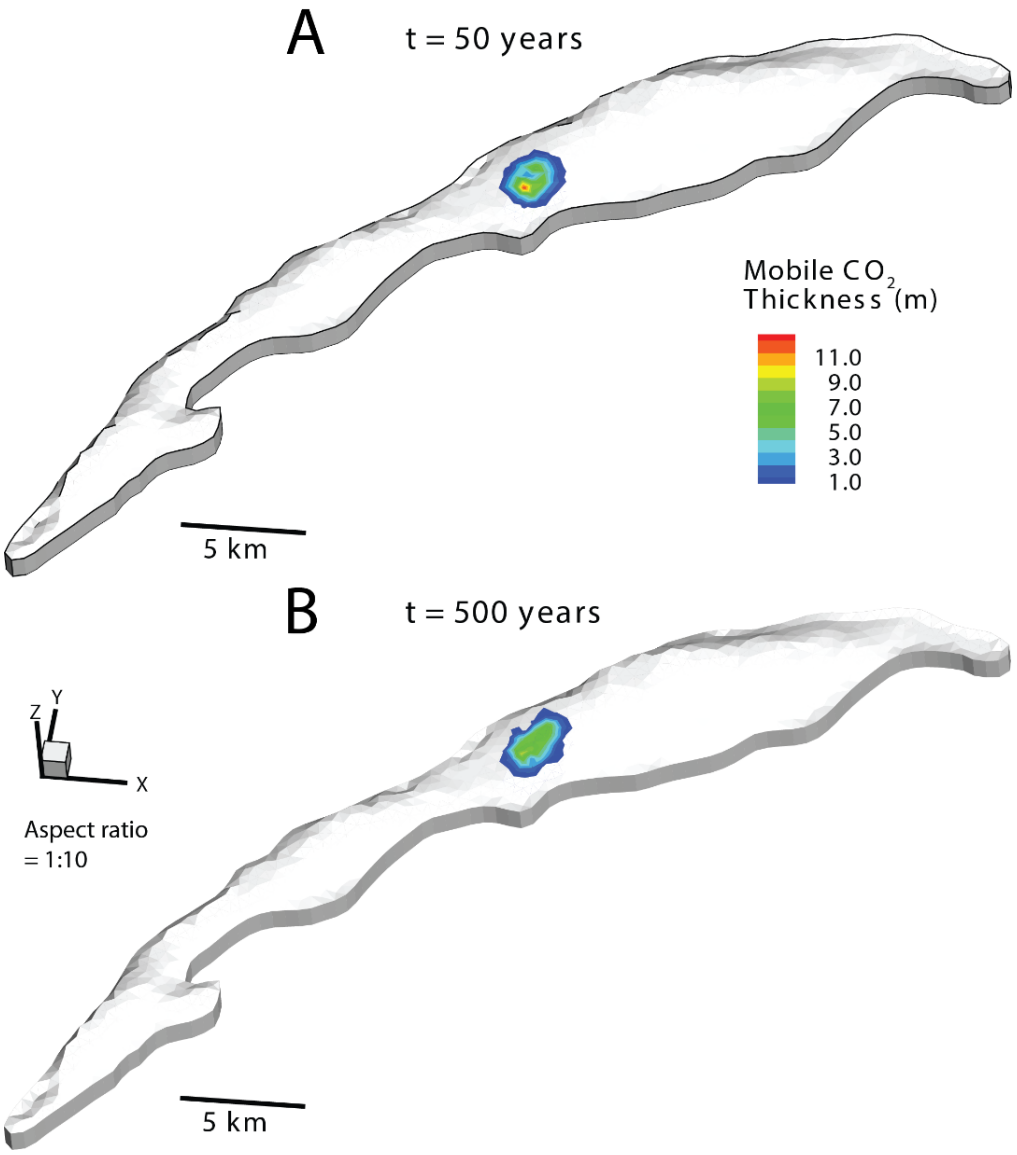

Figure 11. Mobile CO_2 plume migration by the CO_2 injection with the rate of 0.3 Mt CO_2/year for 50 years. (a) 50 years after injection, (b) 500 years after injection.

20.5 Conclusions

We have explored the effects of CO_2 injection in the submarine brine aquifers of Dalders Monocline and Dalders Structure, by modeling fluid pressure evolution and CO_2 plume migration during and after the injection. Three different injection scenarios varying the number of wells and injection rates were considered using the vertical equilibrium modeling approach. Based on the results, we can conclude the following:

1. With given hydrogeological parameters and an injection rate of 0.5 $MtCO_2$/year, the single-well injection could produce 70% ~ 80% overpressure ratio at the injection well after 50 years of injection.

2. The multiple-well injection could exacerbate overpressure evolution, and the location of the injection well is also shown to be important, in order to avoid high overpressures and potential risk of the caprock failure/fault reactivation. The injection well situated very close to the closed fault zone could induce an extreme overpressure of over 200% in the vicinity of the well.

3. Both 0.5 $MtCO_2$/year and 1.0 $MtCO_2$/year injection scenarios to the Dalders monocline create CO_2 plumes of less than 15 km with several meters thickness. The migration distance over 500 years is relatively small and insignificant considering the size of the monocline.

4. The 0.3 $MtCO_2$/year injection in the Dalders structure produced ~20% of overpressure and 3~4 km of CO_2 plume after 50 years of injection. The plume also shows a relatively strong topographically driven migration to the higher elevation area, driven by the buoyancy effect.

20.6 References

Bear J (1972) *Dynamics of Fluids in Porous Media*. Dover Publications, Inc., New York.

Gasda SE, Nordbotten JM, & Celia MA (2009) Vertical equilibrium with sub-scale analytical methods for geological CO_2 sequestration. *Computational Geosciences* **13**, 469-481, doi:10.1007/s20596-009-9138-x.

Gasda SE, Nordbotten JM, & Celia MA (2012) Application of simplified models to CO_2 migration and immobilization in large-scale geological systems. *International Journal of Greenhouse Gas Control* **9**, 72-84, doi:10.1016/j.ijggc.2012.03.001.

Gasda SE, Nilsen HM, Dahle HK, & Gray WG (2012) Effective models for CO_2 migration in geological systems with varying topography. *Water Resources Research* **48**, W10546, doi:10.1029/2012WR012264.

Gray WG, Herrera PA, Gasda SE, & Dahle HK (2012) Derivation of vertical equilibrium models for CO_2 migration from pore scale equations. *International Journals of Numerical Analysis and Modeling* **9**, 745-776.

Juanes R, MacMinn CW, & Szulczewski ML (2010) The footprint of the CO_2 plume during carbon dioxide storage in saline aquifers: storage efficiency for capillary trapping at the basin scale. *Transport Porous Media* **82**, 19-30, doi:10.1007/s11242-009-9420-3.

Szulczewski M & Juanes R (2009) A simple but rigorous model for calculating CO_2 storage capacity in deep saline aquifers at the basin scale. *Energy Procedia* **1**, 3307-3314, doi:10.1016/j.egypro.2009.02.117.

PART E

21.0 ESTIMATING CO_2 PLUME MIGRATION SPEED AND DISTANCE IN THE UP-DIP DIRECTION

Zhibing Yang, Saba Joodaki and Auli Niemi

Supercritical CO_2 injected into the Dalders monocline can migrate mainly in the up-dip direction below the cap-rock (an Alum shale layer), due to the gravity force (i.e., the density difference between brine and supercritical CO_2). This post-injection migration may constitute a concern of leakage risk e.g. at the Gotland island which is about 120 km away from a potential injection point. In order to evaluate the possibility of CO_2 plume reaching Gotland, we perform numerical simulations and analysis to address this issue based on all the available geological information.

21.1 Scenario

Since the CO_2 migration will be dominated by the sliding motion along the slope at large times, we consider a two-dimensional scenario (Figure 1) for investigating the potential of CO_2 up-dip migration. In this scenario, we cut a 2D vertical slice (1 m width) along the slope. Note that this is conservative in terms of CO_2 migration potential, as we ignore the expansion of CO_2 to direction other than the up-dip direction.

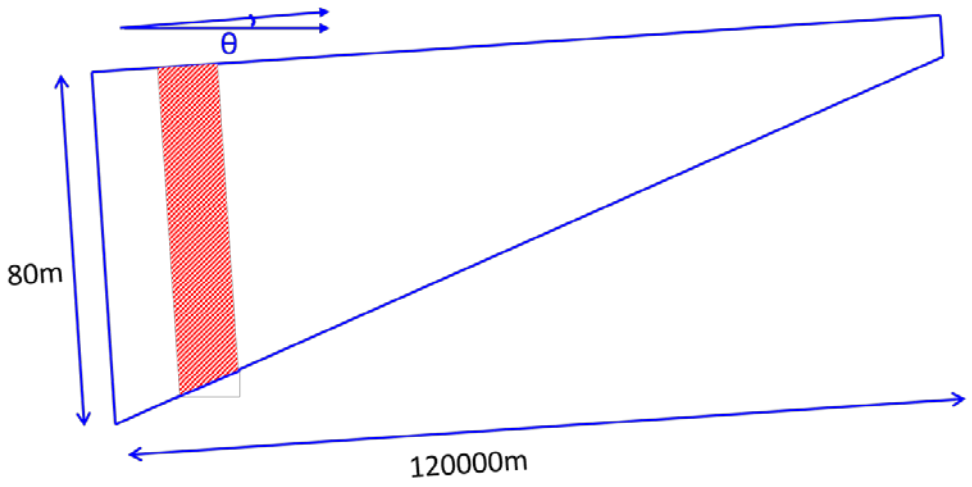

Figure 1. Schematic for the two-dimensional scenario considered in this study. The shadowed part shows the initial CO_2 plume placed in the domain

We use TOUGH2/ECO2N to simulate the migration of CO_2 in the formation. The simulation domain is discretized into 5540 grid blocks. We use a one-meter slice of the aquifer with an initial CO_2 plume of 1 km width. The initial plume is place at x = 14~15 km. The simulation results can provide CO_2 migration patterns and plume tip migration velocities.

The parameters used for the simulations are taken as the best estimates from the available information for the aquifer (Middle Cambrian sandstone). The slope of the aquifer is 0.5 degrees. The initial CO_2 plume depth is set as 1200 m. We test two different permeabilities: 30 and 100 mD, corresponding to the most probably range of permeability values. The thickness of the aquifer varies from 80 m at the deeper end of the aquifer to 5 meters at the shallower end of the aquifer. The porosity of the formation is assumed to be uniformly 0.1.

Capillary pressure and relative permeability functions are based on the Brooks-Corey function with parameter $\lambda = 0.670$, residual brine saturation $S_{lr} = 0.3$. We consider three different residual gas (CO_2) saturation values $S_{gr} = 0.1$, 0.2 and 0.3 to investigate parameter sensitivity. According to the measurement of residual CO_2 saturation for four different sandstones by Krevor et al. (2012), the more realistic values of S_{gr} would be in fact above 0.2 or even 0.3.

21.2 Simulation results

21.2.1 CO_2 saturation patterns

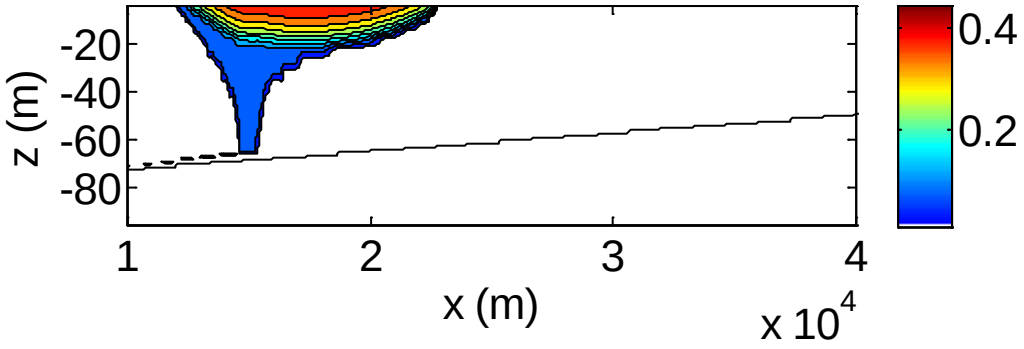

Figure 2. Simulated CO_2 saturation for the case of k=30 mD, residual CO_2 saturation 0.1, at time 2000 years.

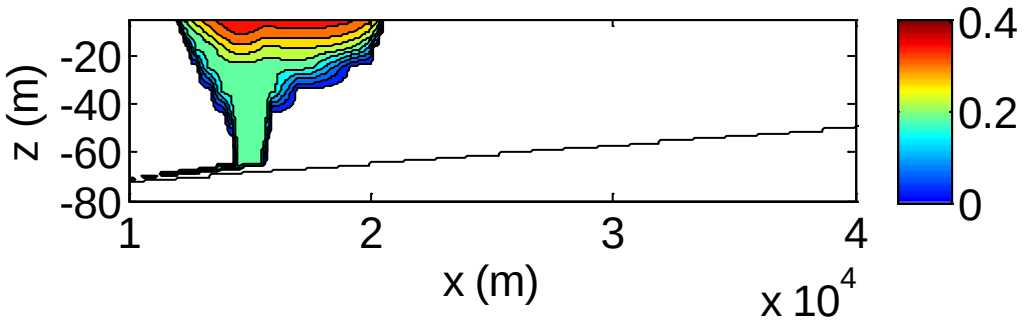

Figure 3. Simulated CO_2 saturation for the case of k=30 mD, residual CO_2 saturation 0.2, at time 3000 years.

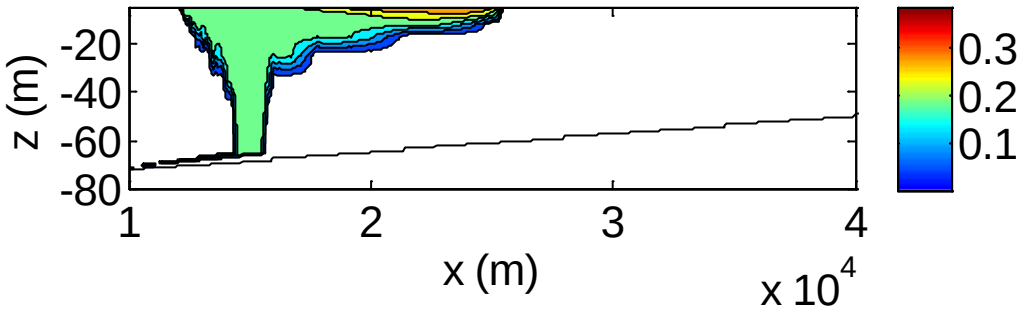

Figure 4. Simulated CO_2 saturation for the case of k=100 mD, residual CO_2 saturation 0.2, at time 2000 years.

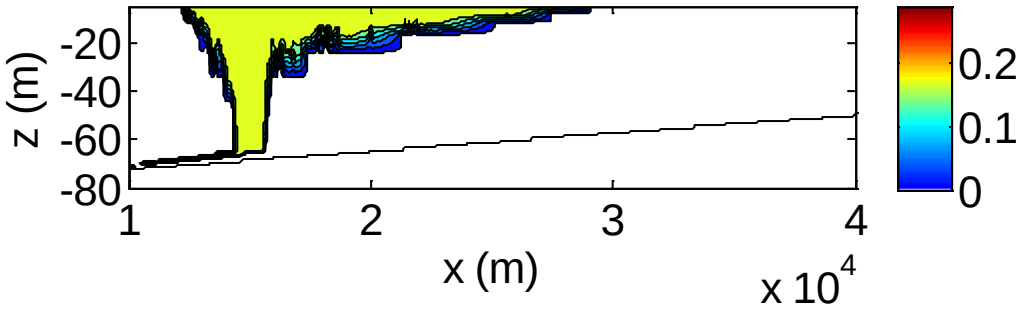

Figure 5. Simulated CO_2 saturation for the case of k=100 mD, residual CO_2 saturation 0.2, at time 4000 years.

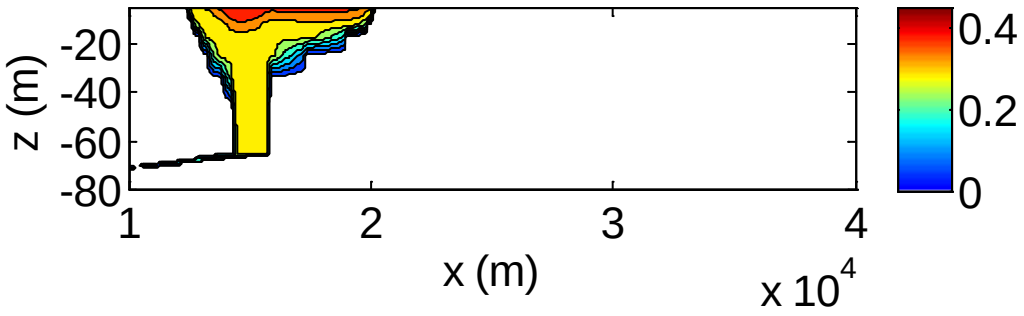

Figure 6. Simulated CO_2 saturation for the case of k=100 mD, residual CO_2 saturation 0.3, at time 2000 years.

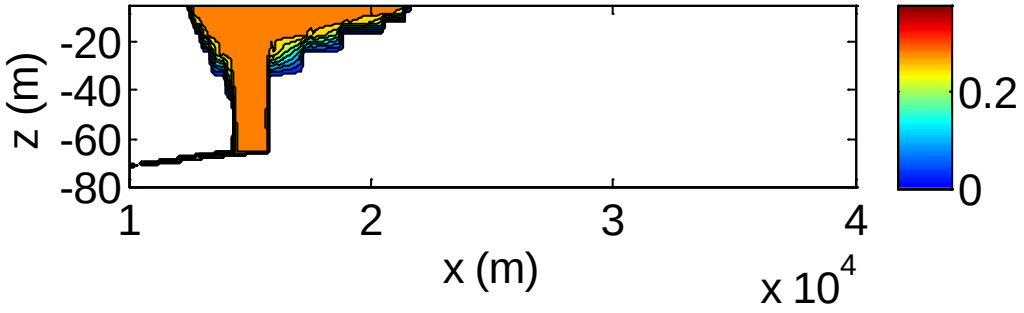

Figure 7. Simulated CO_2 saturation for the case of k=100 mD, residual CO_2 saturation 0.3, at time 4000 years.

Figures 2-7 show some of the simulated CO_2 saturation patterns at different (large) times for different permeabilities and residual gas saturations. It can be seen that the plume extends in the sloping direction and its thickness at the tip gradually decrease as the tip travels farther. These patterns all show the dependence of plume migration on the main parameters (formation permeability and residual gas saturation).

The CO_2 plume in these figures can be divided into two parts: the mobile part where CO_2 saturation $S_g > S_{gr}$ and the trapped (immobile) part where $S_g \leq S_{gr}$. The mobile CO_2 keeps migrating in the up-dip direction until all CO_2 becomes trapped as residual or dissolves in to the brine. For example, in the case of k= 100 mD and $S_{gr} = 0.2$, all mobile CO_2 has depleted and the migration has stopped after 4000 years. The plume tip has migrated about 14 km.

From Figures 2-7, we can see that plume thickness decreases from about 30 m just outside of the initial plume region to 0 m at the plume tip, for the scenario considered here. We note that the thickness of plume depends on the system parameters, especially the injected CO_2 volume. As a first order estimate, we may simply calculate an average thickness for the extended plume (excluding the initial plume zone) to be 15 m. With this average plume thickness and the residual

gas saturation, we can roughly estimate the volume of the CO_2 'footprint' and thus the plume tip distance if given a total CO_2 volume.

21.2.2 Plume tip migration distance and velocity

Parameters that can affect the migration of CO_2 plume in a sloping aquifer mainly include: permeability (and its anisotropy), residual CO_2 saturation, relative permeability of CO_2, slope, density difference between CO_2 and brine, CO_2 viscosity, etc. For the scenario considered in this study, the two most important parameters which are uncertain are the permeability and the residual gas saturation of the aquifer material.

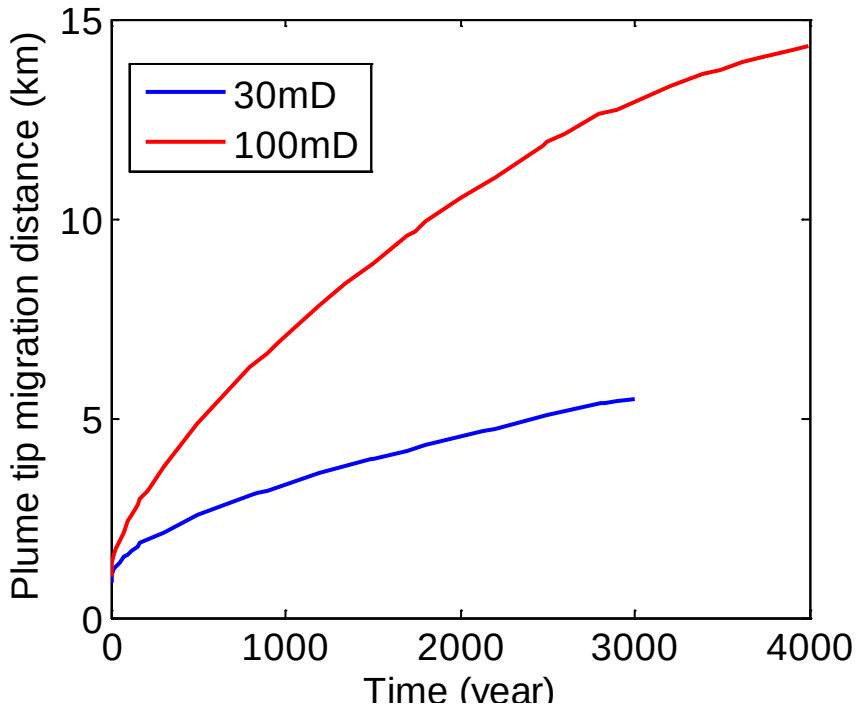

Figure 8. CO_2 plume tip migration distance as a function of time for permeabilities 30 and 100 mD. Residual gas saturation is 0.2 for both cases.

Figure 8 shows that permeability significantly affects the tip migration velocity. When k = 100 mD the plume tip migrated about 14 km in 4000 years, while for the case of k = 30 mD, the tip migrated less than 6 km in 3000 years.

Residual gas saturation has a large impact on the migration of CO_2 plume. As shown in Figure 9, increasing S_{gr} can greatly decrease the tip migration speed and the maximum migration distance. The plume tip has migrated less than 7 km in 4000 years when S_{gr} = 0.3, in comparison to 14 km when S_{gr} = 0.2. In the case of S_{gr} = 0.1, the plume tip migrates much faster, reaching 14 km in about

1250 years. However, 0.1 may be an unrealistically low value for residual gas saturation, given the measurements of typical sandstones relevant for CO2 storage by Krevor et al. (2012).

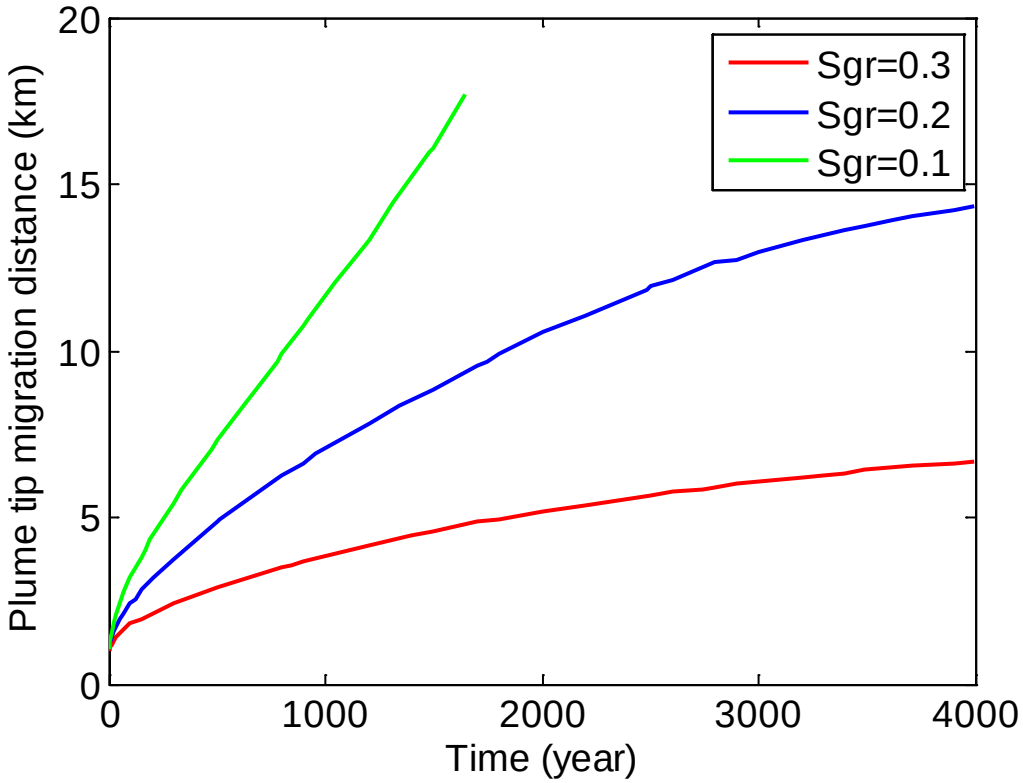

Figure 9. CO_2 plume tip distance as a function of time for different residual gas saturation values. Permeability k = 100 mD.

21.3 Discussion and conclusions

In the above simulations we have not included the effect of caprock topographic roughness (undulation) and the effect of convective mixing (or convective dissolution). Besides, in this 2D analysis, the expansion of the plume to outside of the 2D plane is not taken into account, which will slow down the migration and at the same time decrease the migration distance, especially in the case considered here with a slope of only 0.5 degree for the Monocline. Therefore, the analysis on the plume migration potential is conservative (i.e., the distance will be larger than the actual in the field).

The 2D scenario here can be thought of as a one-meter slice in the middle of the injected CO_2 cylindrical plume in a 3D view. In this 3D perspective, the scenario may correspond to about 3 Mt CO_2 for the injection point. According to the above results, the plume tip will migrate a maximum

distance of about 14 km and come to a stop within 4000 years, for the case of k = 100 mD and S_{gr}= 0.2. Again, these two important parameters are chosen to be conservative.

If we instead consider 30 Mt injected CO_2 for one injection point (well), this corresponds to an initial CO_2 mass of about 1.7×10^7 kg in the 2D scenario. If S_{gr}= 0.2, a simple volumetric calculation may yield a potential maximum migration distance of about 50 km, taking into account the plume shape (with average thickness for the part of plume extending to direction of the slope assumed to 15 m) and equilibrium dissolution within the plume. According to the average speed of migration (3.5 km/1000 year, which may be obtained from Figure 9) a migration distance of 50 km would take about 14000 years. Given this distance and the especially long time, we can also calculate the dissolution trapping capacity of this 2D slice aquifer, i.e., assuming convective mixing to reach its full effect. The mass that can potentially be dissolved in our considered system (50 km long 2D slice) is about 9×10^6 kg, which is more than half of the initial CO_2 mass. This means that, in this case, convective dissolution has the potential to significantly drag the plume migration, and that the plume migration distance will be actually much smaller than 50 km.

21.4 References

Krevor SCM, Pini R, Zuo L, & Benson AM (2012) Relative permeability and trapping of CO_2 and water in sandstone rocks at reservoir conditions. *Water Resour. Res.* **48**, W02532, doi:10.1029/2011WR010859.

Additional Note on Capillary Pressure and Relative Permeability Functions

The different models used in the previous chapters used different assumptions and thereby the treatment of so-called characteristic functions for the two-phase flow are treated differently in the different models. To allow the reader an easy comparison, we explain the use of these functions in the three models here

Capillary pressure functions

In the semi-analytical model for pressure buildup and in the vertical equilibrium (VE) numerical model, capillary pressure is ignored. Capillary pressure would have negligible impact on the pressure buildup (Mathias et al. 2011, WRR 47, W12525). Neglecting capillary pressure in the VE numerical model is justified as the VE model is a a much simpler model than the full-physics TOUGH2 model and the advantage of the VE model is its numerical efficiency.

Capillary pressure functions are only used in the TOUGH2 simulations. Because of a lack of experimental data on two-phase flow properties of the formation rock, we have assumed that the capillary pressure is a van Genuchten function with typical literature parameter values of m=0.457 and S_{wr} = 0.3. Parameters in the similar range have also been used in, e.g., Doughty (1997, Energy Conversion and Management, 48, 1768-1681) and Zhou et al. (Ground Water, 2010, 494-514).

Relative permeability functions

In the VE model, the saturation within the CO_2 occupied region is assumed to be constant (full gas saturation in this case). Thus relative permeability effects are not really taken into account. Through a vertical integration procedure, one can see that the vertical averaged relative permeabilities (pseudo-relative permeabilities) are linear functions of the thickness of the CO2 plume.

Again, in the TOUGH2 simulations we have to use the literature values of the relative permeability functions due to the lack of data.

Using the analytical model presented in Chapter 17, we can evaluate the impact of relative permeability parameters used on injection overpressure. A comparison of relative permeability functions used in the semi-analytical model for pressure buildup and in the TOUGH2 simulations is presented in Figure 1 below. It can be seen that there is notable differences between the two sets

of curves. However, the pressure buildup difference due to the different relative permeability functions is small (Figure 2 below, that can be compared to figures in the appendix A (Chapter 17) of the report).

Nevertheless, it would have been beneficial for modeling if more field data and core measurements especially regarding two-phase flow properties could be obtained. This is one of major sources of uncertainty. In future modeling work, we will refine the analysis by taken into account the uncertainty in the capillary pressure and relative permeability functions.

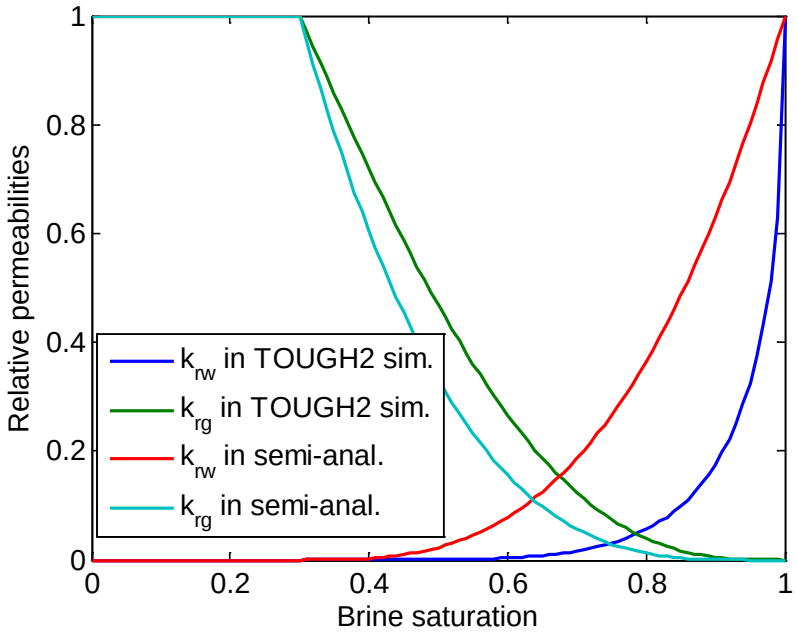

Figure 1. Relative permeability functions used in the semi-analytical model for pressure buildup and in the TOUGH2 simulations.

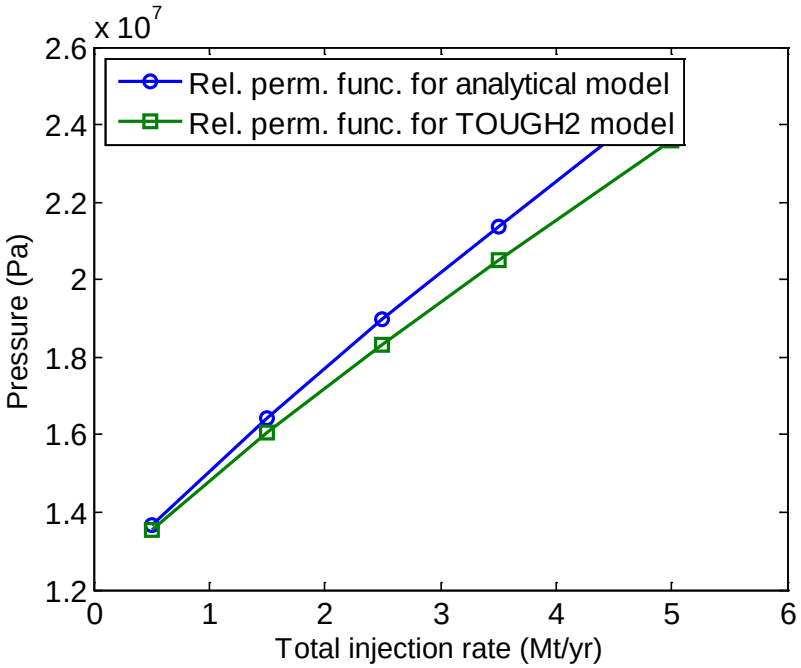

Figure 2. Comparison of pressure buildup from the semi-analytical model with two different sets of relative permeability functions from Figure 1.

Doughty, C. (2007), Modeling geologic storage of carbon dioxide: Comparison of non-hysteretic and hysteretic characteristic curves, *Energy Convers. Manag.*, *48*(6), 1768–1781.

Mathias SA, González Martínez de Miguel GJ, Thatcher KE, & Zimmerman RW (2011) Pressure buildup during CO_2 injection into a closed brine aquifer. *Transport in Porous Media* **89**, 383–97.

Zhou, Q., J. T. Birkholzer, E. Mehnert, Y.-F. Lin, and K. Zhang (2010), Modeling Basin- and Plume-Scale Processes of CO2 Storage for Full-Scale Deployment, *Ground Water*, *48*(4), 494–514.